TECHNICAL AND ECONOMIC EVALUATION OF NANOFLUID-ALTERNATING-BRINE FLOODING FOR ENHANCED OIL RECOVERY IN NIGER DELTA RESERVOIRS

Yetunde Aderonke OMOTOSHO

TECHNICAL AND ECONOMIC EVALUATION OF NANOFLUID-ALTERNATING-BRINE FLOODING FOR ENHANCED OIL RECOVERY IN NIGER DELTA RESERVOIRS

BY

Yetunde Aderonke OMOTOSHO

B.Sc. Petroleum Engineering, M.Sc. Petroleum Engineering (Ibadan)

MATRIC NO: 117542

A Thesis in the Department of Petroleum Engineering,
Submitted to the Faculty of Technology
in partial of fulfilment of the requirement for the Degree of

DOCTOR OF PHILOSOPHY

of the

UNIVERSITY OF IBADAN

FEBRUARY, 2022

CERTIFICATION

I certify that this work was carried out by Mrs Yetunde Aderonke OMOTOSHO in the Department of Petroleum Engineering, Faculty of Technology, University of Ibadan.

…….

(Supervisor)

O. A. FALODE

B.Sc. (Jos), M. Sc., Ph. D. (Ibadan)

Professor of Petroleum Engineering,

Petroleum Engineering Department, University of Ibadan, Nigeria

DEDICATION

This thesis is dedicated to all female researchers who juggle work, career and family life with unwavering determination to fulfil their dreams.

ACKNOWLEDGEMENTS

I am eternally indebted to the Almighty God for keeping me through the thick and thin of this research work and for giving me great and wonderful by-fruits in the course of the programme. I am in awe of Him for the success of it all.

I would like to acknowledge my supervisor, Prof. O.A. Falode, who has been fathering and mentoring me right from my undergraduate days since 2003. Thank you for believing in me. I want to unreservedly express my gratitude for your constant support and guidance in the course of this study. Ab initio, your hands were full but you still made room to supervise me. Your impact in my life remains indelible and undebatable.

I want to appreciate Dr Lateef Akanji of the University of Aberdeen, who warmly received me during my visit to the University of Aberdeen to carry out the analyses pertaining to this work. Thank you for always provoking me to excellence.

I am especially thankful to a father and mentor, Dr Lateef Akinpelu, whom I had been understudying since my undergraduate days. I never knew I would slide into your shoes after your retirement. It was not easy though, but by divine arrangement, it became possible. Thank you for constantly showing me the way of kindness, empathy and dedication.

My immense gratitude goes to Dr Olufemi Omoniyi, for his financial support. I am greatly appreciative.

I would like to acknowledge and appreciate the academic staff members of Petroleum Engineering Department, UI. I would like to thank Prof. Isehunwa for his fatherly counsel and guidance in the course of the programme; Dr Oluwatoyin Akinsete, a dedicated postgraduate coordinator, for his unrelenting effort and exceptional administrative skill in making the thesis flow frictionlessly from one level to the other; Dr Julius Alawode, for your advisory tips while putting the work together; Dr Princess Nwankwo, for making me to realise that it is possible to juggle all together and still come out shining; Dr Sarah Akintola and Engr Seyi Orisamika, for their moral support. I am also grateful to the technical staff members of the department viz., Mr Adebola Adebanjo for providing

guidance during the preliminary stage of the work; Mr Adeniyi Adenuga and Mr Ope Oni for sacrificing their time and effort and giving helpful tips during part of my bench work.

My profound gratitude goes to the entire staff members of the Department of Petroleum Engineering, Covenant, University, Otta, for accepting and supporting me during part of my bench work at their reservoir engineering laboratory. I am specifically grateful to the head of department, Prof. O.D. Orodu; the head of the laboratory, Mr Daramola as well as Mr Temilola Ojo, who had to do several sleepless nights in the laboratory to ensure the experiments went smoothly.

My gratitude goes to members of staff of Centre for Petroleum, Energy Economics and Law, now Department of Mineral, Petroleum, Energy Economics and Law, for their support while working as a member of staff of the Centre.

I am grateful to my spiritual and academic friends and sisters, Nkechi Oranye, Dr Rita Onolemhemhen, Dr Olamide Mustapha, Dr Nike Oluleye, Mrs Adeola Oremule, Mrs Yewande Ayimode, Mrs Olutola Olatunji, Temilade Shodipe, Taiwo and Kehinde Shodipe, Tomiwa Shodipe, Mrs Bukola Olanisebe and the host of others whom time and space will not permit me to list. I will never forget the impact of my academic brother, Dr Akinsanoye, who appeared on the scene at the tail of this research and gave me ideas on how to improve on my write-up.

I want to appreciate my Pastors, Pastor (Dr) Ayo and Ibidun Olude for their moral and spiritual support in the course of this journey. Thank you for your constant word of encouragement, parental counsel and prayers. They are way beyond what words can convey. Your reward remains untainted.

I also want to appreciate my parents, Mr and Mrs Agbolade Oshinibosi and Mr and Mrs James Omotosho for their parental, moral and spiritual support during this research voyage. Thank you very much for your parental advice and prayers. May you witness greater celebrations of your children in life.

I want to unreservedly appreciate my brother, Ajibola Oshinibosi, for always provoking me to excellence and for sponsoring part of the research work; my sisters, Motunrayo Akinboye and Odunayo Oshinibosi for being a great source of encouragement

I greatly indebted to my Pastor and husband, Dr Oladipo Olufemi Omotosho, who has been a great pillar of financial, moral and physical support in the course of this research. I acknowledge the constant help you enthusiastically give when the need arises, especially with the children. No doubt the children are more used to you. Thank you for all the prayers, words of encouragement and for seeing that glorious future in our union ahead of the nuptial knot.

To my children, Ifeoluwa and Inioluwa Omotosho, both of you are fruits of this Ph.D. journey. It has been so exciting mothering you both. You babies are full of inspiration.

ABSTRACT

Nanofluid flooding in the petroleum industry has generated growing interest because of its potential to greatly improve oil recovery. However, studies have reported that injection of nanofluid could lead to impaired permeability due to adsorption of nanoparticles on reservoir rocks thereby incurring high costs. The use of single Nanofluid Flooding (NF) has not appreciably reduced permeability impairment. This study was therefore, designed to investigate the technical and economic viability of Nanofluid-Alternating-Brine Flooding (NABF) for enhanced oil recovery in Niger Delta reservoirs.

Eight sandstone core samples obtained from Niger Delta, were characterised for porosity and permeability using Helium-Porosimeter and Permeameter, respectively. Densities and viscosities of crude oil samples and brine (Salinity: 32.2g/L) were determined using pycnometer and viscometer, respectively. Core samples were initially saturated with brine and drained with crude oil, to determine the initial Water Saturation (SW_i). Silica nanoparticles of size: 20-70 nm, were dispersed in brine at concentrations ranging from 0.01 to 3.00 wt%. Interfacial Tensions (IFT) between oil and nanofluids were measured. Brine Flooding (BF) of core samples was conducted at 2.00 cm^3/min. The Optimum Concentration (OC) and Optimum Injection Rate (OIR) during NF were determined by injecting each nanofluid concentration at 0.50, 1.00, 2.00 and 3.00 cm^3/min. The NABF was carried out at OC and OIR. The Oil Recovery Factors (ORF) for all experiments were computed using material balance. The images of pre-flooded and post-flooded core samples were obtained using Scanning Electron Microscope. Nanoskin factors (S_n) were determined for NF and NABF and compared with the analytical model developed from Darcy's equation. The ORF obtained were upscaled for field application and evaluated for Threshold Oil Price (TOP). Risk analysis with varying ORF, Capital Expenditure (CAPEX) and Operating Expenses (OPEX) was carried out using a commercial software. Data were analysed using ANOVA at $\alpha_{0.05}$.

Porosity and liquid permeability for the samples were 17.0-30.0% and $1.1x10^{-8}$ -$1.6x10^{-8}$ cm^2 (1104.9-1584.0 md), respectively. The densities of crude oil and brine were 0.88 and 1.02 g/cm^3, while their viscosities were $3.0x10^{-4}$ $kgms^{-2}$ (3.0 cp) and $1.0x10^{-4}$ $kgms^{-2}$ (1.0

cp), respectively. The SW_i were 11.0-18.4%. The IFT were $1.9x10^{-2}$ -$2.3x10^{-2}$ N/m (18.5-23.0 dynes/cm) while the OC and OIR for NF were 2.00 wt % and 2.00 cm^3/min, respectively. The ORF for BF, NF and NABF were 68.9-73.1, 63.8-66.2 and 83.8-86.2%, respectively. The pre-flooded cores had evenly distributed grain matrices void of external particles while permeability impairment was observed for NF. Permeability impairment reversal was observed during NABF. The predictive model for S_n agreed with the experimental result. Economic analysis revealed that for unit CAPEX (N13,985.56/bbl; $34.00/bbl) and OPEX (N1,867.48/bbl; $4.54/bbl), at discount rate of 10.0%, TOP was N20,196.79/bbl ($49.10/bbl). Risk analysis on profitability showed that TOP for proved, probable and possible ORF were 33,400.81, 19,197.24 and N12,545.87/bbl (81.20, 46.67 and $30.50/bbl), respectively. The order of impact of the economic variables on profitability was ORF>CAPEX>OPEX.

Improved oil recovery in Niger Delta reservoirs was achieved using nano-alternating-brine flooding with minimal permeability impairment. The method is also profitable within the stipulated oil price regime.

Keywords: Nano-enhanced oil recovery, Nanofluid flooding, Nanofluid, Nanoskin, permeability, Threshold oil price

Word count: 498

TABLE OF CONTENTS

LIST OF FIGURES

LIST OF TABLES

LIST OF ABBREVIATIONS

BF	Brine Flooding
EOR	Enhanced Oil Recovery
IFT	Inerfacial Tension
C_N	Cost of Nanofluid
C_{nf}	Nanofliluid Concentration, wt %
k_{nf}	Nanofluid permeabilty, md
k_o	End point permeability of oil, md
k_w	End point permeability of brine, md
LHP	Lipophobic Hydrophilic Polysilion
NABF	Nanofluid-Alternating-Brine Flooding
NF	Nanofluid Flooding
ORF	Oil Recovery Factor, fraction or per cent
P_{OT}	Threshold oil Price, $/bbl
PV	Pore Volume
RPT	Relative Permeability Tester
S_{oi}	Initial Oil Saturation, fraction or per cent
S_n	Nanoskin factor
S_{or}	Residual Oil Saturation, fraction or per cent
SEM	Scanning Electron Microscopy/Microscope
S_{wi}	Initial Water Saturation, per cent
q_{inj}	Nanofluid injection rate, cm^3/min
q_o	Oil flow rate, cm^3
q_w	Water flow rate, cm^3
μ_{nf}	Nanofluid viscosity, cp
μ_o	Oil viscosity, cp
μ_w	Brine viscosity, cp
W_{np}	Weight of nanoparticle, g
MMbbl	Million Barrels

CHAPTER ONE

INTRODUCTION

1.1 Background to the Study

Majority of the conventional oil fields in the Niger Delta basin are already or almost at their peak production phase, which is a precursor to the declining production phase. The current task then becomes optimising recovery of hydrocarbon from the conventional fields and delaying their time to abandonment in a cost effective manner as well as exploiting the unconventional reservoirs. Additional reserves are usually achieved by the development of new discoveries and improvement of oil recoveries from existing reservoirs. Oil recoveries from existing reservoirs may be achieved through three major phases. The first phase is the natural recovery phase also known as the primary recovery phase. In this phase, oil recovery results from the utilisation of the natural or inherent energy within the reservoir. The mechanisms involved in this phase include rock and liquid expansion, solution gas drive, gas cap drive, gravity drainage or a combination of two or more of the aforementioned mechanisms. Only 10-15% of the original oil in place (OOIP) is recoverable because some of the hydrocarbons are normally trapped within the porous media during this phase (Carcoana, 1992). Trapping occurs as a result of capillary forces which are influenced by interfacial forces and wettability. The next phase is the secondary oil recovery phase which uses conventional methods (waterflooding and gas injection) to achieve increased recovery and recovery may be up to about 50% during this phase. The residual oil after secondary recovery which remains largely as isolated, trapped droplets (ganglia) are usually confined within the pores or films around the rock particles depending on rock wettability. Mobilisation of the residual oil after the exhaustion of the secondary energy methods then becomes the target of enhanced oil recovery (EOR) (Ahmed, 2010). Figure 1.1 depicts the phases of oil recovery in reservoirs.

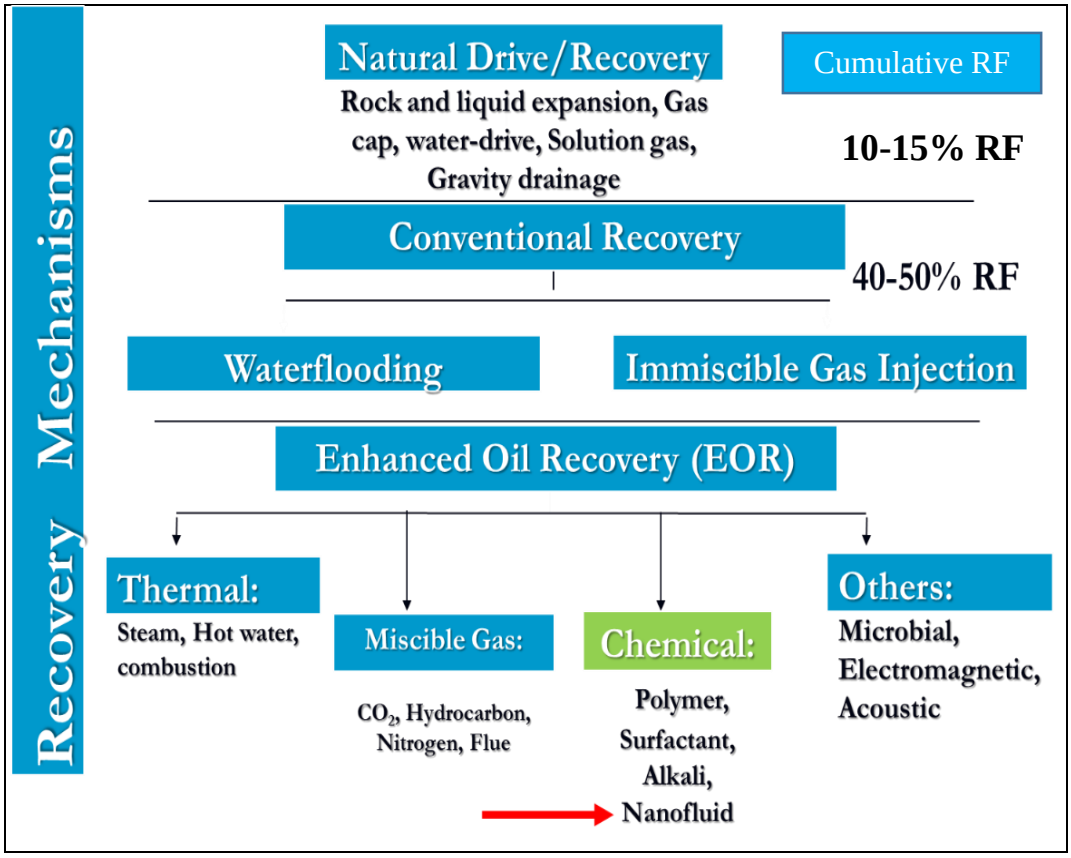

Fig. 1.1: Categorisation of oil recovery mechanisms (After Carcoana, 1992)

EOR involves the addition of supplementary energy from heat, miscible gases, chemicals or other agents, to a depleted reservoir or heavy oil reservoirs to achieve incremental oil recovery. EOR methods could be classified into thermal, miscible gas, chemical, microbial, electromagnetic, acoustic methods depending on the agents used to achieve additional oil recovery (Shafiai and Gohari, 2020). Displacement of residual oil during EOR processes may be microscopic; which is at pore scale or macroscopic at the volumetric scale.

The oil recovery phases or methods need not be applied in chronological order, especially in the case of heavy oil reservoirs where thermal injection is usually the only feasible method of recovery. As resources are becoming more expensive and risky to explore in new terrains, enhanced oil recovery techniques have increasingly become the new focal areas. EOR techniques achieve recovery by improving mobility ratio between injected and in-place fluid, hence improving sweep efficiency; and eliminating or reducing capillary and interfacial forces thus improving displacement efficiency (Latil *et al.*, 1980). Phenomena such as oil swelling, wettability modifications, emulsification of oil and oil viscosity reduction also account for these improved recoveries. The conventional EOR methods such as thermal, chemical and miscible gas methods have seen limited field applications because of certain challenges surrounding their deployments in reality. Most of these limitations centre around high costs, loss of injection fluids, unfavourable mobility ratios and environmental risks. Some of these limitations of conventional EOR methods are summarised in Figure 1.2.

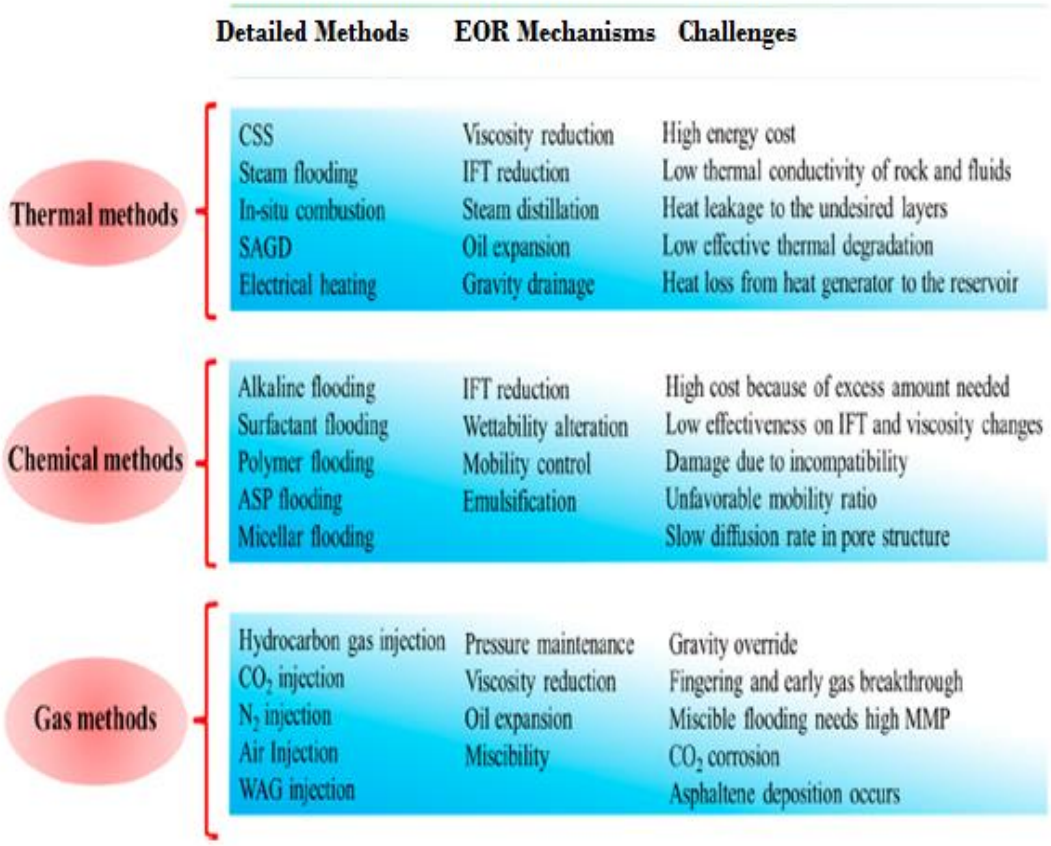

Fig. 1.2: Categories of EOR Technologies and their Challenges (Sun *et al.*, 2017).

Nanotechnology has the potential to mitigate some of the current issues in the oil and gas industry. It has the ability to change EOR methods and processes. Introduced by Feyman in 1959, nanotechnology is precisely an idea of manipulating molecules and atoms on a nanoscale (10^{-9}). The smaller these particles become, the less they are affected by gravity and then, van der Waals forces and surface tension become more prominent. Nanotechnology has been applied and has been proposed for application in many areas. Some of these areas include biomedicine, electronics, food and agriculture, manufacturing industry, to mention a few. Figure 1.3 shows some of the areas of application of nanotechnology. It has been applied to petroleum drilling and cementing operations to a reasonable extent. Nevertheless, it has yet to be widely used in oil and gas exploration and production technology.

At least one dimension of a nanoparticle is between 1 and 100 nm. Fullerenes (C_{60}), graphene, carbon nanotubes, quantum dots, polymeric metals, and metallic oxides are some examples of nanoparticles. At the nano-scale, the surface and quantum mechanics phenomena become important. As a result, nanoparticle behaviour differs significantly from that of their bulk counterparts (Kapusta *et al*., 2011).

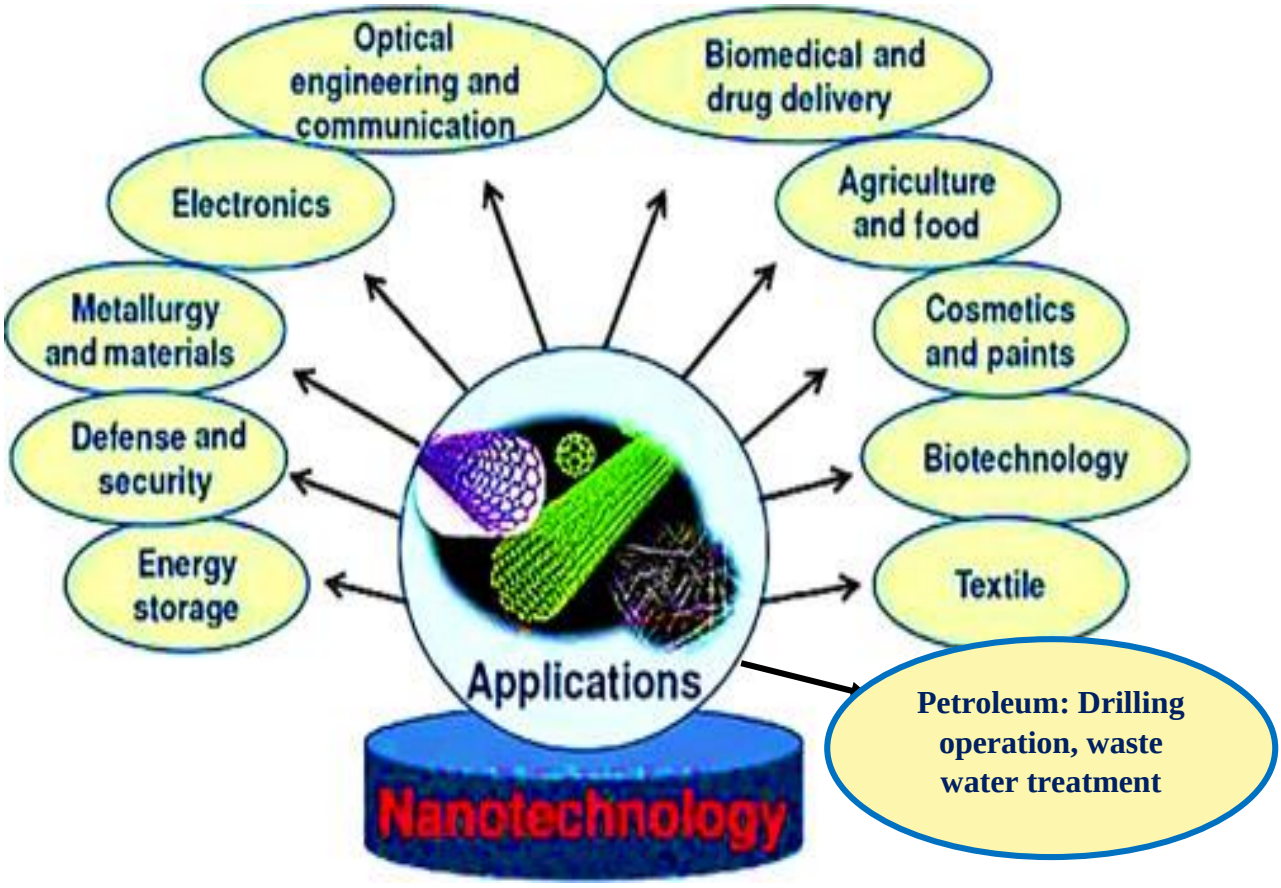

Fig. 1.3: Nanotechnology Applications in Different Areas (After Nasrollahzadeh *et. al*., 2019)

Nanoparticles have the unique and advantageous ability to alter some reservoir rock-fluid interaction properties such as wettability and fluid-fluid interaction properties such as interfacial tension (IFT). Apart from those, their small size allows them to pass through porous media with relative ease. They have the ability to allow for the release of chemicals at certain locations in the formation which can create or break emulsions. In addition, they can improve fluid properties such as viscosity. Laboratory testing shows that small concentrations (<1 wt %) of nanoparticles can raise the viscosity of water-based fluids without significantly changing their density and could offer potential improvement in the efficiency of oil recovery (Kapusta *et al*., 2011)

A dispersion where solid particles in nano-sizes are carried in suspension in a base fluid or heat-transfer fluid, usually water, brine, ethanol, oil, ethylene glycol or gas, is referred to as **nanofluid**. Recent research has demonstrated that nanoparticles distributed in fluids can mobilise trapped oil in porous formations, and that they can be combined with surfactants/polymers to improve their effects and range of mobilization (Negin *et al.*, 2016; Rostami, 2019). Pore channels in rocks are larger than nanoparticles indicating their ability to penetrate through hydrocarbon formations without much retention (Li *et al.*, 2013). Nanofluids have been offered as a low-cost, ecologically friendly alternative to surfactants and polymers, which are both expensive and possibly harmful to the environment (Dahle, 2014).

An inorganic ceramic material composed of Silica dioxide (SiO_2) or Silica is normally used as a nanoparticle in most EOR nanofluid as seen in many studies (Ju *et al*., 2006; Li *et al*., 2013; Dahle, 2014). Silica nanoparticles are commonly used because they are cheap and easily accessible. They also provide other advantages because their surface can easily be coated to alter their chemistry for more favourable application; rheological, heat and mechanical properties (surface chemistry, shape and size) can be adjusted for specific objective as well as improvement in sedimentation stability because surface forces counteract gravity (Miranda *et al*., 2012).

Other types of nanoparticles which have been investigated for EOR process include the oxides of Zinc, Aluminium, Magnesium, Tin, Zirconium, Iron and Nickel. Aluminium, Nickel and Iron oxides were concluded as effective candidates for nano-enhanced oil recovery process. This could be inferred from the improvement in thermal conductivity of the crude oil and viscosity reduction caused by breaking of Carbon-Sulphur bond by Aluminium and increase in viscosity of the carrying fluid (brine in this case) induced by Nickel and Iron; both of which resulted in favourable mobility ratio for the process. Zinc and Magnesium oxide fell into disfavour owing to the resultant permeability damage they caused in the process (Ogolo *et al.*, 2012).

Two main nanofluids characteristics make them widely different from other EOR agents. First is their large surface area to volume. In comparison to other EOR agents such as surfactants, a smaller amount of nanoparticles is required to accomplish the same impact (Almahfood and Bai, 2018). Secondly, their quantum effects can affect the optical, electric and magnetic behaviour of that material (Nanowerk, 2016). Nanofluids target improvement of microscopic displacement efficiency since it is concerned with wettability alteration and IFT reduction. It is a chemical EOR technique.

1.2 Statement of the Research Problem

Nanoparticle dispersions in injection water (nanofluids) have been shown in studies to boost oil recovery by up to 65% (Hendraningrat *et al.*, 2013a; Li *et al.*, 2013). However, in certain situations, damage to the formation has been observed, thereby incurring high formation remedial costs, with recovery limited to less than 10% (Torsater *et al.*, 2013). The damage is described by a novel concept called **nanoskin**, as shown in Figure 1.4. Nanoskin is defined as a continuous thin sheet formed as a result of accumulation of nanoparticles at the rock pore surface and pore throat, limiting oil recovery. No appreciable permeability reduction has been achieved from previous attempts of using nanofluid flooding alone, and in fact, the potential of synergism of nanofluid-alternating-water flooding for reversal of permeability impairment is yet to be investigated within the limit of all literature reviewed (Ju *et al.,* 2006, Zhang, 2014, Li *et al.,* 2013) . The nanofluid "slugs" could potentially

mobilise more oil, while the brine can desorb retained particles and prevent major porosity/permeability impairment.

Several factors affect nanofluid flooding recovery; these include concentration of nanoparticles, size of nanoparticles, salinity, temperature, wettability of nanoparticles, the rock grain size, the clay content, reservoir permeability, and injection rate. Increase in concentration has proved to improve the displacement efficiency of nanofluids because of the consequent increase in viscosity and spreading of nanoparticles on the surface. However, according to Maghzi *et al.* (2012) and El-Diasty (2015), a concentration beyond 3.0 wt % has been found to reduce ultimate recovery due to blockage of pores and throats by dispersed nanoparticles. The optimal concentration of nanoparticles for maximum recovery is the one at which the adsorption sites on the pore walls are saturated with nanoparticles. For nanoparticles concentration above the optimal concentration, the effect of permeability reduction is more than that of wettability alteration such that the overall effect is reduction in the recovery factor. With increasing concentration, the rate of nanoparticle retention on the pore surfaces and the pore spaces increases, which causes further reduction in permeability. Consequently, a reduction in the overall recovery efficiency occurs despite the wettability alteration effect, which results from the adsorption of these particles through the porous media. An appropriate combination of concentration and other factors, becomes very key to minimisation of particle retention, potentially resulting in the elimination of nanoskin, leading to improved oil recovery. Defining optimal conditions for these factors therefore becomes imperative. Apart from the combination of nanoparticle size, concentration as well as salinity, less attention has been received for other factors.

In addition, one of the major factors that make an EOR method attractive is its unit cost of implementation per barrel of recovered oil which determines the threshold crude oil price per barrel for profitable implementation. To achieve this, the impact of technical and economic factors on implementation of EOR becomes paramount. Limited emphasis has however, been placed on this in previous studies (Ju *et al*., 2006, Li *et al.*, 2013).

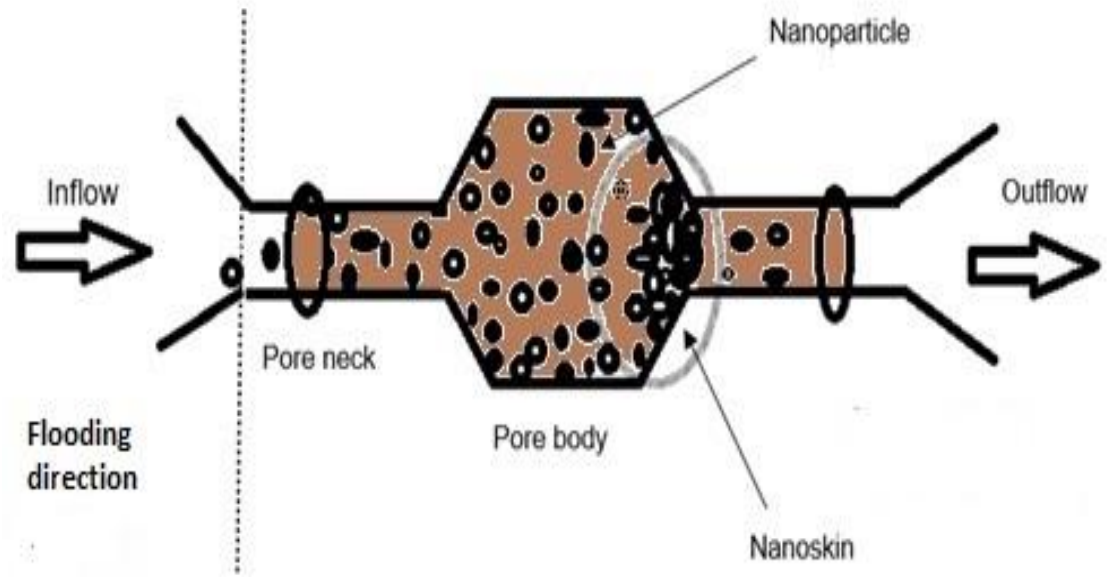

Fig. 1.4: Pictorial Representation of the Nanoskin Formation at the Pore Throat of a Reservoir Rock (Modified after El-Diasty, 2015)

1.3 Significance of the Study

Nanofluid flooding is a relatively new chemical EOR method that has proven to be more effective than other types of chemical EOR (Alkali, Polymer, Surfactant flooding), recovering an appreciable amount of oil initially in place. Investigation of nanofluid flooding in Niger Delta reservoirs is still sparsely studied, necessitating wider research for its potential enhancement of oil recovery.

Most of the reservoir rocks in the Niger Delta region are water-wet; nanoparticles have the tendency to alter the wettability to neutrally wet, reducing residual oil to critically low saturation and thus, improving recovery efficiency. At relatively predetermined high concentration, nanofluid serves as a mobility control agent and may be employed after waterflooding and later followed by same to achieve maximum recovery efficiency in EOR. This synergism of brine and nanofluid is apparently more environmentally friendly than other flooding processes requiring the use of surfactants and some other toxic chemicals, alongside nanofluid flooding. Nanofluid flooding with silica nanoparticles is relatively cheaper and easy to manage alternative compared to other chemical EOR methods.

In addition, the recent continuous plunge and general instability in global oil prices makes the design of threshold oil price for investment in nano-EOR highly imperative.

1.4 Research Aim and Objectives

The main goal of the research was to establish the technical and economic viability of nanofluid flooding (NF) alternately with brine flooding (BF) in typical Niger Delta sandstone core samples. The technical and economic viability of silica NF for enhanced oil recovery in Niger Delta has been established by Ajulibe *et al.* (2018). However, a combination of nanofluid, reservoir rock and fluid properties are responsible for improved recovery efficiency during NF. Critical to the improved recovery efficiency is the ability to prevent or minimise positive nanoskin effect, caused by high retention of nanoparticles at the rock pore throats which ultimately leads to formation damage. If reservoir rock and fluid properties are held as control and two nanofluid conditions, i.e., concentration and injection rate, are varied, possible minimisation of nanoskin effect and consequently, improved oil

recovery efficiency may be achieved. Hence, the overall objective of the study was to boost recovery efficiency using synergism of nanofluid-alternating-brine flooding (NABF) at optimal nanofluid concentration and injection rate and evaluate the economics of NABF in typical Niger Delta reservoirs

The specific objectives include:

i. To carry out preliminary characterisation of eight core samples and crude oil sample obtained from typical Niger Delta reservoir,
ii. To formulate and characterise brine solution, nanofluids of concentrations ranging from 0.01-3.00 wt % using brine as the base fluid and measure the interfacial tension (IFT) between the brine and crude oil sample, in the presence of each nanofluid concentration,
iii. To determine initial water (or brine) saturation of core samples using vacuum saturation,
iv. To perform coreflood (drainage) experiment to determine initial oil saturations of core samples,
v. To investigate oil recovery efficiencies under brine flooding (unsteady state method). This will serve as the control,
vi. To investigate and compare recovery efficiencies under NF using a range of concentrations of silica nanofluids at different injection rates,
vii. To find the best nanofluid concentration and injection rate for optimal recovery efficiency.
viii. To investigate oil recovery efficiency under NABF,
ix. To compare the Scanning Electron Microscopy (SEM) of the core samples investigated for BF, NF and NABF,
x. To develop an analytical model for estimating nanoskin factor and compare with experimental results,
xi. To perform technical evaluation of NABF flooding for a case field from upscaled experimental results and
xii. To perform economic evaluation for the estimation of deterministic oil price threshold and risked-oil price threshold for NABF implementation.

1.5 Scope of the Study

The scope of the study was on tertiary flooding with silica nanoparticles. The critical factors; namely concentration and injection rate, and mechanisms influencing recovery by flooding with silica nanofluid were studied at laboratory scale. Measurements of fluid petrophysical properties such as rock porosity and permeability, fluid viscosity and API gravity were carried out in the laboratory. Interfacial tension (IFT) tests were done for both the control fluid (brine) and nanofluid. IFT tests served as screening tests to obtain low IFT nanofluids and served as confirmatory tests for the incremental recoveries during NF and NABF. The experimental approach involved materials and specimen preparation, coreflood test. SEM analyses of the states of pore surface and pore geometry prior and post-flooding served as a basis for comparison of brine flooded, nanofluid and nanofluid-alternating-brine flooded core samples.

The economic analysis was limited to the definition of threshold oil price, which is the minimum oil price for profitable implementation of NABF. Risk analysis of uncertain technical and economic input variables *viz.*, oil recovery, capital expenditure and operating expenses were carried out to define a degree of confidence for the threshold oil price

1.6 The Study Area

The study area was the Niger Delta Agbada Formation where the sandstone core and crude oil samples were obtained. The Niger Delta is a prominent and prolific hydrocarbon producing basin in Nigeria where intensive exploration and production activities have been going on since early 1960's as a result of the discovery of commercial oil in Oloibiri-1 well in 1956. The Niger Delta Basin is situated in the West African continental margin at the apex of the Gulf of Guinea, between latitudes 30^0N West and 60^0N and longitudes 50^0E and 80^0E (Reijers *et al*., 1996). The Niger Delta is bordered on the northwest by a subsurface extension of the West African Shield, the Benin Flank. The eastern edge of the basin overlaps the Calabar Flank to the south of the Oban Masif (Murat, 1972). Well sections through the Niger Delta generally display three vertical lithostratigraphic subdivisions: an upper delta top facies; a middle delta front lithofacies; and a lower pro-delta lithofacies (Reijers *et al.,* 1996). These lithostratigraphic units correspond respectively with the **Benin**

Formation (Oligocene-Recent), **Agbada** Formation (Eocene-Recent) and **Akata** Formation (Paleocene-Recent) according to Short and Stauble (1967). The Akata Formation is the primary source rock and is composed mainly of marine shales, with sandy and silty beds which are thought to have been laid down as turbidites and continental slope channel fills. It is estimated that the formation is up to 7,000 metres thick (Doust and Omatsola, 1990).

The Agbada Formation is the major petroleum-bearing unit in the Niger Delta. The formation consists mostly of shore face and channel sands with minor shales in the upper part, and alternation of sands and shales in equal proportion in the lower part. The interbedded marine shale of the lowermost Agbada Formation is possibly a contributor to the primary source rock of the Niger Delta. The thickness of the formation is over 3,700 metres. The Niger Delta contains one petroleum system referred to as the tertiary Niger Delta (Agbada-Akata) Petroleum System (Ekweozor and Daukoru, 1994; Kulke, 1995).

The Benin Formation is made up of continental sands and gravels and is about 280 meters thick, but can be up to 2,100 metres thick in the area of maximum subsidence (Whiteman, 1982). The Delta is divided into structural and stratigraphic belts called depobelts by major growth-fault trends that prograde from northwest to southeast. Hydrocarbons can be found in all of the Niger Delta's depobelts, in high-quality sandstone reservoirs that are part of the major deltaic sequence (also known as the 'paralic sequence'). Each of these depobelts has a deltaic sequence that is distinct in age and characterizes consecutive phases in the delta's history. The majority of the bigger accumulations occur in roll-over anticlines in the hanging-walls of growth faults, where they might be trapped in dip or thrust.

The area contains as much as 34.5 billion barrels ($5.5x10^9$ m^3) of recoverable oil and 94 trillion cubic feet ($2.7x10^9$ m^3) of proved natural gas reserves and up to 600 trillion cubic feet of possible reserves (1.7×10^{13} m^3) of associated and unassociated gas since more than 60 years of discovery. The oil and gas fields contain thousands of individual reservoirs, most of which are sandstone pockets trapped within oil-rich shale strata. The Niger Delta region has as many as 574 fields discovered (481 oil and 93 natural gas fields). The Success rate of hitting oil in the past has been as high as 45% (Akintola *et al.*, 2015). Most fields are small, ranging up to 315 Million barrels (50×10^6 m^3), though several larger fields have

recoverable reserves in excess of 503 Million barrels (80×10^6 m^3). The hydrocarbons are found in multiple pay sands with relatively short columns, and adjacent fault blocks usually have isolated accumulations (Doust, 1990). Figure 1.5 reveals the regional stratigraphy of the Niger Delta cutting across several formations.

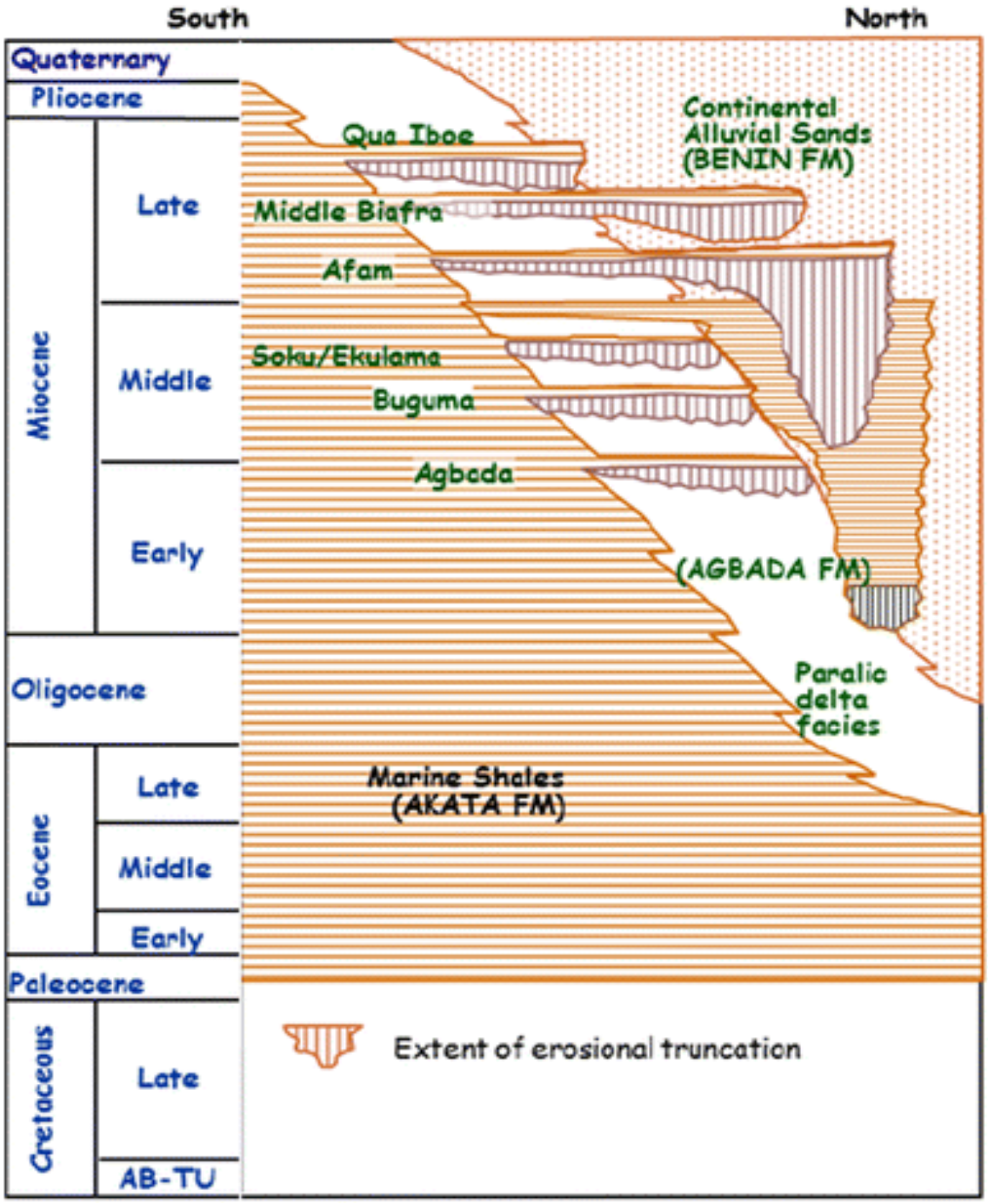

Fig. 1.5: Regional stratigraphy of the Niger Delta showing different formations (After Ozumba, 2013.

The Agbada Formation comprises principally sandstones and unconsolidated sands from which most petroleum in the Niger Delta is produced. The depositional environment and depth of compaction constitute the predominant factors that formed the characteristics of the Agbada Formation. The reservoirs range in thickness from less than 15 meters to more than 45 meters in thickness (Evamy *et al*., 1978) and are Eocene to Pliocene in age. The thicker reservoirs are most likely layered channel composite bodies (Doust and Omatsola, 1990). The principal Niger Delta reservoirs, according to Edwards and Santogrossi (1990), are Miocene paralic sandstones with 40 percent porosity, 2 darcys permeability, and a thickness of 100 meters. Growth faults in the down-thrown block, where reservoir thickness is greatest, are the most powerful controlling factor for lateral variation in reservoir thickness (Weber and Daukoru, 1975). The reservoir sandstone has a wide range of grain sizes, with fluvial sandstones being coarser than their delta front counterparts; point bars fine upward, while barrier bars have the best grain sorting. Much of this sandstone is nearly unconsolidated, with some argillo-silicic cement as a minor component (Kulke, 1995). Because of the young age of the sediment and the coolness of the delta complex, porosity decreases with depth.

Niger Delta fields are composed of mainly structural traps although few stratigraphic traps have been discovered. The development of the structural traps is associated with synsedimentary deformation of the Agbami paralic sequence (Evamy *et al*., 1978). These traps stretch form the north (older depobelts) to south (younger depobelts); a reflection of progressive instability of the shale under compaction and over pressure. Multiple growth faults, antithetic faults and collapsed crest structures including simple rollover structures and clay filled channels, constitute some of the structural trapping elements (Doust and Omatsola, 1990) in the province. On the flanks of the delta, stratigraphic traps are likely as important as structural traps (Beka and Oti, 1995). In this region, pockets of sandstone occur between diapiric structures. Towards the delta toe (base of distal slope), this alternating sequence of sandstone and shale gradually grades to essentially sandstone.

The primary seal rock in the Niger Delta is the interbedded shale within the Agbada Formation. The shale provides three types of seals—clay smears along faults, interbedded sealing units against which reservoir sands are juxtaposed due to faulting, and vertical seals

on the flanks of the delta, major erosional events of early to middle Miocene age formed canyons that are now clay-filled (Figure 1.5). These clays form the top seals for some important offshore fields (Doust and Omatsola, 1990).

For the purpose of the research, a field in an onshore mature lease located in the northern Niger Delta was used as a case study. Oil and gas were first discovered in the lease in 1967 and production came on stream in 1972. The licence covers an area of approximately 358 km² (88,464 acres). It comprises seven producing fields and two single well discoveries that had been produced in the past but are currently shut-in. The total number of production and injection wells in the lease are 94 of which 24 are currently producing. The case study field has 12 wells with 6 currently producing. It is also currently being waterflooded to maintain pressure. The produced water-oil-ratio (WOR) is relatively high, having reached 5 stb/stb.

For the case study field, we assumed a direct line drive pattern; i.e. one injection well to one producer. Current oil production rate is 5,000 bbls per day with about 50% original oil in-place (OOIP) estimated to be unrecoverable after waterflooding. Primary recovery factor before waterflooding was 30%. Estimated additional recovery factor from waterflooding was 20%. Average reservoir thickness was about 23 metres and well spacing was 121, 406 sq. metres (30 acres).

CHAPTER TWO

LITERATURE REVIEW

Manipulating a matter on an atomic or a molecular scale is referred to as Nanotechnology. It is defined as the construction of functional materials, device and systems by controlling matter at the nano-scale level (one-billionth meter), and the exploitation of their novel properties and phenomena that emerge at that scale. Reportedly, one nanometer-scale polysilicon material could change the wettability of porous surfaces of sandstone and consequently affect the flow of water and oil when injecting the suspension of the nanoparticles in an oil reservoir (Ju and Dai, 2002).

2.1 Nanotechnology as a Possible EOR Technique

By producing better materials, nanoparticles have been applied to upstream petroleum operations. They have been utilised as tracers, and nanoparticle dispersions have been used to treat asphaltene, scale, and paraffin deposition issues. The development of new forms of smart fluids is another growing application of nanotechnology in the petroleum business. Surfactants/polymers, microemulsions, colloidal dispersion gels, and other nano-formulas utilised in drilling, oil recovery, and other applications are among these innovative nano-formulas (Dahle, 2014).

Cocuza *et al*. (2011) provided an overview of nanotechnology applications and critically highlighted the potential benefits that can come from transposing the same or adapted solutions to the oil industry. For enhanced or improved oil recovery purpose, the new-generation nano-agents should both affect the properties of the injected fluid, in terms of viscosity, density, thermal conductivity and specific heat, and modify the fluid-rock interaction properties, for example in terms of wettability. These nano-agents, according to reports, include two different types of polysilicon nanoparticles in oil fields to improve oil

recovery and enhance water injection. These are Lipophobic Hydrophilic Polysilicon (LHP) and Hydrophobic Lipophilic Polysilicon (HLP) nanoparticles. Two approaches exist for building nanoparticles, these are the top-down and the bottom-up approaches. The top-down approach is also referred to as miniaturized technology that are employed in integrated circuits, sensors, telecommunications, environmental monitoring or bio-oriented diagnostics. Nevertheless, the true nano-revolution relies on the full exploitation of the bottom-up approach, i.e. the creation of smart materials by exploiting their self-organisational capacity. It can be seen as the attempt to emulate nature in its intrinsic ability to build up and organise itself into complex structures starting from elementary atoms and molecules.

Greff and Babadagli (2011) reported that Nickel improved the recovery of the steam stimulation process by 10%. Nanoparticles are distinguished by nearly 100 times larger specific surface area than microparticles. The sample experimented contained 0.5 wt % of the particles. The Nano-sized particles showed higher viscosity reduction than micron-sized particles. The larger specific area of nanoparticles resulted in more reactivity compared to the microparticles owing to more contact area with the oil phase of the former compared to the latter. The first pilot field tests using nano-sized particles as catalyst were in Liaohe oil fields, northeastern China (Li *et al.*, 2007).

In addition, extraordinary materials such as nano-scale sensors are likely inventions that can enhance oil recovery under harsh conditions, like deep water and areas with low temperature and salinity (Zhang, 2014).

2.2 Principles of Nano-enhanced Oil Recovery

According to Enslayed and Fattah (2014), the applications of Nanotechnology in EOR can be summarised in three approaches; **Nanocatalysts, Nanoemulsions and Nanofluids**. Nanocatalysts are defined as metallic nanoparticles injected into heavy oil reservoir for the purpose of breaking carbon sulphur bond in the asphaltenes (present in the heavy oil). The nanocatalysts are injected along with steam and the resultant breaking of C-S bonds in the heavy oil increases the proportion of saturates and aromatics. This chemical reaction,

referred to as aquathermolysis, leads to irreversible viscosity reduction in the heavy oil. Nickel and iron are catalysts and have proven to catalyse such reactions.

Nanoemulsion is a kind of pickering emulsion that is stabilized by nanoparticles instead of surfactant and is more stable under harsh condition of temperature and salinity. The large viscosity of nano-stabilised emulsions can help to manage mobility ratio during flooding which provides a viable method to push highly viscous oil from the subsurface, rather than polymers that are relatively large and have high retention on reservoir rock. The nanoparticle-stabilised emulsion droplets are tiny enough to allow to pass through most pores, and flow freely through the reservoir. Due to irreversible adsorption on their droplet surfaces, they also remain stable in harsh circumstances in reservoirs.

2.3 Displacement Mechanisms of Nanofluid Flooding

2.3.1 Structural Disjoining Pressure

Experimental investigations of the recovery mechanisms in EOR application of nanofluids have been carried out by several authors (Wasan and Nikolov, 2003; Chengara *et al*., 2004; Wasan *et al.*, 2011). The recovery mechanism was referred to as structural displacement mechanism and authors have attributed the mechanism to Brownian motion and electrostatic repulsion between nanoparticles. The electrostatic force of repulsion increases with the concentration of nanoparticles but decreases with particle size.

The authors revealed that nanoparticles present in the three phase region between oil, water and rock tend to force themselves between the discontinuous phase and the solid rock surface. They create a wedge-like structure which separates the formation fluid (oil) from the pore wall and enhances the spreading behaviour of nanofluid (Fig. 2.1).

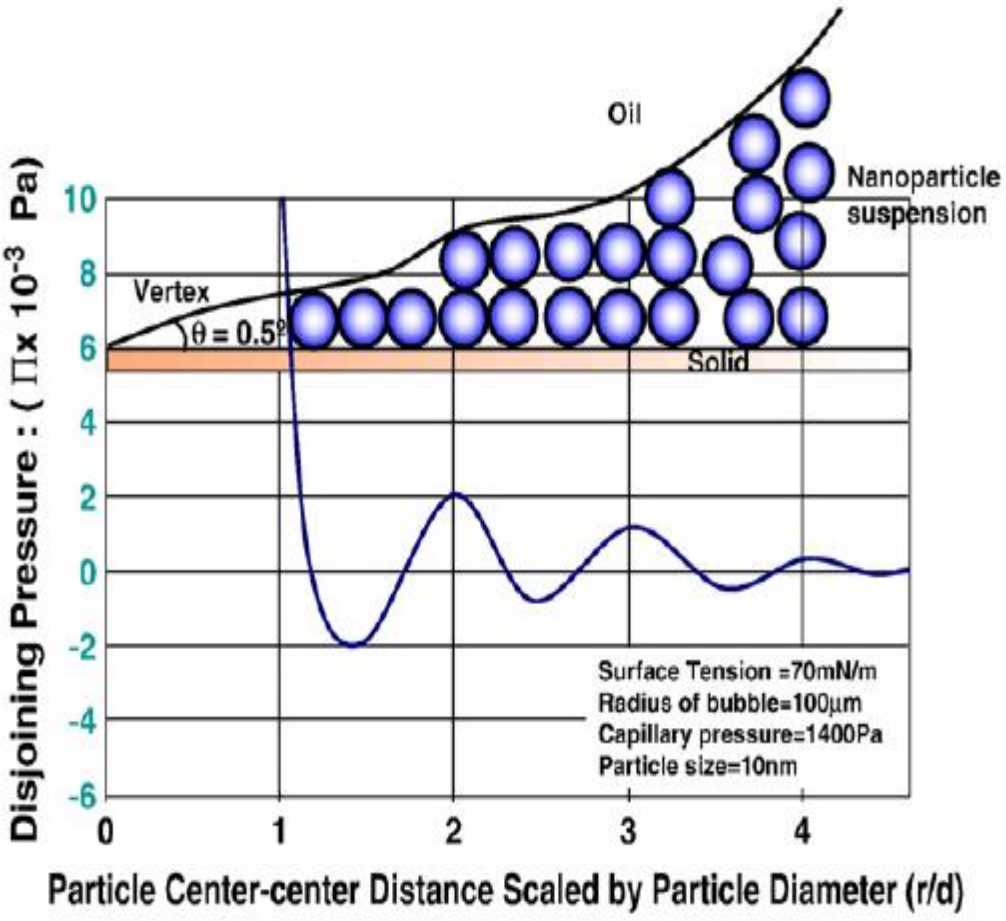

Fig. 2.1: Disjoining Pressure in the Wedge Structure (Wasan and Nikolov, 2003)

The displacement efficiency of nanofluids increased with decrease in particle sizes. The smaller the particle sizes, the higher the charge density, the greater the electrostatic force of repulsion and the stronger the structural disjoining pressure. The mechanism of displacement of nanoparticle in particle dispersion (NPD) may be explained by the principle of structural disjoining pressure. A film of wedge-shape assemblage, which separates the discontinuous phase(s) (oil, gas, water or paraffin) from the surface of the formation, is normally formed. This results in the additional recovery than would be possible with conventional additives or fluids (McElfresh, 2012).

Hendraningrat *et al*. (2013b), in their work, studied the parameters involved in structural disjoining pressure mechanism such as lowering of interfacial tension (IFT) and alteration of wettability. Water-wet Berea core plugs with permeability in the range 9-400 mD were investigated in laboratory coreflood experiments using different nanofluid concentrations. Nanofluid concentrations of 0.01, 0.05 and 0.1 wt% were synthesised with synthetic brine. It was observed that IFT decreased as nanofluid concentration increased indicating a potential for EOR. Another challenge that was discovered is the impairment of porosity and permeability as nanofluid concentration increased.

El-Diasty (2015) also carried out an experiment to investigate the effects of nanoparticle size and concentration on oil recovery in Bahariya formation in Egypt. Different silica nanoparticle sizes of 5, 20, 40 and 60 nm and concentrations 0.01-3.00 wt% were investigated. A size of 20 nm for silica nanoparticles and concentration of 3.0 wt% were considered optimum for injection rate of 2 cc/min. The nanofluid (20 nm - 3.00 wt%) flooding recovered 65% of the Initial-Oil-In-Place (IOIP) at breakthrough compared to that of water flooding which yielded 36% of IOIP at breakthrough

2.3.2 Displacement by Interfacial Tension Reduction and Wettability Alteration

After waterflooding, almost all the remaining oil is immobile. The discontinuous residual oil which is the target of the nanofluid exists in the form of small spherical globules behind pore throats and cannot pass through them (Anderson, 1987). Oil recovery by nanofluid results from two main mechanisms. These include IFT reduction and Wettability alteration.

The alteration to wettability can be from water wet to oil wet depending on the nature and type of the nanoparticles.

1. Effect of Nanofluid on Interfacial Tension

At the oil and water interface, the force acting tangentially to the interface is referred to as interfacial tension. Reduction of interfacial tension decreased the work of deformation needed for oil droplets to move through the pore throat. Therefore, the trapped oil packets are mobilised and can pass through the pore throat easily. In addition, capillary pressure acts as a barrier in pore throat for the displacement of mobilized oil from one pore to another (Fig. 2.2) (Roustaei *et al*., 2012).

Nanoparticles are known to structure themselves at the oil/brine interface, thereby reducing the contact between the two phases. This results in the lowering of the IFT. The IFT reduces as the concentration of the nanofluid increases (Li *et al*., 2013a; Dahle, 2014).

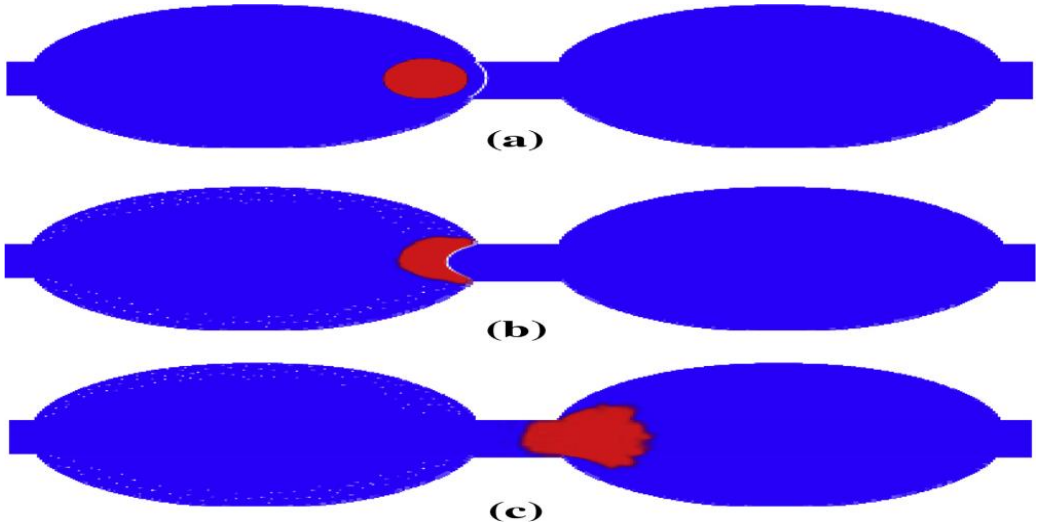

Fig. 2.2: Role of nanoparticles in wettability alteration and consequently direction of capillary curvature in the pore throat before (a) and after surface modification with nanoparticles (b and c) (Source: Roustaei *et al.*, 2012).

2. Effect of Nanofluid on Wettability

Wettability is the tendency of a fluid to spread on to a solid surface in the presence of another immiscible fluid. The preferential spreading occurs as a result of the individual fluid differential adhesion to the solid surface and the interfacial tension. A surface may be oil wet or water wet; a contact angle is formed due to force balance between the spreading coefficient of the solid surface in equilibrium contact between oil and water (Agi *et al*., 2018).

Ju *et al.* (2002) investigated the mechanism of oil recovery in Lipophilic Hydrophilic Polysilicon (LHP) nanoparticles for changing the wettability of porous media theoretically. To quantitatively anticipate changes in relative and effective permeability of the oil and water phases, as well as oil recovery in sandstone after waterflooding, a one-dimensional two-phase mathematical model was presented, and a simulator was created. The distribution of particle concentration, the reduction in porosity and liquid permeability, the LHP volume retention on pore walls and pore throats across a dimensionless distance, and oil production performance were all studied using numerical models. They recommended LHP concentration in the range of 0.02-0.03%wt to enhance oil recovery; any further increase in concentration will lead to formation damage due to reduction of permeability. In addition, they concluded that oil recovery can be obviously improved by flooding with LHP.

Wettability alteration by silica nanoparticles in glass micro models had been established using experimental and numerical approaches (Rostami *et al*., 2019). Initially water-wet and imposed oil-wet micromodels were investigated.-and flooded with nanofluids. Comparisons of experimental flooding scenarios and numerical simulation results were done for the two differently saturated glass micromodels. The result of the two agreed and

3. Effect of Nanofluid on Mobility

Jikish (2012) conducted a research on the use of nanoparticles as stabilising agents for CO_2 flooding. Nanoparticle-stabilised foams could be a novel way to create superior CO_2 EOR mobility control agents. Surfactant-produced foams may disintegrate in tough reservoirs due to adsorption on reservoir rock and high temperature, therefore aqueous nanoparticle

dispersions may be a viable option. Commercial fumed nanosilica can be purchased at very low cost, at less than USD 4/lbm. The costs can be reduced further by use of other nanoparticles (e.g., nanoclays or fly ash). Proof-of-concept tests in real porous media have shown that it is possible to propagate these dispersions through a porous medium without the adsorption or trapping of nanoparticles in pores. The results are promising at laboratory scale. More tests are needed to show the ability of nanofoam to improve conformance for better volumetric sweep efficiency. Although this technology is still in its early development, some operators have expressed interest in limited field testing.

2.4 Synergy of EOR Methods for Oil Recovery Optimisation

One of the ways to overcome the limitations of EOR processes, which have been investigated, is synergising two or more EOR methods to leverage on the advantages of individual methods and also nullify their individual shortcomings.

For example, Orodu *et al.* (2019) investigated the enhanced oil recovery potential of nanocomposites formed from the combination of Al_2O_3 nanoparticles and uncommon biopolymers. These investigation were based on rheology and stability of the biolymer. Niger Delta region and Berea sandstone core plug samples were used. The incremental oil recovery after waterflooding (secondary recovery) was 5–12% and 5–7% for potato starch nanocomposite (PSPNP) and gum Arabic nanocomposite (GCNP) respestively.

Akanji *et al*. (2019) examined the applicability of the synergy of alkaline-surfactant-polymer-flooding in comparison with surfactant-polymer flooding for EOR in Angolan field. Poly (vinyl) alcohol was used as the polymer agent while rhamnolipid and Sodium hydroxide (NaOH) were used as the surface-active agent (surfactant) and alkaline medium respectively. The alkaline-surfactant-polymer combination presented more reduction in surface tension and Interfacial tension (IFT). Another investigation was carried out by Udoh *et al.* (2018) to assess the prospect of combining environmentally friendly bio-surfactants with controlled salinity water injection. The bio-surfactants used were rhamnolipid and protein enzyme. Combined controlled salinity water injection with protein enzyme indicated reduction in IFT from 3.4-2.50 mN/m, while with rhamnolipid, IFT increased from 0.11-0.34 mN/m.

2.5 Transport of Fluids in Porous Media

Darcy's law governs the flow of fluid in porous media. Hence, for incompressible Newtonian flows, the continuity equations of oil (o) and water (w) phases are given by:

$$\frac{\partial}{\partial t}(\Phi S_l) - \frac{\partial}{\partial t}\left(\frac{K_l}{\mu_l}\frac{\partial P_l}{\partial x}\right) = 0, \quad f = o, w \tag{2.1}$$

With initial and boundary conditions at S_f=S_{f0} and P_f=P_{f0} at t=0;

$\frac{K_w}{\mu_w}\frac{\partial P_w}{\partial x} = q \ at$ x=0,

$\frac{K_w}{\mu_w}\frac{\partial P_w}{\partial x} + \frac{K_o}{\mu_o}\frac{\partial P_o}{\partial x} = q \ \ at \ x = L,$

where *x* is the distance from the inlet of the core or porous medium, *t* is time, Φ is the porosity, P_f, S_f, and μ_f are pressure, saturation and viscosity of phase f, respectively, and effective permeability of phase f is k_f=k_r/*k.*

Capillary force is given by equation (2.2) (Donaldson *et al.,* 1991):

$$P_c = P_o - P_w = (a + bS_w) / (1+cS_w) \tag{2.2}$$

where *Sw* is water saturation and where constants *a, b* and *c* are empirical parameters.

2.5.1 Transport of Nanofluids in Porous Media

The interaction between nanoparticles and pore walls is caused by five different types of energy. Attractive potential energy of London-van der Waals repulsion, energy of electric double layers, Born repulsion, acid-base interaction, and hydrodynamic energy are some of these. The attraction force between nanoparticles and porous walls is stronger than the repulsive force when the total energy is negative, resulting in more nanoparticle adsorption Khilar and Fogler (1999). Desorption of nanoparticles from porous walls will occur otherwise. The total energy between particles and porous walls controls the dynamic equilibrium between adsorption and desorption. Blocking occurs when the diameter of LHP

particles exceeds the pore throat size, or when several LHP particles smaller than the pore throat size clump together to clog the pore throat. Ju *et al*. (2006) based the model for simulating the transport of nanofluids (Lipophobic and hydrophilic polysilicon (LHP)) in porous media on the assumptions below:

i. Under isothermal conditions, flow is one-dimensional, and the rock and fluids are assumed to be incompressible;

ii. Aqueous LHP solution is homogeneous;

iii. Flow of oil and water in porous media follows Darcy's law, and gravity force is ignored;

iv. LHP particles are discretized into n size intervals;

v. Fluid viscosity and density are constant, and both oil and water are Newtonian

vi. Chemical reactions are not taken into account

LHP can only exist in water (hydrophilic). Because the nanoparticles' diameters range from 10 to 500 nm, Brownian diffusion effects should be taken into account. As a result, the continuity equation for the nanoparticle size interval i in phase *f* can be written as

$$u_w \frac{\partial C_i}{\partial x} + \Phi S_w \frac{\partial C_i}{\partial t} - \frac{\partial}{\partial t}\left(\Phi S_w D_i \frac{\partial C_i}{\partial x}\right) + R_i = 0 \qquad (2.3)$$

$C_i=0$, at t=0

$C_i=C_{i,\,in}$ at x=0, at initial conditions

where C_i is the volume concentration of LHP particles in interval *i* in the water phase, D_i is the dispersion coefficient of LHP particles in size interval *i* in the water phase, R_i is the net losing rate of LHP particles in interval *i* in the water phase, and $C_{i,in}$ is the concentration of LHP particles in interval *i* in the injected fluids.

2.6 Preparation of Nanofluids

In the preparation of nanofluid, stability of the suspension is an important consideration to achieve a considerable efficiency both at the microscopic and macroscopic levels. Several methods are employed to enhance the stability (Devendiran and Amirtham, 2016). Some of them include:

1. pH Value Alteration**:** The pH value at which a particle carries zero charge electric charge or where minimal forces of hydration are observed is known as the isoelectric point (IEP). When IEP gets close to the pH of nanofluids, instability occurs. The Zeta Potential is zero at the IEP, and the repulsive forces between NPs in suspension are low, with a propensity to consolidate at the suspension's base. Russel *et al.*, 1992). Therefore, a high hydration force is requisite for the enhancement of stability (Wen and Ding, 2005).
2. Using surfactants: Surfactants can act as a link between NPs and base fluids, allowing for continuity between the two. Hydrophilic NPs, such as oxide NPs, will disperse readily in polar base fluids such as water. When hydrophobic NPs must be dispersed in polar base fluids and hydrophilic NPs must be dispersed in non-polar base fluids, surfactants must be added to stabilize the nanofluids. The inclusion of surfactant has an effect on the thermophysical properties of nanofluids, which should be noted (Yu *et al.*, 2012).
3. Using ultrasonic vibration: Ultrasonication baths or probe-based ultrasonic devices are often employed to disperse NP aggregates. Ultrasonic devices with probes operate at a very high frequency. As a result of the separation of extremely small metal particles from the surface of the metal probe, there is a risk of contamination of nanofluids. This could have a negative impact on nanofluid stability (Ruan and Jacobi, 2012).

2.7 Retention of Nanoparticles in Porous Media

Continuous deposition of nanoparticles on pore surfaces and pore throats cause particle retention (Ju *et al.,* 2006). Under the influence of colloidal and hydrodynamic forces, resorbed particles could be desorbed. However, there is a possibility of re-adsorption on different pore body sites or pore throat trapping.

By modifying the Liu and Civan's model (1993), *Ri* in Eq. (2.3) is given by

$$R_i = \frac{\partial (V_i + V_i^*)}{\partial t} \tag{2.4}$$

where V_i is the volume of LHP particles i in contact with the water phase available on the pore surfaces per unit bulk volume of sandstone, $V_i^*$is the volume of LHP particles i entrapped in pore throats from water phase per unit bulk volume of sandstone due to plugging and bridging.

2.8 Economic Evaluation of EOR Processes

The field applicability of any EOR process will depend greatly upon its economic implication. Oil price and costs of implementation of an EOR technique are key factors that drive its application. During the regime of high oil prices, many EOR techniques usually come on stream. In the period of low prices, careful scrutiny of the process and economic analysis is imperative.

Conventional economic evaluation involves the use of net present value (NPV), internal rate of return (IRR), unit technical cost (UTC) and profitability index (PI). Sometimes, the pay-back period could also serve as a useful economic decision tool. However, the above approaches are usually applied deterministically and thus, do not account for uncertainties that come with using single-point estimates of inputs into the economic model. Some authors have pointed out the shortcomings with deterministic approach some of which include inability to incorporate managerial flexibilities, uncertainties emerging from price and cost volatilities, assumption of irreversibility of the decision.

Apart from economic uncertainties, technical uncertainties may pose a great challenge in the implementation of an EOR process. Alkhatib and King (2011), for instance, pointed out that challenges arise due to uncertainty in field application e.g. reservoir heterogeneity, surfactant absorption, etc. for wide scale implementation of surfactant EOR. They emphasised that managing these uncertainties is essential for optimal implementation policy. Surfactant flooding has been proposed as a feasible way of evaluation and decision making using real options theory. The Real options technique was based on the Least Squares Monte Carlo (LSM) algorithm. Scenarios based on a synthetic reservoir model were used to test the algorithm.

Finding the best timing to start the surfactant flood was one of the options considered. The reservoir's expected life was ten years. The start of years 4, 5, 6, and 7 were chosen as the decision nodes. The Schlumberger ECLIPSE was used as the numerical simulator for the surfactant flood, and a MATLAB code was used to conduct the various simulations and the LSM algorithm. The variables which include residual oil after chemical flood (S_{orc}) and surfactant adsorption (Ds), were assumed to be the state variables at different time and then at the same time. The ideal surfactant flood beginning times were discovered to be at year 6. In comparison to the no-option scenario of starting the flood at the beginning of the reservoir life (year 0), the optimal injection policies recommended achieved, on average, an increase in recovery efficiencies of 0.123, 0.147 and 0.141 for Cases 1, 2 and 3 respectively in contrast to the no-option scenario of initiating the surfactant flood at the start of the reservoir life (year 0). These values represent the value of the flexibility in initiating surfactant flooding. This method is being considered for more complex and realistic situations.

Fathi and Ramirez (1983) have previously looked into the best injection policies for surfactant flooding. The goal of the optimization was to optimize the amount of oil recovered while lowering the cost (or amount) of chemicals utilized. To solve this dynamic computational problem, a steepest-descent gradient method was employed as the computational methodology. The algorithm's performance was tested for surfactant injection in a one-dimensional flooding situation. Two types of interfacial tension (1FT) behavior were considered. These are Type A system where the 1FT is a monotonically

decreasing function with solute concentration and Type B system where a minimum 1FT occurs at a nominal surfactant concentration. For Type A system, the shape of the optimal injection strategy was not unique; however, there was a unique optimum for the amount of surfactant needed. For Type B system, the shape of the optimal injection as well as the ·amount injected) was unique.

Joshi *et al.* (1998) applied Monte Carlo Simulation to the Wilmington steamflood project to quantify the risk and uncertainties associated with the project. For the determination of production rates and economic analysis, Monte Carlo Simulation was used. Production calculations accompanied economic analysis were done based on statistical models, serving as a sensitive method confirming the convergence of the Monte Carlo Simulation. Stochastic assumption were made for the main inputs, such as porosity, net pay and oil saturations and distributions that followed the assumption included triangular, normal and triangular ($10^{th}/90^{th}$) distribution. Probabilistic Net Cash Flow (NCF), Net present Value (NPV) and Internal Rate of Return (IRR) were presented as the simulation outputs in form of probability density curves, probability density curves, cumulative probability density curves, tornado diagrams, etc.

Zhong *et al.* (2013) used Black and Scholes model and Differential Equation to evaluate the value of a polymer injection project in the North oil fields of China. They pointed out the sources of uncertainty in the application of EOR techniques which include external risks, .i.e., from the macroeconomic environment, global oil market, financial market, competitors, government policy, natural disasters, and internal risks which may originate from employee's skills, change in management, occasional events. Technical risks arise from reserve estimates and estimated production data. The uncertainties were captured by parameters which were incorporated in the Differential equation. The input to their model had some assumptions. The assumptions include Geometric Brownian Motion of oil price, no risk-free arbitrage opportunity, no transaction costs, taxes, etc. an option value, V above the value obtained from the traditional NPV was obtained from their models.

Ajulibe *et al.* (2018) investigated the viability of silica nanofluid for EOR application in Niger Delta with focus on the economics. Using a comparative economic approach, the

evaluation of the economic feasibility of Alkali-Surfactant-Polymer (ASP), Water-Alternating Gas (WAG) and Silica nanofluid EOR projects were investigated using discounted cash flow method. The NPVs for ASP, WAG and Silica naofluid were $15.45M, $25.30M and $57.88M, respectively. The IRR for all the EOR options were all above the hurdle rate 15.0% that was used. Hence, all three projects were profitable, however, silica nanofluid options was the most potentially profitable.

CHAPTER THREE

METHODOLOGY

3.1 Materials

The materials used for the study were eight representative sandstone core samples (labelled Y1, Y2, Y3, Y4, Y5, Y6, Y7 and Y8) and crude oil obtained from Agbada Formation in the Niger Delta region; silica nanoparticles and reconstituted brine. The equipment included digital weighing balance, vernier caliper, porosimeter, permeameter, soxhlet extraction apparatus, scanning electron microscopy (SEM) apparatus, viscosimeter, pycnometer, vacuum saturator and relative permeability tester (core-flood set-up)

3.2 Preliminary Experimental Set Up

The experimental set up could be broadly categorised into two; namely preliminary experimental set up and main experimental set up. The preliminary set up involved preparation, formulation and characterisation of materials, measurement of interfacial tension (IFT) as well as vacuum saturation of core samples, while the main set up involved the coreflood set up. The coreflood set up could further be categorised into four parts which include drainage (also referred to as oil flooding) and BF, NF and NABF. The BF was the control while NF and NABF were the experimented methods.

3.2.1 Preparation of Core Samples

The core samples were cleaned using soxhlet extraction, which is the most popular procedure for cleaning core samples, as shown in Figure 3.1. Methanol was heated to the boiling point of 65-70^{o}C during soxhlet extraction. The vapour rose through the core and into the condenser, where it was condensed by cool flowing water. The re-condensed methanol dripped into the thimble's core sample, cleaning it of any water or other contaminants. The condensed liquid was mechanically discharged into the boiling flask

when it reached the top of the tube. After cleaning, the samples were dried in 70^{o}C oven for 6 hours and then cooled for another 6 hours.

Fig. 3.1: Soxhlet Extraction Apparatus

3.2.2 Characterisation of Core Samples

i. Weight, Volume and Density Measurements

The dry weight, W_c, of each core sample was measured using a digital weighing balance while the diameter, d_c and length, l_c were measured using a vernier caliper. The bulk volume, V_b and bulk density, ρ_c of each core sample were calculated using equations (3.1) and (3.2) respectively.

$$V_b = \pi \frac{d_c^4}{4} \tag{3.1}$$

$$\rho_c = \frac{W_c}{V_b} \tag{3.2}$$

ii. Porosity Measurement

The porosity measurements of the core samples were done using the Helium Ultrapore Porosimeter and liquid saturation method. The Helium porosimeter measures porosity of a dry core sample. In a closed cell, it uses the principle of gas expansion. The core sample was placed in the Helium Ultrapore Porosimeter and helium gas in a reference cell expanded into a sample cell, at constant temperature. Using Boyle's law, the helium porosimeter determines the volume of the sample chamber, as shown in equation (3.3).

$$V_c = \frac{(P - P_r)V_r}{P_c - P} \tag{3.3}$$

Where the initial pressure in the reference cell and sample chamber are P_r and P_c respectively, and the equilibrium pressure once the valve is opened, is P. The difference in the volume of the empty reference cell V_r and the chamber of core sample V_c, is the grain volume V_g. The grain density, ρ_g, is also computed from the ratio of weight and grain volume of the core sample. The scale on Helium porosimeter is graduated in volumes and

so, volumes are directly read from it, and effective porosity may be determined as ratio of pore volume, V_{pHe} to bulk volume, V_b, as shown in equation (3.4)

$$\Phi_{He} = \frac{V_{pHe}}{V_b} = \frac{V_b - V_g}{V_b} = \frac{V_b - (V_c - V_r)}{V_b} \quad (3.4)$$

The Helium porosimeter is preferable over other porosimeters because Helium gas is inert and so, does adsorb on pore surface. In addition, the particle size of the gas is small and thus can penetrate the tiny pores. The gas also has high diffusivity and hence useful in measuring low permeability rocks.

The liquid saturation method employs the difference in weights between the dry core sample W_c, and the saturated core sample, W_s, to obtain the liquid saturated pore weight, W_l (which in this case, is brine) as shown in equation (3.5). The pore weight is then converted to pore volume, V_{pl}, by dividing it by the liquid density, ρ_l . The resulting pore volume is then divided by the bulk volume, V_b to obtain the liquid saturation effective porosity, Φ_{ls}, in %, defined by equation (3.6). The porosity values used for the flooding experiments in this study, were those obtained from the liquid saturation method since the experiment fluids were in liquid state.

$$W_l = W_s - W_c \quad (3.5)$$

$$\Phi_{ls} = \frac{\rho_l \, X \, W_l}{V_b} \quad (3.6)$$

iii. Permeability Measurement

Liquid permeabilities, *k*, of the core samples were estimated using a liquid Hassler permeameter. The permeability measurement was based on Darcy's law by measuring the flow time of a single fluid through a constricted tube. The experiment was repeated for three times to estimate the average liquid permeability of the core plug.

3.2.3 Formulation and Characterisation of Injection Brine

Synthetic brine was made from 32.2 g of laboratory grade Sodium Chloride dissolved in 1000 cm^3 (1 litre) of de-ionised water. The 32.2 g/litre concentration of NaCl is revealed by PVT analysis of formation water found in Niger Delta. Brine density and viscosity were then measured by pcynometer and viscosimeter, respectively.

3.2.4 Characterisation of Crude Oil

Degassed and de-watered crude oil sample obtained from the same Niger Delta region using decantation method. Its properties such as density and viscosity were measured. The density was measured using a pycnometer while the dynamic and kinematic viscosities were estimated using a viscosimeter.

3.2.5 Formulation and Characterisation of Different Nanofluid Concentrations

Nanofluid was formulated by suspending LHP nanoparticles (size range: 20-70 nm, surface area: 135-140 m^2/g and purity: 98.0-99.5%), procured from Burgoyne Urbidges Laboratory, India in the synthetic brine. The suspension was prepared in four distinct concentrations: 0.01, 0.50, 2.00 and 3.00 wt%, labelled Si_1, Si_2, Si_3 and Si_4, respectively. These were concentrations of nanoparticles that gave lower IFT values with crude oil, as compared to IFT value of brine and crude oil. A magnetic spinner was used to mix the nanofluid suspensions to achieve uniformity for up to 5 minutes. The density and viscosity of each nanofluid concentration were measured using pycnometer and viscosimeter.

3.2.6 Measurement of Interfacial Tension between Nanofluid and Crude Oil

Interfacial tension (IFT) between each nanofluid concentration and crude oil was measured to ensure that its value was within low IFT range. The IFT measurement was carried out using a ring tensiometer. The ring tensiometer uses a metallic ring lowered below the interface of two fluids. The metallic ring was lowered below the interface of the nanofluid and crude oil. The force required to pull the metal ring through the interface between the nanofluid and crude oil to the nanofluid medium is the interfacial tension and is read off in dynes/cm on the scale of the tensiometer. The experimental was repeated three times for each concentration to establish the range of values. Figure 3.2 depicts the picture of a tensiometer.

Fig. 3.2: Ring Tensiometer

3.2.7 Vacuum Saturation with Brine

The core samples were saturated with brine in the vacuum chamber of a saturator (made by VINCI technologies) as shown in Figure 3.3, for about 24 hours. The saturation pressure was 2,100 psia, typical of pressure obtained at reservoir condition. The saturated weight of each core sample was measured. To obtain the volume of brine in each saturated sample, the sample was weighed and the weight of the dry sample was subtracted from the weight of the saturated sample. The differential weight obtained was divided by the density of the reconstituted brine to obtain the volume of brine in each sample as shown in equation (3.7).

Initial volume of brine in the saturated sample,

$$\mathrm{V_{iw}} = \frac{W_{ls} - W_c}{\rho_w} \quad , \tag{3.7}$$

Where W_{ls} =weight of brine saturated sample, g; W_c= weight of dry sample, g; ρ_w = density of brine, g/cm^3

Fig. 3.3: Vacuum Saturator

3.3 Coreflood Set Up

The coreflooding process was carried out using a reservoir permeability tester (RPT). The RPT is a complex system that consists of a core holder with three accumulators for water (brine), oil and EOR fluid; as well as interconnection of pipes, tubing, pumps, pressure gauges, regulators and pressure valves and flow valves to control flow direction. It also consists of digital and analogue metres for adjusting and monitoring flow conditions. The vacuum pump is used to control flow of fluid into each of the accumulators before flooding begins. The effluent is collected at the core holder's outlet. The picture of the coreflood set-up is as shown in Figure 3.4. The schematic of the coreflood set up is illustrated in ure 3.5

The brine saturated core sample was loaded in the sleeve of the core holder and kept in place with spacers to avoid unsolicited invasion of fluid into the space around the core chamber during fluid injection. The fluid pump was then switched on and corresponding valves open to admit fluid (brine, oil and nanofluid) into the accumulators. The temperature condition in the RPT was maintained at 28 ^{o}C.

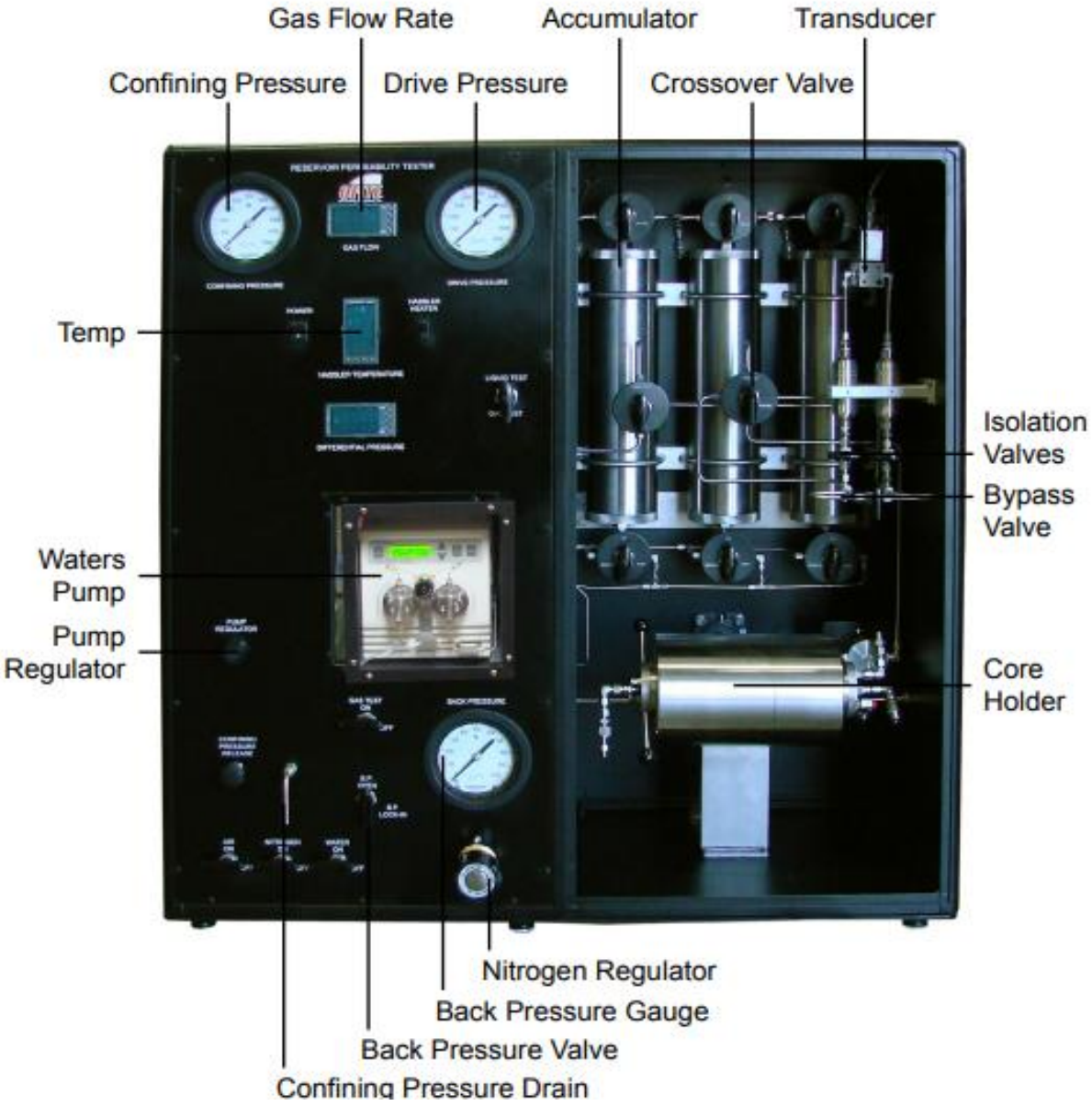

Fig. 3.4: Relative permeability tester used for coreflooding

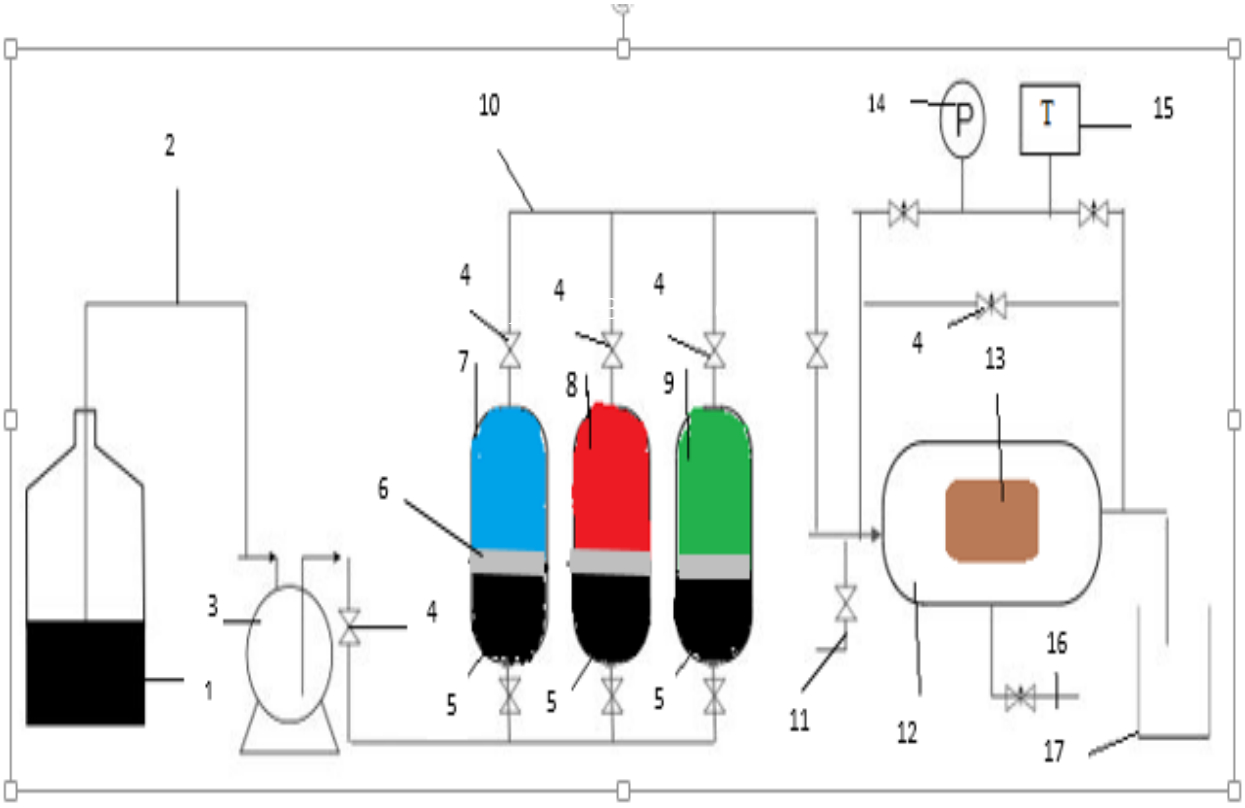

Fig. 3.5: Schematic diagram of the coreflood set up showing: 1) Pump fluid; 2) Injection line; 3) Fluid pump; 4) Valve 5) Pump fluid in accumulator A; 6) Piston plate; 7) Brine in accumulator –A; 8) Oil in accumulator–B; 9) Nanofluid in accumulator–C; 10) Oil line; 11) fluid line; 12)Core holder; 13) Core plug in the core holder 14) Pressure gauge; 15) Temperature gauge; 16) Sleeve pressure; 17) Effluent collector

3.3.1 Primary Drainage Process (Oil Flooding)

The degassed and dewatered crude oil pumped into accumulator B as shown in Figure 3.5 above, was injected into the brine saturated core sample (containing initial saturation of 100% brine). The drainage process was performed at a confining pressure of 300 psia and a flow rate of 2 cm^3/min to displace brine until no brine flowed into the effluent collector. 3-5 pore volume (PV) of crude oil was injected to reach a point of further displacement of brine from the core. The initial water saturation, $S_{wi,}$ was determined through material balance (i.e. initial volume of brine in the saturated sample minus volume of brine produced; hence, the OOIP was estimated from the volume of brine produced. The core plug was then aged for 24 hours for wettability restoration and oil-water distributions refinement at pore level. This process was repeated for all the core samples (Y1, Y2, Y3, Y4, Y5, Y6, Y7 and Y8). A similar flow rate of 2 cm^3/min was used for all the flooding processes to achieve uniform basis.

The initial water saturation can be calculated as shown in equation (3.8)

$$S_{wi} = \frac{V_{iw} - V_{pw}}{V_{iw}} \tag{3.8}$$

where V_{iw} = initial volume of brine in the saturated sample, V_{pw} = volume of brine produced, or *original oil in place (OOIP), cm^3*

3.3.2 Secondary Brine Flooding (BF)

Before secondary brine flooding, the core samples were at initial water, S_{wi} and initial oil saturations, S_{oi}. The secondary brine flooding served as the control. By opening the brine accumulator A (Fig. 3.5), each sample ((Y1, Y2, Y3, Y4 and Y5) was flooded with brine at 2cm^3/min and volumes of effluents produced and pressure drop were measured and recorded as a function of time. The flooding continued until no more oil was produced. However, when stable pressure was obtained, end-point permeability of the core to water k_w (at residual oil saturation) was calculated using Darcy's law. Material balance was used to calculate the residual oil saturation S_{or} (i.e., OOIP minus volume of oil produced). Also, the

core was aged for 24 hours for wettability restoration and oil-water distributions refinement at the pore level.

The brine flooding oil recovery factor is determined as depicted in equation (3.9)

$$ORF_{BF} = \frac{V_{wr}}{OOIP} \quad , \qquad (3.9)$$

where ORF_{BF} *is brine flooding oil recovery factor,* V_{wr} *= volume of oil recovered during brine flooding,* cm^3*;* $OOIP$ *= original oil in place,* cm^3

3.3.3 Nanofluid Flooding (NF) with Changing Concentration and Injection Rate

Accumulator C (Fig. 3.5) was opened and nanofluid containing concentration of 0.01 wt% was injected at 0.5 cm^3/min into the core chamber containing core Y1 that was previously flooded with brine (secondary brine flooding), until no more oil was recovered. The volume of oil recovered was subtracted from the residual oil volume before NF to obtain residual oil saturation after NF at the initial rate. The rate was then increased to 1.0, 2.0 and 3.0 cm^3/min and oil volume recovered was recorded. The flooding procedure was repeated with the other core samples (Y2, Y3 and Y4) for nanofluid concentrations of 0.5, 2.0 and 3.0 wt%, respectively, using injection rates ranging from 1.0 to 3.0 cm^3/min step-wisely for each of the core samples. The combination of nanofluid concentration and injection rate which yielded the highest oil recovery was recorded. These were the optimum nanofluid and injection rate. For the purpose of SEM analysis and comparison, Y5 was left only as a brine flooded core.

The NF recovery factor can be written as:

$$ORF_{NF} = \frac{V_{NF}}{OOIP}, \qquad (3.10)$$

where ORF_{NF} is the oil recovery factor for NF, V_{NF} is the volume of oil recovered during NF, cm^3; $OOIP$ is the original oil in place, cm^3

3.3.4 Nanofluid Flooding (NF) with Optimal Concentration and Injection Rate

Accumulator C (Fig. 3.5) was emptied and refilled with the optimal nanofluid concentration. Core sample Y6 which had only been drained during the primary flooding process was placed in the core chamber of the RPT. This was then flooded with the optimal nanofluid concentration at the optimal injection rate recorded in the previous experiment in section 3.3.3. Oil produced was collected in an effluent collector until no more oil droplet was produced.

3.3.5 Nanofluid-Alternating-Brine Flooding (NABF)

Accumulator A and C (Fig. 3.5) were filled with brine and nanofluid with optimal concentration, respectively. Core sample, Y8, initially drained during the primary oil flooding process was placed in the core holder of the RPT. Nanofluid was first injected into the core sample at the optimal injection rate and confining pressure of 300 psia until no more oil was recovered. Accumulator A was then opened and brine was pumped at the optimal injection rate into the core sample until no more oil was produced. The volume of oil recovered under each flooding process was recorded and residual oil saturations were estimated using material balance.

3.4 Scanning Electron Microscopy

Scanning Electron Microscopy was carried out using the Scanning Electron Microscope (SEM) to obtain high resolution images and compare the changes that occurred on the pore surfaces of each of the core samples before and after the completion of the flooding processes. The SEM uses highly accelerated electron beam, producing higher resolutions compared to optical microscope, to investigate the surface texture, chemical composition, crystalline structure and orientations of materials which the sample is made up of. The electron beam interacts with atom of the sample to produce imagery of the surface topography and composition of the sample. Areas ranging from approximately 1 cm to 5 microns in width can be imaged in a scanning mode using conventional scanning electron microscopy techniques (magnification ranging from 20X to approximately 30,000X, spatial resolution of 50 to 100 nm). A thin section of each core plug (Y5, Y6, Y8) was analysed

with SEM at a magnification of 5,000X and resolution of 2 μm. SEM with smaller and larger magnifications and resolutions were also captured. Y5 is the BF core, Y6 is the NF core while Y8 is NABF core. The SEM sections of the three core samples were interpreted and compared.

3.5 Model Development for Nanoskin Factor

3.5.1 Physical Description

The concept of nanoskin was introduced by the author and is defined as a thin sheet of nanoparticles deposited and retained in the reservoir rock pore surfaces and throats during nanofluid flooding which causes porosity and permeability impairment and subsequent formation damage. As shown earlier in Figure 1.4, nanoskin formation could be explained by the principle of adsorption of nanoparticles and the removal of nanoskin, by the principle of desorption. The nanoskin factor is analogous to skin factor caused by mud cake deposition during drilling operations, which affects oil production. While flooding with nanofluid, same effect can occur but unlike skin effect, the nanoskin effect is not restricted to the well bore region but also propagates further to the reservoir.

Many factors such as nanoparticle size, nanofluid concentration, salinity, injection pressure, injection rate, pore geometry, reservoir rock properties, temperature, contribute to nanoskin effect, however, for the purpose of this study, the factors were be limited to two, *viz.*, nanofluid concentration and injection rate. The model for nanoskin factor was developed using Darcy's equation.

3.5.2 Simplifying Assumptions

The assumptions for the development of the model include:

1. Homogenous system
2. Fluids are incompressible
3. Two-phase flow
4. Linear piston-like displacement
5. No injection fluid loss

6. Saturation of a fluid is the same throughout the porous medium (core plug)

3.5.3 Mathematical Model

The nanoskin model is a linear model. The model consists of reservoir rock parameters such as porosity, permeability, cross-sectional area; reservoir fluid parameters, viscosity; flow parameters such as oil and water flow rates; oil recovery factor, and injection fluid properties such as nanofluid concentration, nanoparticle surface area and injection rate. Nanoskin factor, S_n, is the dependent variable while nanofluid concentration, C_{nf} and injection rate, q_{inj}, are the independent variable while other variables are fixed.

3.5.4 Governing Equations

i. Darcy's equation

Darcy's law for a linear flow may be expressed as given in equation (3.11a)

$$\frac{\Delta P}{\Delta L} = \frac{-qA}{k\mu} \tag{3.11a}$$

where $\frac{\Delta P}{\Delta L} = normal\ Pressure\ drop,$

q=flow rate,

k =permeability

A =cross-sectional area of flow

ii. Frontal Advance Equation

This is modification of Darcy's equation and is governed by the principle of conservation of mass

Rate of mass flow in-Rate of accumulation =Rate of mass flow out

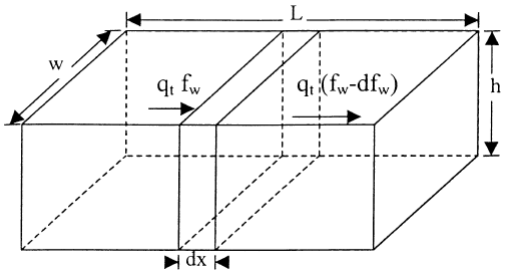

The frontal advance equation is given by equation (3.11b)

$$\left(\frac{dx}{dt}\right)_{Sw} = \left(\frac{q_t}{\phi A}\right)\left(\frac{df_w}{dS_w}\right)_{S_w} \qquad (3.11b)$$

Where v_{sw}=velocity of any specified value of S_w

A= Cross-sectional area in cm^2

q_t = Total flow rate (cm^3/min)

ϕ= Porosity, fraction

$\left(\frac{df_w}{dS_w}\right)_{S_w}$ = Slope of curve of f_w vs. S_w at S_w

Since we assume that saturation is the same throughout the porous medium,

$$\left(\frac{df_w}{dS_w}\right)_{S_w} = 1$$

Equation (3.11b) then becomes

$$\left(\frac{dx}{dt}\right)_t = \frac{q_t}{\phi A} \qquad (3.11c)$$

$\left(\frac{dx}{dt}\right)_t$ = total velocity of the two phases (oil and water)

$q_t = q_o + q_w$

q_o= flow rate of the water phase

q_w= flow rate of the oil phase

3.5.5 Model Development

During injection of nanoparticles into the well, an additional pressure drop results due to formation of nanoskin. Hence, total pressure drop may be given as:

$$\frac{\Delta P}{\Delta L}\Big|_{\text{total}} = \frac{\Delta P}{\Delta L}\Big|_{\text{ns}} + \frac{\Delta P}{\Delta L}\Big|_{\text{normal}} \tag{3.12}$$

This may be expressed as

$$\frac{\Delta P}{\Delta L}\Big|_{\text{total}} = \frac{1}{A}\left[\frac{\mu_w q_w}{k_w} + \frac{\mu_o q_o}{k_o}\right](1 + S_n) \tag{3.13}$$

We introduce the porosity term to account the effective flow from equation (3.11b). In addition, since the pressure drop is due to flow of the injectant; equation (3.13) becomes

$$\frac{\Delta P}{\Delta L}\Big|_{\text{ns}} = \frac{1}{\phi A}\left[\frac{\mu_w q_w}{k_w} + \frac{\mu_o q_o}{k_o}\right] S_n = \frac{q_t \mu_{nf}}{A_{nf} k_{nf}} \tag{3.14}$$

$q_t = q_{inj}$, assuming no fluid retention/loss (although nanoparticles could be retained); hence,

$$s_n = \frac{\frac{q_{inj}\,\mu_{nf}}{A_{np} k_{nf}}}{\frac{1}{\phi A}\left[\frac{\mu_w q_w}{k_w} + \frac{\mu_o q_o}{k_o}\right]} \tag{3.15}$$

wt % Nanofluid concentration =Weight of nanoparticles/Weight of brine

$C_{nf} = W_{np}/W_w$, (3.16)

Hence, $W_{np} = C_{nf} * W_w$ (3.17)

Surface Area, SA= Area/Weight (3.18)

$SA = A_{np}/W_{np}$ (3.19)

$A_{np} = SA * W_{np}$ (3.20)

$A_{np} = SA * C_{nf} * W_w$ (3.21)

Hence,

$$S_n = \frac{\frac{q_{inj}\ \mu_{nf}}{SA*C_{nf}*W_w*k_{nf}}}{\frac{1}{\phi A}\left[\frac{\mu_w q_w}{k_w}+\frac{\mu_o q_o}{k_o}\right]} \quad (3.22)$$

$$q_o = ORF * q_{inj} \quad (3.23)$$

$$q_{inj} = \frac{q_o}{ORF} \quad (3.24)$$

Substitute for q_{inj} in equation (3.22) using equation (3.24)

Hence, equation 3.22 becomes

$$S_n = \frac{\frac{q_o * \mu_{nf}}{ORF*SA*C_{nf}*Ww*k_{nf}}}{\frac{1}{A\phi}\left[\frac{\mu_w q_w}{k_w}+\frac{\mu_o q_o}{k_o}\right]} \quad (3.26)$$

where:

q_{inj} = *Nanofluid injection rate, cm^3/min*

q_o = *Oil flow rate, cm^3/min*

q_w = *Water flow rate, cm^3/min*

μ_{nf} = *nanofluid viscosity, cp*

A_{np} =

$Portion\ of\ area\ occupied\ by\ nanoparticles,\ a\ function\ nanofluid\ concentration,$ cm^2

$k_{nf} = Nanofluid\ permeability,\ md$

$S_n = Nanoskin\ factor$

μ_w = *Brine viscosity, cp*

μ_o= *Oil viscosity, cp*

k_w= *end permeability point of brine, md*

k_o= *end permeability point of oil, md*

C_{nf} =*Nanofluid concentration, wt %*

W_{np} = *Weight of nanoparticle, g*

ORF= Oil recovery factor, % or fraction

3.5.6 Solution Method

The equation is solved by substituting all relevant input variables while assuming values for the test variable(s).

3.5.7 Application

Because of the number assumptions of the model, the model may only be applied at the laboratory scale with little error. Pilot studies and field application require modifications to eliminate the assumptions of the equation.

3.6 Technical Evaluation of Nanofluid-Alternating-Brine Flooding for a Case Reservoir in Niger Delta

The volumetric model was used in the estimation of oil reserves for the case study field described in section 1.6. The method assumes that reservoir is homogenous (i.e. uniform distribution of porosity, permeability and fluid saturation; constant reservoir thickness and drainage area)

Estimated oil recovery for NABF for the case study field is therefore given in equation (3.25)

$$NpNABF = (ORF_{NABF} - ORF_{B\,NABF}) * (1-S_{wi})*Ah\phi \quad (3.25)$$

Where:

NpNABF = Oil recovered during NABF flooding, m^3

ORF_{NABF} = recovery efficiency of the NABF

ORF_{BNABF} = cumulative recovery efficiency before NABF

h = average reservoir thickness, metres

S_{wi} = connate water saturation, %

A = drainage area or well spacing, sq. metres

ϕ = the average reservoir porosity, %

3.6.1 Upscaling of Experimental Results

Upscaling will be done using ratio of laboratory and reservoir parameters

Reservoir pore volume of nanofluid injected,

$$P_{VRN} = \frac{P_{VLN} \, x \, V_{BR}}{V_{BL}} \quad (3.26)$$

where:

P_{VLN} = core pore volume of nanofluid injected, cm^3

V_{BR}= reservoir bulk volume, cm^3

V_{BL}= core bulk volume, cm^3

Reservoir pore volume of brine injected is also as expressed in equation (3.27) below

$$P_{VRW} = \frac{P_{VLW} \, x \, V_{BR}}{V_{BL}} \quad (3.27)$$

where:

P_{VLW}= core pore volume of brine injected

V_{BR}= reservoir bulk volume, cm^3

V_{BL}= core bulk volume, cm^3

Weight (g) of nanofluid required, $W_N = C_{op} * P_{VRN}$ (3.28)

where

C_{op} =optimal nanofluid concentration, wt %.

Assumptions

i. No viscous fingering

ii. Homogeneous reservoir

iii. Linear flow

3.7 Economic Evaluation of Nanofluid-Alternating-Brine Flooding for a Case Reservoir in Niger Delta

3.7.1 Deterministic Approach

The economic evaluation was carried out using the net present value (NPV) approach. No cost of drilling injection well was incurred because the production wells were converted to injection wells. Major CAPEX was the cost of procuring and installing the injection pumps and flow lines. Using the rule of thumb (Mian, 2011), fixed OPEX is 5% of engineering CAPEX. In deterministic approach, the volume of oil recovered after NABF was estimated as a single value (point estimate) without any consideration for uncertainty.

Fixed OPEX= 5%* CAPEX (3.29)

The variable OPEX, i.e., cost of injection per depth is $8,330 per foot. Cost of silica nanoparticle injectant is $0.5 per gram.

Cost of Silica nanofluid ($), $C_N = W_N * 0.5$ (3.30)

Total Cost/ bbl, C_T= CAPEX/bbl + Total OPEX/bbl+ C_N/bbl (3.31)

NCF/bbl= Oil Price/bbl–C_T –Royalty/bbl – Tax/bbl (3.32)

Net Present Value/bbl= $\sum_{t=o}^{n} \frac{NCF/bbl}{(1+i)^t}$ (3.33)

where

i= real discount rate, %

t= time, years

If the threshold oil price is P_{OT} and given that royalty is 20% and tax rate is 30% with a desirable undiscounted profit margin of P_M% of P_{OT}, then P_{OT} may be expressed as:

$(P_{OT} – 0.2* P_{OT} - C_T)* (1-0.30) = P_M*P_{OT}$ (3.34)

Equation 3.34 then becomes

$$P_{OT} = \frac{0.7C_T}{0.56 - P_M} \quad (3.35)$$

If P_M is 0% then,

$$\boldsymbol{P_{OT} = 1.25 * C_T} \quad (3.36)$$

If P_M is 20% then, $\boldsymbol{P_{OT} \approx 2 * C_T}$ (3.37)

Threshold oil price, $P_{OT,}$ is the minimum oil price that will give the minimum expected profit margin.

3.7.2 Probabilistic Approach

The probabilistic approach employed was Monte Carlo Simulation. The oil recovery for NABF ($\mathbf{N_{pNABF}}$), cost of materials, CAPEX, and OPEX constitute a high level of uncertainty in the oil and gas business. So, rather than use point estimates, continuous distributions were assigned to uncertain variables and a range of oil prices beyond which NABF would not be realistic, was generated.

A range of values for N_{pNAB} was obtained by simulating the extreme and mean values of the input variables (ORF_{NAB}, A, h, ϕ, S_{wi}) for estimating N_{pNABF} as given in equation (3.25). P_{10}, P_{50} and P_{90} reserves then served as inputs into the economic model. Variable OPEX is also subject to changes since it varies with external factors such as inflation rate which affects the general prices of goods and services. Hence, a triangular distribution of OPEX per foot drilled ranging from \$8,000 per foot to \$10,000 per foot was assumed. The point-estimate value of \$8,330 per foot served as the most likely OPEX. Fixed OPEX was assumed to be 5% of CAPEX; since fixed OPEX is dependent on CAPEX, it would not be used as a risked variable.

CAPEX, on the other hand, changes gradually. The values are normally distributed about a mean. Hence, we assumed a normal distribution for total CAPEX with a standard deviation of 10% of the mean. Taxes and royalties are not usually subject to sudden changes.

However, the operator may not be immune to uncertain charges such as NDDC levy, hydrocarbon taxes, to mention a few.

CHAPTER FOUR

RESULTS AND DISCUSSION

4.1 Characterisation of Core Samples

4.1.1 Weight, Volume and Density Measurements

The weight, length and diameter were preliminary measurements for the computation of porosity of each of the core samples. The dry weight, W_c, ranged from 114.0 to 175.1 g while the length, l_c, ranged from 5.4 to 7.0 cm. The diameters of the samples, d_c, were similar as expected, giving a value of 3.8 cm. The bulk volumes, V_b, ranged from 61.2 to 79.4 cm^3 while the bulk densities, ρ_c , ranged from 1.8 to 2.0 g/cm^3. Table 4.1 illustrates the parameters, with means and their mean deviations.

The mean and mean deviations of the samples dry weights, lengths, diameters, bulk volumes and bulk densities were 143.4 g and 19.0 g; 6.4 cm and 0.6 cm; 3.8 cm and 0.0 cm; 72.7 cm^3 and 6.6 cm^3; and 2.0 g/cm^3 and 0.1 g/cm^3, respectively. These values are reflections of similarities among the values of the samples' parameters.

Table 4.1: Weight, Dimension, Volume and Density Measurements

Sample No	W_c, **g**	l_c, **cm**	d_c, **cm**	V_b, **cm^3**	ρ_c, **g/cm^3**
Y1	115.1	5.5	3.8	62.4	1.8
Y2	150.4	6.9	3.8	78.3	1.9
Y3	124.2	6.0	3.8	68.0	1.8
Y4	114.8	5.4	3.8	61.2	1.9
Y5	175.1	7.0	3.8	79.4	2.2
Y6	155.9	6.9	3.8	78.3	2.0
Y7	153.7	6.8	3.8	77.1	2.0
Y8	158.0	6.8	3.8	77.1	2.0
Mean	143.4	6.4	3.8	72.7	2.0
Mean Dev.	19.0	0.6	0.0	6.6	0.1

4.1.2 Porosity

The dry weights, W_c, grain volumes, V_g, grain densities, ρ_g, bulk weights, W_s , liquid saturated pore weights, W_l of the eight core samples, are as shown in Table 4.2(a). These parameters were precursors for the calculation of pore volumes and by extension, the porosities. The mean and mean deviation of these aforementioned parameters were 143.4 g and 19.0 g; 54.5 cm^3 and 7.1 cm^3; 2.6 g/cm^3 and 0.0 g/cm^3; 161.7 g and 18.6 g; and 18.3 cm^3 and 1.7 cm^3.

Table 4.2 (b) shows the Helium pore volumes, V_{pHe}, liquid saturated pore volumes, V_{pl} and the corresponding porosities; Φ_{ls} and Φ_{He} for the eight core samples. V_{pHe} ranged from 13.8 to 20.9 cm^3 while V_{pl} ranged from 12.3 to 19.0 cm^3. Φ_{He} ranged from 17.4 to 30.9% while Φ_{ls} ranged from 16.8 to 30.4%. The difference in porosity values of the two methods is an indication that they were some dead ends and tinier pores that could not be saturated by the liquid in the liquid saturation method. The Helium porosities includes pores of the non-liquid saturated zones, hence their higher values. The mean and mean deviation of Φ_{ls} and Φ_{He} are 26.0% and 3.2% and 25.4% and 3.2%, respectively.

Table 4.2(a): Preliminary Data for the Calculation of Porosities of the Core Samples

Sample No	W_c**, g**	V_g**, cm^3**	ρ_g**, g/cm^3**	W_s**, g**	W_l**, cm^3**
Y1	115.1	43.4	2.7	134.1	19.0
Y2	150.4	58.2	2.6	170.5	20.1
Y3	124.2	47.6	2.6	144.6	20.4
Y4	114.8	43.9	2.6	132.1	17.3
Y5	175.1	66.1	2.6	188.4	13.3
Y6	155.9	58.8	2.7	175.4	19.5
Y7	153.7	58.0	2.7	172.8	19.1
Y8	158.0	59.6	2.7	175.5	17.5
Mean	143.4	54.5	2.6	161.7	18.3
Mean Dev.	19.0	7.1	0.0	18.6	1.7

Table 4.2(b): Porosities of the Core Samples

Sample No	V_{pHe}**, cm^3**	V_{pl}**, cm^3**	Φ_{He}**, %**	Φ_{ls} **, %**
Y1	19.3	19.0	30.9	30.4
Y2	20.9	17.9	26.7	25.7
Y3	20.7	16.8	30.4	30.0
Y4	17.5	15.4	28.6	28.3
Y5	13.8	12.3	17.4	16.8
Y6	19.8	15.4	25.3	24.9
Y7	19.5	15.2	25.3	24.8
Y8	17.8	14.9	23.1	22.7
Mean	15.9	26.0	25.4	25.4
Mean Dev.	1.5	1.7	3.2	3.2

Figure 4.1 shows the plot of Φ_{He} and Φ_{ls}. Φ_{He} values are regarded as more accurate because the Helium Porosimeter uses Helium gas which is inert. Hence, Φ_{ls} values were compared to Φ_{He} to estimate the errors in their measurements. The mean error was 0.5% and mean deviation of errors was about 0.2%.

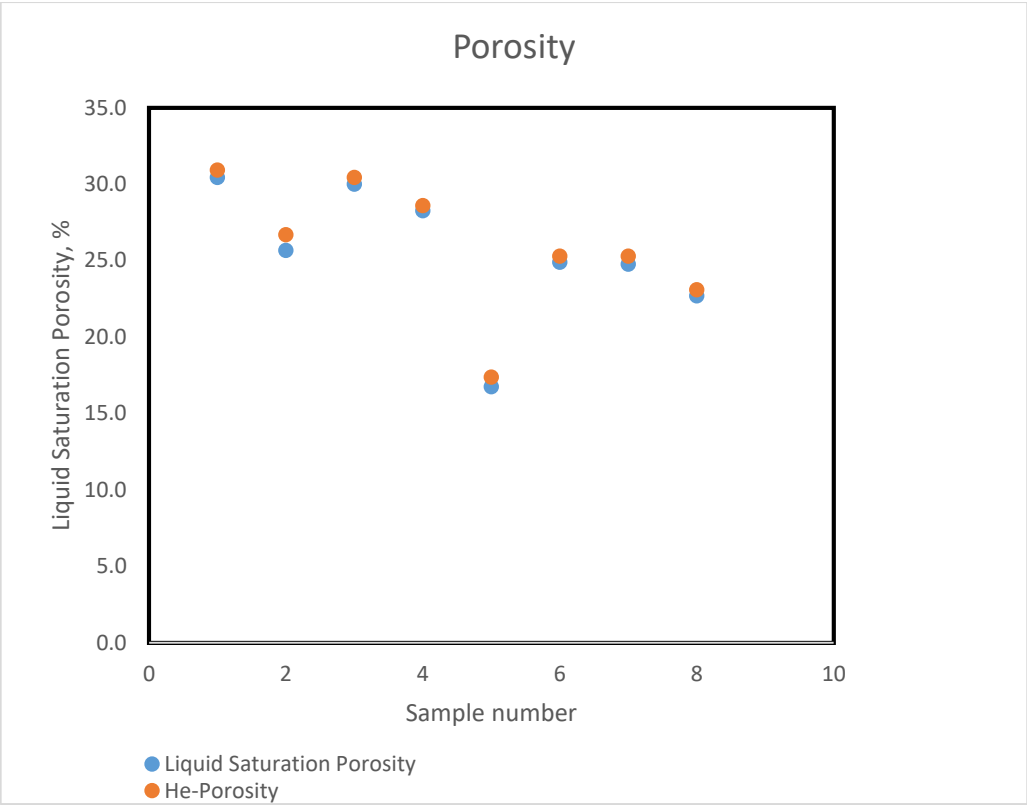

Fig. 4.1: Plot of Helium and Liquid Saturation Porosities

4.1.3 Permeability

Liquid permeability, *k*, measurement revealed relatively high permeability values from 1104.9 to 1589.0 md. This is the reflective of high permeability property of Niger Delta sandstone reservoirs. Figure 4.2 reveals the plot of the liquid permeabilities of the eight core samples. The mean of the permeabilities was 1226.9 md, while the mean deviation was 116.6 md.

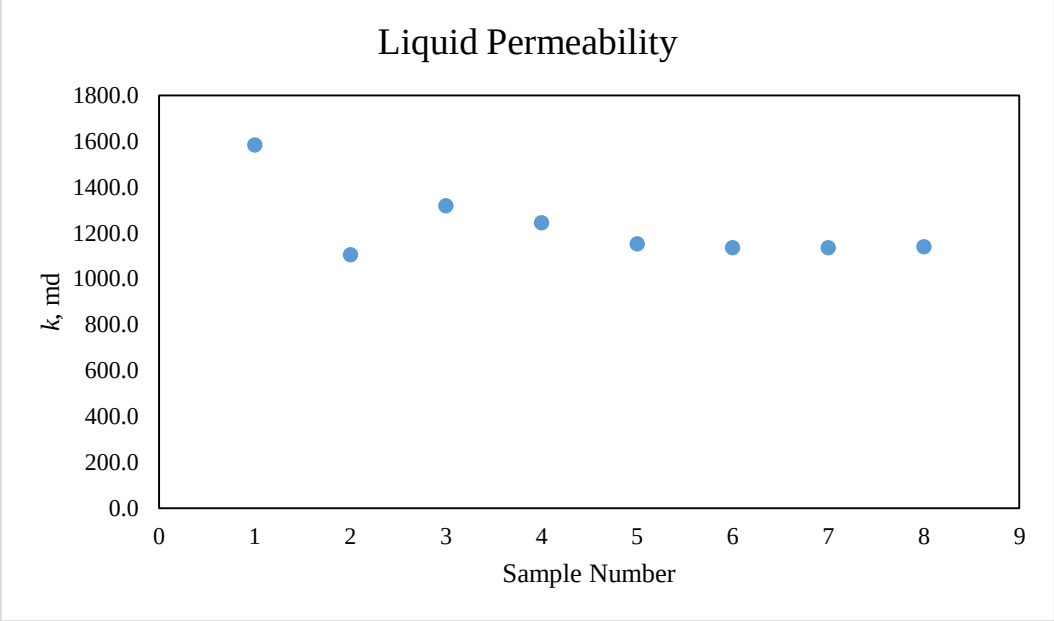

Fig. 4.2: Liquid Permeability Plot for the Core Samples

4.1.4 Summary of Sample Characterisation

The summary table of results of the characterisation of the 8 core samples are as shown in Table 4.3. The ranges of the parameters are depicted to see how close or far apart the values of the properties of the core samples are. Among these properties, the porosity and permeability values are crucial, and may not be too far apart, in order to reduce experiment bias. Moreover, the measured parameters should be representative of those from typical Niger Delta core samples. From Table 4.3, it could be seen that the values of the porosities and permeabilities were close to those reported by Onyeonkwu and Ogolo, with a standard mean errors of 1.8% and 27.1%, respectively (2010).

Table 4.3: Summary Table for Sample Characterisation

Sample No	**Dry weight, g**	**Length, cm**	**He-Porosity, %**	**Liq. Porosity, %**	**Liq. Permeability, k (md)**
Y1	115.1	5.5	30.9	30.4	1584.0
Y2	150.4	6.9	26.7	25.7	1104.9
Y3	124.2	6.0	30.4	30.0	1318.4
Y4	114.8	5.4	28.6	28.3	1244.5
Y5	175.1	7.0	17.4	16.8	1152.3
Y6	155.9	6.9	25.3	24.9	1135.8
Y7	153.7	6.8	25.3	24.8	1135.0
Y8	158.0	6.8	23.1	22.7	1140.2
Range	60.3	1.6	13.5	13.6	479.1

4.2 Formulation and Characterisation of Injection Brine

The density and viscosity of the injection brine prepared at a concentration 32. 0 g/litre are as provided in summary Table 4.4 below. The average density was 1.023 g/cm^3 while average viscosity was 1.0 cp.

4.3 Characterisation of Crude Oil Sample

The density and viscosity of crude oil are as provided in summary Table 4.4 below. Average density and average viscosity of the crude oil were 0.882 g/cm^3 and 2.981 cp respectively.

4.4 Formulation and Characterisation of Different Nanofluid Concentrations

The density and viscosity of each prepared silica nanofluid concentration are as provided in the summary Table 4.4 below. The average densities ranged from 1.011 1to 1.021 g/cm^3 while the average viscosities were from 1.005 to 1.020 cp.

Table 4.4: Summary of Fluid Characterisation

Fluid	Concentration, wt %	Density, g/cm^3	Kinematic Viscosity, cp
Brine	0.35	1.023	1.000
Si_1	0.01	1.011	1.005
Si_2	0.50	1.018	1.014
Si_3	2.00	1.020	1.018
Si_4	3.00	1.021	1.020
Crude oil	-	0.882	2.981

4.5 Interfacial Tension

The interfacial tension (IFT) values between the brine and crude oil and that of each nanofluid and crude oil are as depicted in Table 4.5. The average IFT of the brine and crude oil was 23.0 dynes/cm while those of $Si_1 – Si_4$ was ranged between 17.5 and 20.0 dynes/cm, confirming that the range of nanofluid concentrations used in the experiments were those below the IFT between brine and crude oil. As seen in table, the IFT values decreased with increasing concentration of nanofluid, however, at 3.0 wt % nanofluid concentration, it rose to 20.0 dynes/cm. Figure 4.3 shows the relationship between IFT and nanofluid concentration. The relationship follows third order polynomial trend and may be extended to other nanofluid concentrations.

Table 4.5: IFT Measurements

Fluid	Concentration, % wt	IFT between crude oil and Fluid, dynes/cm
Brine	0.35	23.0
Si1	0.01	19.0
Si2	0.50	18.5
Si3	2.00	17.5
Si4	3.00	20.0

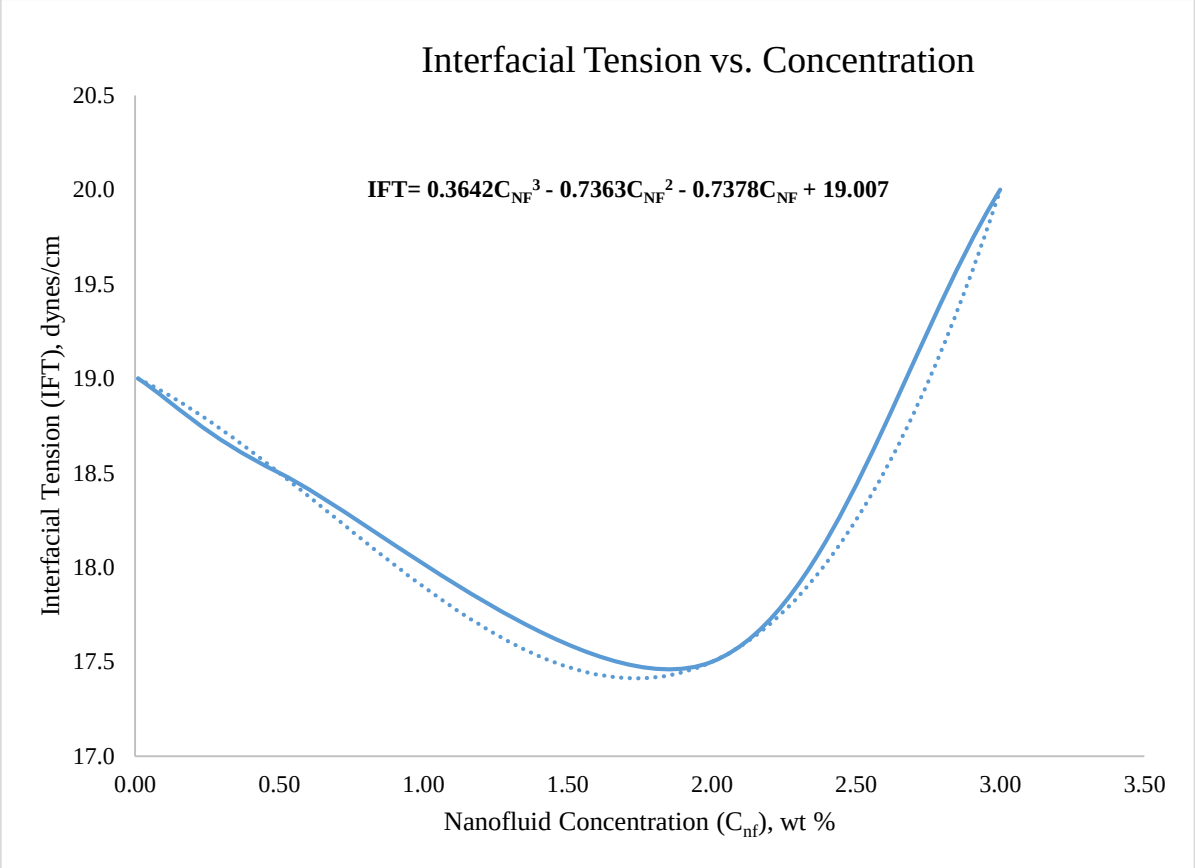

Fig. 4.3: Plot of Interfacial tension (IFT) against Nanofluid Concentration (C_{NF})

4.6 Vacuum Saturation Results for Initial Water Saturation

The vacuum saturation with brine for all the core samples are as illustrated in table 4.6. If all pore spaces in the core samples were fully saturated, the imbibed water saturation would be 100%. However, when Φ_{He} of each core sample was compared to Φ_{ls} , there was a slight difference, showing that some parts of the sample were not invaded by brine. Hence, the brine saturation, computed as a ratio of Φ_{ls} and Φ_{He}, is as presented in the table. Sample Y4 has the highest water saturation of 98.9% while Y2 has the lowest saturation of 96.2%. The range of the water saturation was therefore 2.7%.

Table 4.6: Vacuum Saturation Results

Sample No	He- Porosity, %	Liquid Saturation Porosity, %	Water Saturation, %
Y1	30.9	30.4	98.4
Y2	26.7	25.7	96.2
Y3	30.4	30.0	98.6
Y4	28.6	28.3	98.9
Y5	17.4	16.8	96.4
Y6	25.3	24.9	98.5
Y7	25.3	24.8	97.9
Y8	23.1	22.7	98.3

4.7 Coreflood Experiments

4.7.1 Primary Drainage Process (Oil Flooding)

Table 4.7 shows the results of the drainage (oil imbibition) experiment. The initial volume of brine in the saturated sample, $V_{iw,}$ is as shown in the table. The initial water saturation, S_{Wi}, for each sample was the volume of brine that could not be displaced by oil. The OOIP defines the volume of oil imbibed, which was used in determining the initial oil saturation, S_{oi}, for each sample, as also depicted in the table.

4.7.2 Secondary Brine Flooding

The volume of oil recovered, V_{wr}, residual oil saturation, S_{or}, and oil recovery factor, after secondary brine flooding, ORF_{BF}, are as shown in Table 4.7 also. Sample Y1 had the highest recovery factor of 60.0%, after secondary brine flooding while sample Y4 had the least (52.0%).

4.7.3 Nanofluid Flooding with Changing Concentration and Injection Rate

The oil recovery factor, $ORF_{NF,}$ for each concentration and their respective injection rates are as shown in Table 4.8. For the 0.01 wt % nanofluid mixture, the injection rate beyond 1.0 cm^3/min yielded no significant recovery. Increase in injection rate from 1.0 to 3.0 cm^3/min was quite important for 0.05 wt % mixture as it guaranteed more recovery. For 2.00 wt % mixture, going beyond 2.0 cm^3/min was not important because it guaranteed no further recovery while for 3.00 wt %, an injection rate beyond 1.0 cm^3/min need not be exceeded for additional recovery.

The 2.0 wt % nanofluid mixture yielded the optimal ORF_{NF} of 36.0% while the 3.0 wt % mixture gave the least ORF_{NF}. The 3.0 wt % nanofluid concentration yielded no significant additional recovery; this was an indication that nanoparticles adsorption at this point, had a negative effect on oil recovery. The structural disjoining pressure which leads to wettability reversal, increases with concentration because of the stronger effects of electrostatic repulsion and Brownian motion (Klaine *et al*., 2008). As much as high nanoparticles

concentration is required to strengthen the effects of the forces mentioned, it is vital to maintain concentration at a level that would not lead to pore blockage. When concentration is higher than required, nanoparticles agglomerate to form thicker nanoskin at the pore surface, causing eventual formation damage. Hence, concentration beyond 2.0 wt % should not be exceeded during flooding with LHP nanoparticles in Niger Delta reservoirs.

Table 4.7: Drainage and Brine Flooding Experiment Results

Sample No	V_{wi}, cm^3	S_{wi}, %	OOIP, cm^3	S_{oi}, %	V_{wr}, cm^3	S_{or}, %	ORF_{BF}, %
Y1	19.0	18.4	15.5	81.6	9.3	32.6	60.0
Y2	20.1	11.0	17.9	89.0	9.8	40.3	55.0
Y3	20.4	15.2	17.3	84.8	10.0	35.8	58.0
Y4	17.3	11.0	15.4	89.0	8.01	42.7	52.0

Table 4.8: Nanofluid Flooding Results

Sample No	**Y1**	**Y2**	**Y3**	**Y4**
Conc , wt %	**0.01**	**0.50**	**2.00**	**3.00**
inj. rate, cm^3/min	**Volume of Oil Recovered, cm^3**			
0.5	2.0	2.3	2.7	0.7
1.0	0.3	1.6	2.6	0.5
2.0	0.0	0.6	1.0	0.0
3.0	0.0	0.1	0.0	0.0
Cumulative oil recovered after nanoflooding, cm^3	2.3	4.6	6.3	1.2
ORF_{NF}	0.15	0.26	0.36	0.08

This trend of recovery factor as concentration increases is as depicted in Figure 4.4. Table 4.9 indicates that 0.01 and 0.50 wt % concentrations gave nanofluid recovery efficiency of 15.0 and 26.0% respectively (highlighted in yellow), while 3.0 wt % concentration gave a recovery efficiency of 8.0 % (highlighted in blue). The optimal nanofluid recovery efficiency of 36.0% was recorded at 2.00 wt% (highlighted in green) nanofluid concentration. In addition the residual oil saturation after brine flooding, $\mathbf{S_{orBF}}$ and nanofluid flooding, $\mathbf{S_{orNF}}$, are indicated accordingly.

The trend of oil recovery factor at different injection rates, specified in the study, is as shown in Figure 4.5. The dotted lines indicate the oil recovery path for waterflooding. An injection rate above 2 cm^3/min for the concentrations experimented did not result in any significant additional recovery. Hence, the injection rate threshold is 2 cm^3/min. The intent of specifying the injection rate threshold for the concentration range under study is first to avoid unnecessary injection of large quantity of nanofluid per unit flow time which would be costlier. Secondly, it is to reduce the possibility of formation of thick nanoskin which causes formation damage due to nanoparticle retention and entrainment.

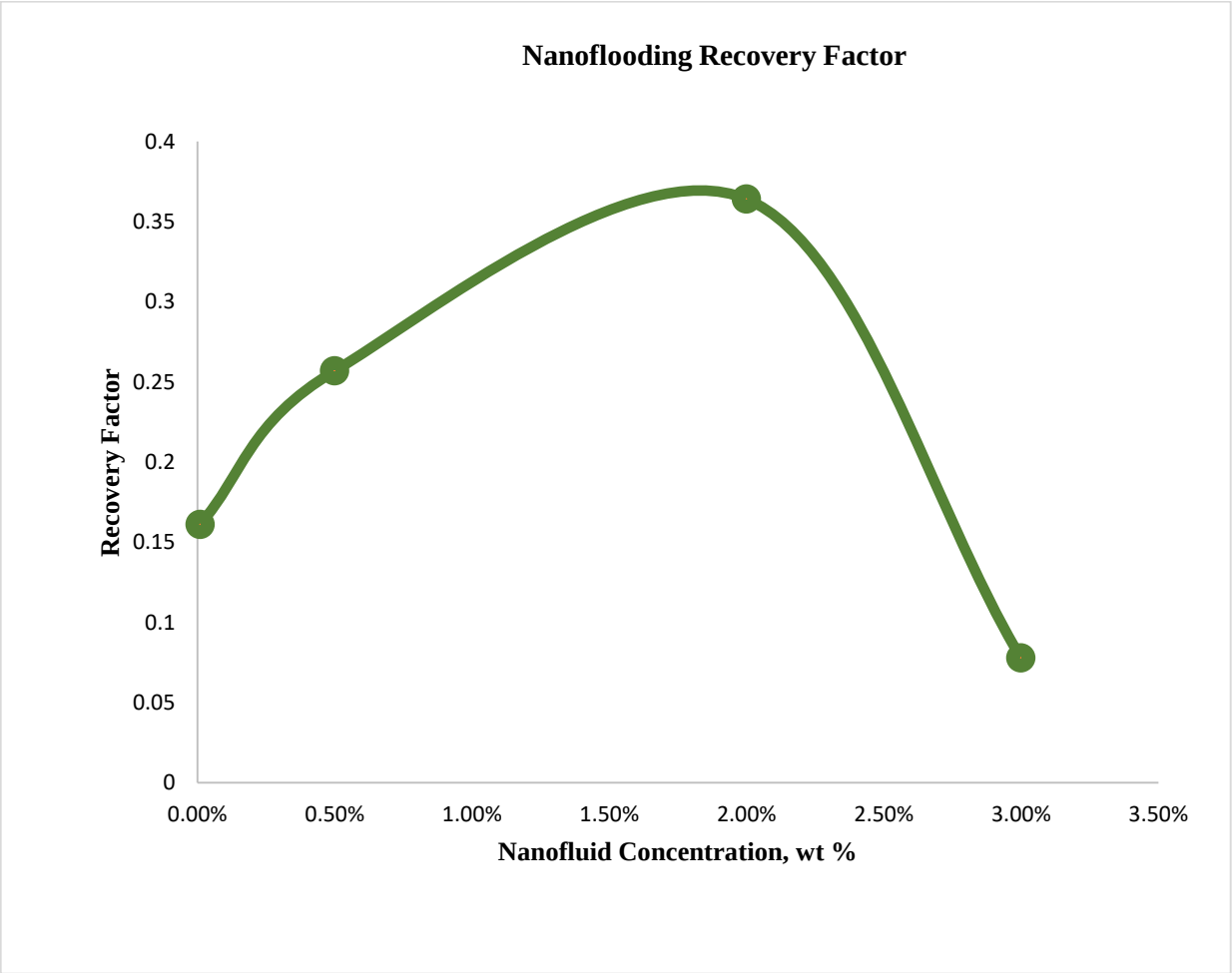

Fig. 4.4: Recovery Factor against Nanofluid Concentration

Table 4.9: Residual Oil Saturation and Displacement Efficiency for Brine Flooding and Nanofluid Flooding for the Four Different Concentrations of Nanofluid

Nanofluid Concentration, wt %	**S_{Wi}**	**S_{oi}**	**S_{orBF}**	**ORF_{BF}**	**S_{orNF}**	**ORF_{NF}**
0.01	0.18	0.82	0.33	0.60	0.21	0.15
0.50	0.11	0.89	0.40	0.55	0.17	0.26
2.00	0.15	0.85	0.36	0.58	0.05	0.36
3.00	0.11	0.89	0.43	0.52	0.36	0.08

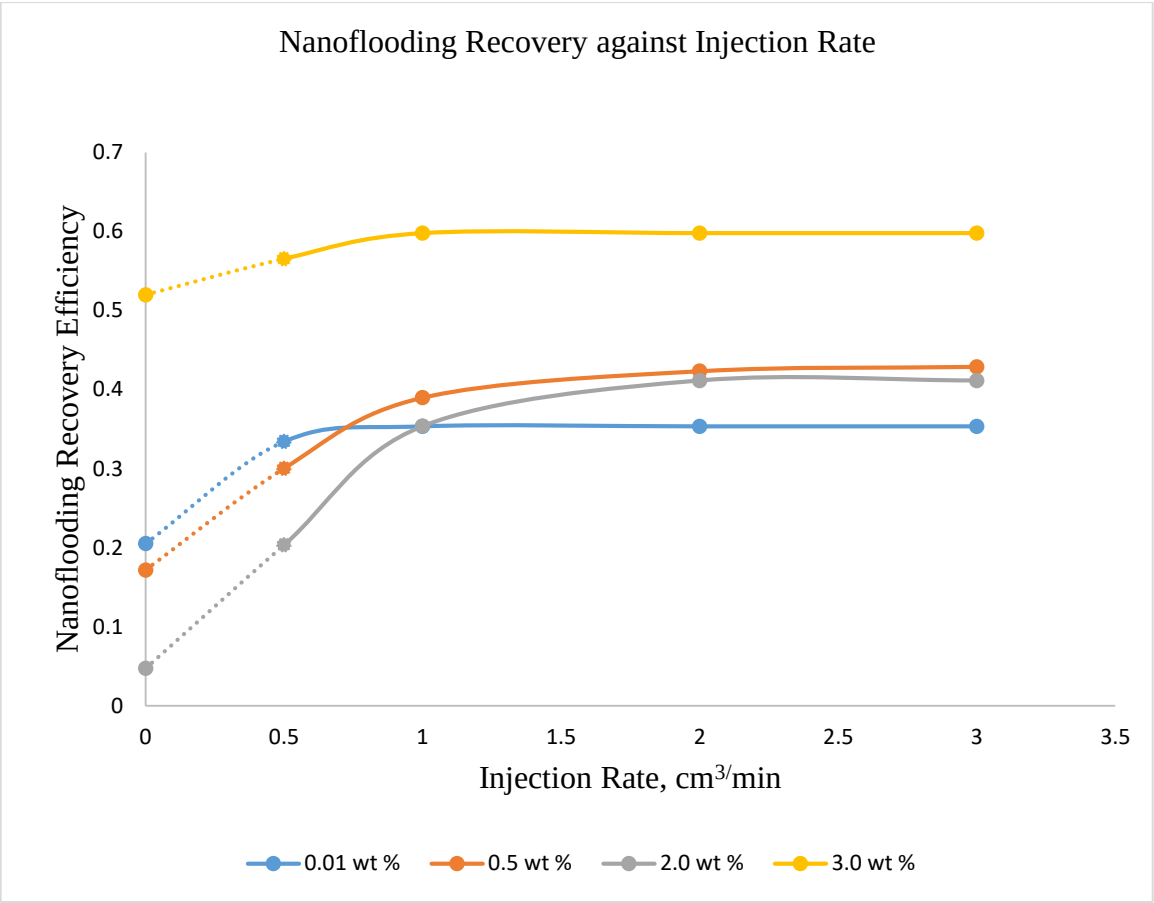

Fig. 4.5: Nanoflooding Recovery Factor against Injection Rate

4.7.4 Oil Recovery for Brine Flooding (Control)

The initial fluid saturations prior to flooding for samples Y5, Y6 and Y8 were 80.0%,77.9% and 77.4% respectively, as shown in Table 4.10. Samples Y5, Y6 and Y8 were flooded with different fluids and the recovery factor obtained after each flooding process was compared.

The secondary brine flooding experiment with sample Y5 was the control experiment. During the injection of the first 2 PV, two-phase flow of oil and brine existed in the porous medium, but only oil was recovered at the collector. This continued up until 3 PV when water breakthrough occurred; at this point, oil recovery factor was approximately 55.0 %. Oil and brine continued to flow as more PV of brine was injected up until 4.2 PV of brine had been injected. At this point, no oil was recovered at the collector and only brine continued to flow. Estimated oil recovery factor was 71.0 % while residual oil saturation was 28.9%. The sample Y5 was not used for tertiary nanofluid flooding as it served as a control sample.

Table 4.10: Initial Fluid Saturations of the Core Samples Y5, Y6 And Y8

Core Sample Number	**Pore Volume, cm^3**	**Water volume drained, cm^3**	**Connate water saturation, S_{wi} %**	**Initial oil saturation, S_{oi} %**
Y5	13.3	10.6	20.0	80.0
Y6	19.5	15.1	22.1	77.9
Y8	17.5	13.5	22.6	77.4

4.8 Nanofluid Flooding with Optimum Concentration and Injection Rate

The nanofluid flooding experiment was carried out using sample Y6 in order to establish oil recovery factor using the optimum nanofluid concentration of 2.00 % wt and injection rate, 2.0 cm^3/min, without prior secondary brine flooding. The ultimate recovery for the process stood at 65.0% which is 6.0% lower than that of the brine flooding process. This means that 35.0% of the oil pore volume still remained unswept after the process.

4.9 Nanofluid-Alternating-Brine Flooding (NABF)

From the nanofluid flooding experiment, the recommended optimum concentration for maximum oil recovery was 2.0 wt %. Although the nanofluid flooding yielded lower ultimate recovery compared to that of waterflooding, it was, however, observed that the alternation of the two flooding processes using sample Y8 resulted in an oil recovery factor far beyond what was obtained from each of the processes. The ultimate recovery was in the region of 85.0 % which translates to a final residual oil saturation of about 12.0 %.

The synergestic effect of NABF may be explained from the principle of adsorption and desorption. LHP nanoparticles adsorption results in wettability alteration or wettability accentuation and IFT reduction, thereby increasing relative permeability of oil. More so, when LHP nanoparticles are adsorbed on the pore walls, they may also be retained in the porous spaces causing displacement of oil globules along the pore throat and leading to increased effective oil pore diameter. However, total pore blockage may occur and cause trapping of some residual oil in the pores. The blockage forms a continuous thin sheet of nanoparticles referred to as nanoskin. When the nanofluid flooding is then succeeded by waterflooding, blockage reversal, due to breaking of the nanoskin by water invasion, may occur and cause displacement of the retained nanoparticles. The displacement of the nanoparticles is referred to as desorption. This explains perhaps, why additional recovery factor of about 10% was obtained after nanofluid flooding process was followed by waterflooding during the NABF experiment.

Figure 4.6 depicts the relationship between oil recovery factor and injected pore volume of fluid. It can be observed that oil recovery was the highest for secondary brine flooding up

until 5.7 PV of fluid was injected and a recovery factor of 71% was attained. Oil recovery continued to increase for NABF up until 12 PV at a recovery factor of about 85%. Single nanofluid flooding was observed to have the lowest oil recovery as injected PV of fluid increase. Oil recovery factor for single nanofluid flooding did not exceed 65%. Table 4.11 compares recovery efficiencies and residual oil saturations of the three flooding experiments, NABF had the highest ORF of 85% with a S_{or} of 11.6%; and surprisingly followed by BF which gave an ORF of 71% and S_{or} of 28.9%. The least favourable results were recorded for NF giving an ORF and S_{or} of 65.0% and 29.4% respectively.

The secondary BF had a higher ORF compared to NABF at lower PV of fluid injected because NABF recovery potential at low PV is limited. Interaction between nanoparticles in the nanofluid and reservoir rock, which causes wettability alteration, becomes more pronounced as the nanoparticles occupy more of the pore spaces.

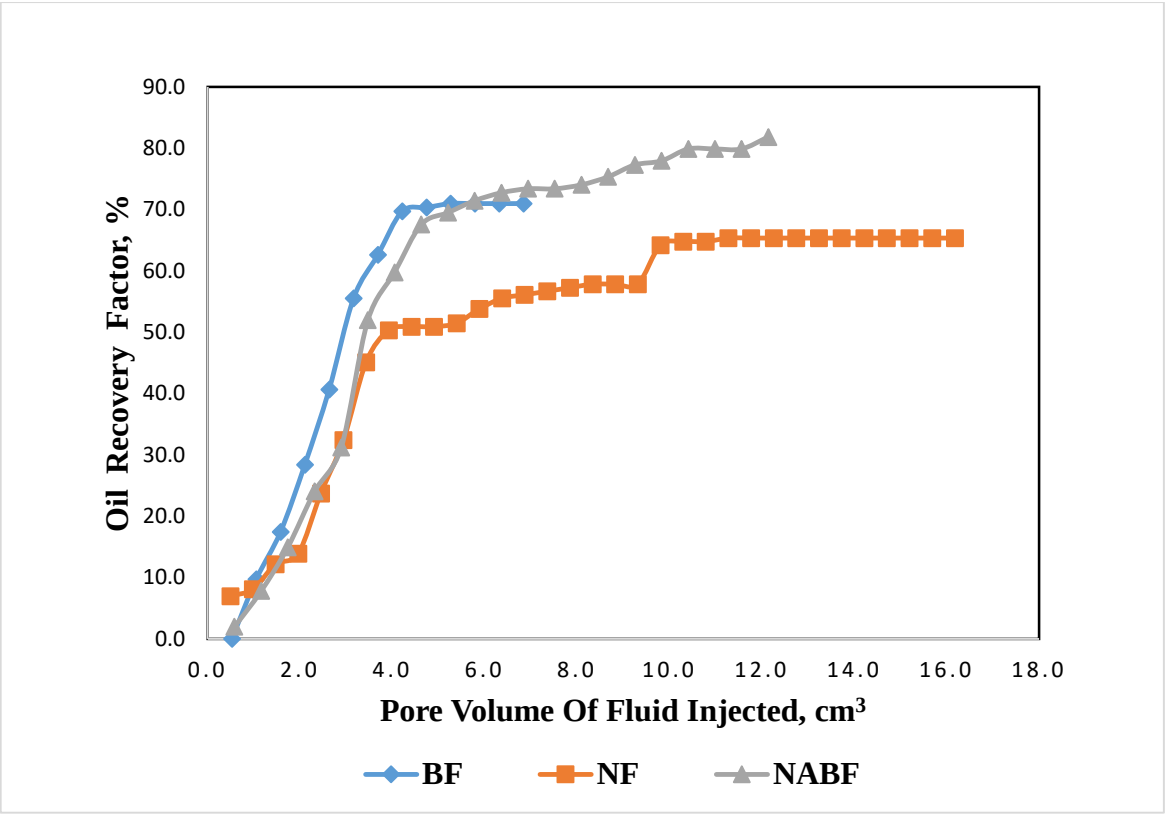

Fig. 4.6: Oil recovery performance against injected pore volume of fluid during BF, NF and NABF.

Table 4.11: Comparison of oil recovery efficiencies and residual oil saturations

Experiment	**ORF, %**	**S_{or}, %**
BF	71.0	28.9
NF	65.0	29.4
NABF	85.0	11.6

4.10 Scanning Electron Microscopy Results for BF, NF and NABF Experiments

Scanning Electron Miscroscope (SEM) was used to obtain high resolution images and compare the changes that occurred on the pore surfaces of each of the core samples (Y5, Y6 and Y8) used for the three flooding processes. Areas ranging from approximately 1 cm to 5 microns in width was imaged in a scanning mode using conventional scanning electron miscropy techniques (magnification ranging from 20X to approximately 30,000X, spatial resolution of 50 to 100 nm).

A thin section of each of the three core samples was analysed with SEM and the results at 5,000 magnification and resolutions of 2 μm are as depicted in Figures 4.7 (a) and (b), 4.8 (a) and (b) and 4.9 (a) and (b).

4.10.1 Brine-Flooded Core

Figure 4.7(a) shows the image of sample Y5 which represents the brine-flooded core sample. Figure 4.7(b) indicates the SEM image of the sample. The surface structure reveals loosely packed crystalline matrix of sub-rounded and sub-angular quartzite mineral particles. The cementation is uneven and apparently moderate as expected of most sandstone cores obtained from the Agbada formation in the Niger Delta area of Nigeria. The pore structure and matrix morphology reveals moderate interconnectedness. The red arrows show the pore surfaces and throats occupied by the residual oil after brine flooding.

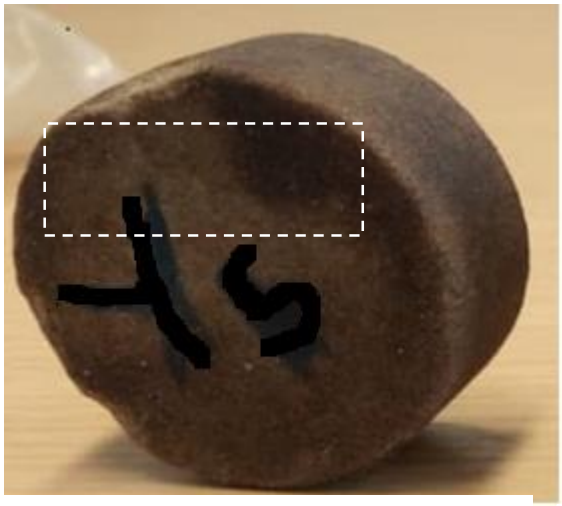

Fig. 4.7(a): Brine flooded sample to residual oil saturation

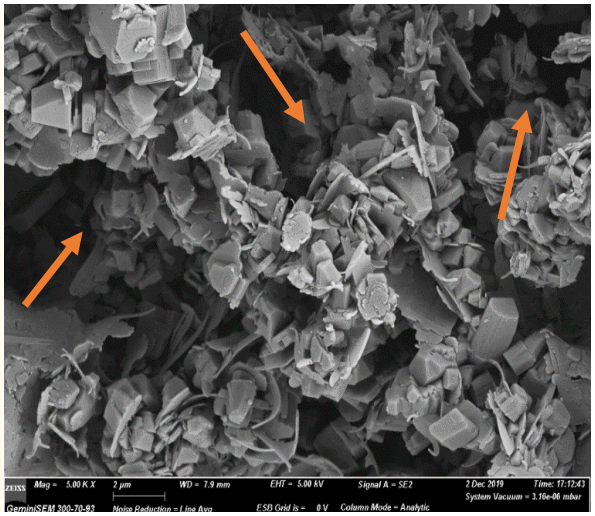

Fig. 4.7 (b): SEM image of sample Y5 (brine flooded sample) under resolutions of 2 µm and magnification of 5000x. The image shows entities such as pores, grain shapes and arrangements**.**

4.10.2 Nanofluid Flooded Core

Figure 4.8 (a) indicates the portion of sample Y6 marked out for SEM analysis. Figure 4.8 (b) reveals the SEM analysis with a superimposition of finer LHP nanoparticles on the surface matrix of the rock as shown by A, after flooding with nanofluid of concentration ranging from 0.01-3.0 wt %. The superimposed layer forms a nanoskin which causes permeability impairment and formation damage. B reveals a microfracture in the rock .

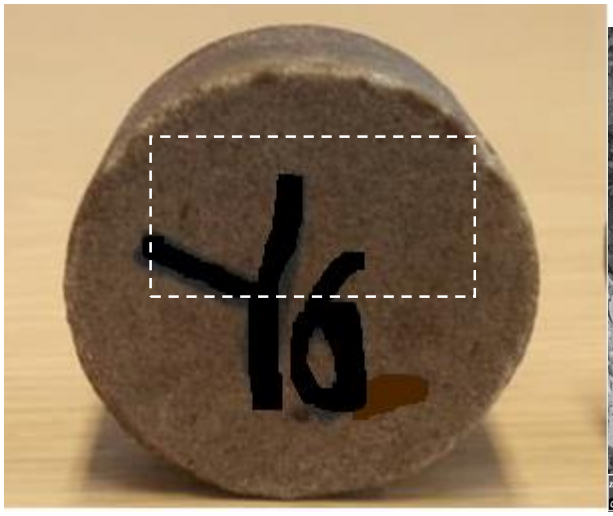

Fig. 4.8 (a): Nanofluid flooded core to residual oil saturation

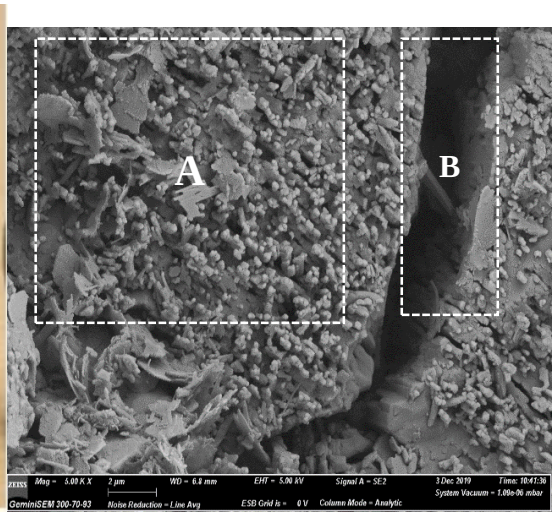

Fig. 4.8 (b): SEM image of sample Y6 under resolutions of 2 µm and magnification of 5000x. The image shows entities such as pores, grain shapes and arrangements. A shows the surface matrix and B shows the microcrack.

4.10.3 NAB Flooded Core

Figure 4.9 (a) reveals the portion of sample Y8 analysed with SEM. Figure 4.9 (b) shows the SEM image of the rock surface when flooded with brine after nanofluid flooding with the optimum concentration of 2.0 wt. %. The figure indicates no retention of the LHP nanoparticles on the pore surface of the rock. This confirms the optimality of the 2.00 wt. % concentration of the nanofluid for flooding the core under investigation and the desorption of adsorbed nanoparticles by brine. The red arrows show pore spaces or pore surfaces occupied by the residual oil after NABF. The green arrow shows a small unswept portion containing nanoparticle retention, too negligible to cause permeability damage.

Fig. 4.9 (a): NAB flooded core to residual oil saturation

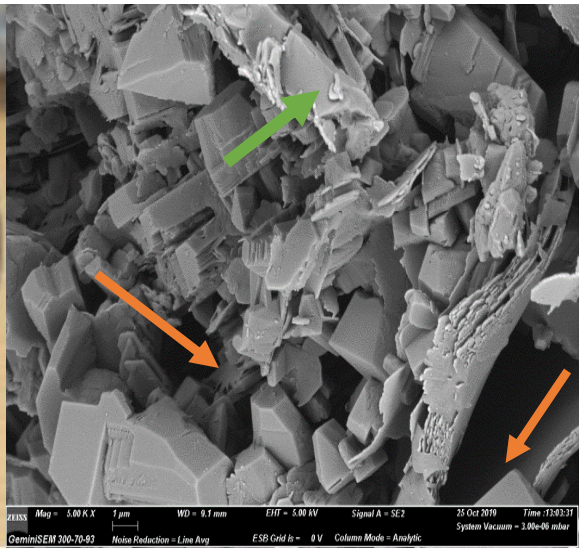

Fig. 4.9 (b): SEM image of sample Y8 under resolutions of 2 µm and magnification of 5000x. The image shows entities such as pores and grain shapes and arrangements.

4.11 Validation of the Model

Substituting all parameters except for q_{inj} and C_{nf} in equation (3.22), gives

$$S_n = 8.33X\ 10^{-4}\ q_{inj}\ /C_{nf} \quad (4.1)$$

The equation (4.1) is true for the limiting concentration of 2.0 wt%. This is because the values of S_n values for concentrations beyond 2.0 wt% are too far from the experimental results.

So using the nanofluids concentration and injection rates from the experiment, gives the results as shown in Table 4.12 (a). To validate the nanoskin factor obtained from the analytical equation, equation (3.26) is used, since ORF was a result generated from the experiment. The results are as shown in Table 4.12(b). Comparing the model and empirical results gives a standard mean error of 17.4%.

Table 4.12(a): Relationship of Nanoskin Factor with Nanofluid Concentration and Injection Rate

C_{nf}, wt %	$q_{inj,\ cm^3/min}$	S_n
0.01	0.50	0.0417
0.50	1.00	0.0017
2.00	2.00	0.0008

Table 4.12(b): Nanoskin Factor Oil Recovery Factor

ORF	**Sn**
0.129	0.0426
0.223	0.0015
0.354	0.0009

4.12 Technical Evaluation

4.12.1 Upscalng of NABF Input and Output Parameters

Table 4.12 (c) presents the average properties of the three core samples used for the BF, NF and NABF processes. The samples were slightly consolidated. Average porosity was 29.57%, average permeability was 1335.78 md.

Using equation (3.25), the incremental oil recovery was estimated. From Table 4.13 estimated incremental recovery from NABF was 14.89 MMbbls. This additional recovery from NABF could extend the life of the field an additional 10 years and guarantee more income which would have been impossible if the field had been abandoned after waterflooding. However, this volume could be subject to myriads of risks and uncertainties as a results of the uncertainties in the input parameters (porosity, draiange area, water saturation, net pay thickness) used for its the computation.

Table 4.14 depicts the results for upscaled pore volume of nanofluid injected from the core sample to reservoir size. Total pore volume required for injection was 580 million cubic metre. Equation (3.26) was used for the estimation.

Table 4.12(c): Average Properties of the Core

Dry weight, g	**Av. Length, cm**	**Av. Diameter, cm**	**Av. Grain Volume, cm^3**	**Av. Bulk Volume, cm^3**	**Av. Pore Volume, cm^3**	**Av. ϕ, %**	**Av. k (md)**	**Av. S_{wi}, %**
118.03	5.63	3.80	44.97	63.87	18.90	29.57	1335.77	21.50

Table 4.13: Estimated Incremental Oil Recovery from NABF

ORF_{NABF}	0.85
$ORF_{B.NABF}$	0.48
A, sq. metre	121,406
h , m	230
ϕ	0.30
Swi	0.22
N_{pNABF}, m^3	2,382,953.88
N_{pNABF}, MMbbls	14.89

Table 4.14: Estimation of the Reservoir Pore Volume of Nanofluid Injected

P_{VLN}, m^3	0.00013272
V_{BL}, m^3	6.39E-06
V_{BR},m^3	27,923,380.00
P_{VRN}, m^3	**580,239,704.65**

4.13 Economic Evaluation

4.13.1 Deterministic Approach

All costs incurred were estimated in $/bbl as shown in Tables 4.15, 4.16 and 4.17 below. In Table 4.15, the nanofluid cost was assumed to be $ 0.5/g based on current average global price. From the technical analysis, an average weight of 11,604,794.09 g would be required for the case field, translating into a total material cost of $5,802MM and a cost per barrel of $0.39, given the estimated reserves of 14.89 MM barrels. Table 4.16 reveals the costs (OPEX and CAPEX) required for implementing the NABF process. The unit OPEX and unit CAPEX were about $4.54/bbl and $34.91/bbl, respectively.

From the analysis, the deterministic or point-estimate threshold oil price that would justify implementing NABF in typical Niger Delta reservoir was $49.10/bbl (N20, 196.79/bbl). The global price of oil (brent) in current terms (January, 2022) is in the range $80.00/bbl - $86.00/bbl; this translates to the applicability of NABF in current economic scenario, since the computed threshold oil price for the process is lower. However, the recommendation may change if oil price dwindles. The deterministic approach for computing the oil price threshold did not account for uncertainties in the input parameters. Input parameters such as recovery factor, are subject to technical uncertainties and need to be defined within an acceptable historical range. In addition, other input data which are intrinsic in the estimation of reserves, such as oil saturation, porosity, drainage area and pay thickness are also subject to technical errors, hence there is need for them to be defined within minimum and maximum ranges based on history. The economic data which are based on costs (CAPEX, OPEX, costs of materials), are also prone to economic risks and uncertainties and as well, need to be defined within realistic highs and lows. This therefore, leads to the probabilistic analysis.

Table 4.15: Nanofluid Cost

Parameter	Value
Cost of nanofluid, $ /g	0.5
W_{np}, g	11,604,794.09
C_{nf}, $	5,802,397.05
C_{nf}, $/bbl	**0.39**

Table 4.16: CAPEX and OPEX Data

Parameter	Value
CAPEX, $	520,000,000.00
Unit CAPEX, $/bbl	34.91
Fixed OPEX, $	26,000,000.00
Variable OPEX, $/foot	8,330.00
Variable OPEX, $/m	27,329.40
TVD, ft	5000.0
TVD, m	1524.0
Variable OPEX, $	41,650,000.00
Total OPEX, $	67,650,000.00
Unit OPEX, $/bbl	4.54

Table 4.17: Cost and Threshold Oil Price Per Barrel

C_T, $/bbl	39.37
P_{OT}, $/bbl (zero profit margin)	49.10

4.13.2 Probabilistic Approach

1. Risked Oil Recovery or Reserves for NABF

The assumptions for the probabilistic approach are as shown in Tables 4.18 and 4.19. Figures 4.10 (a) to (f) give the distribution of each of the risked input parameters for the estimation of reserves for NABF. Figure 4.10 (a) illustrated that P10 and P90 values for NABF recovery efficiency were 95.9% and 74.1 % respectively. Figure 4.10 (b) indicates that cumulative recovery efficiency before NABF had P10 and P90 values of 54.4% and 41.6% respectively. Figure 4.10 (c) shows that P10 and P90 values for the drainage area, A, were 680 sq. m and 707sq. m, respectively. Figure 4.10 (d) shows that P10 and P90 values for reservor thickness, h, were 255.6 m and 204.4 m, respectively.The P10 and P90 values for porosity, Φ, were 32.1% and 27.0%, respectively as shown in Figure 4.10 (e) while the P10 and P90 values for connate water saturation, Sw, were 20.9%, and 23.1%, rspectively.

Figure 4.11 reveals the cumulative ascending probability curve of oil recovery for NABF. The P10 (possible) value was 41.10 MMbbls while the P90 (proved) value was 18.80 MMbbls. In fact, the deterministic value of 14.89 MMbbls never fell within the range between the possible and proved values obtained in the probabilistic analysis. The deterministic value of 14.89 MMbbls was therefore a conservative estimate, as compared to the P90 and P10 values which were determined after the incorporation of risks to the input data for the reserves computation . This is suggestive that the case field is a good prospect for NABF.

Table 4.18: Input Assumptions and Results for Probabilistic Estimation of Oil Recovery after NABF

Parameter	Deterministic Value	Function	Minimum	Mean	Maximum
ORF_{NABF}	0.85	RiskNormal (0.85, 0.085)	-∞	0.85	+∞
ORF_{BNABF}	0.48	RiskNormal (0.48, 0.048)	-∞	0.48	+∞
A, sq. metre	121,406	RiskLognormal(121,406, 12140.6)	-∞	121,406	+∞
h , m	230	RiskNormal (230,20)	-∞	230	+∞
ϕ	0.30	RiskNormal (0.30, 0.02)	-∞	0.03	+∞
Swi	0.22	RiskTriangle (0.20, 0.22, 0.24)	0.20	0.22	0.24
N_{pNABF}, m^3	2,382,953.88				
N_{pNABF}, MMbbls	14.89		18.80		41.10

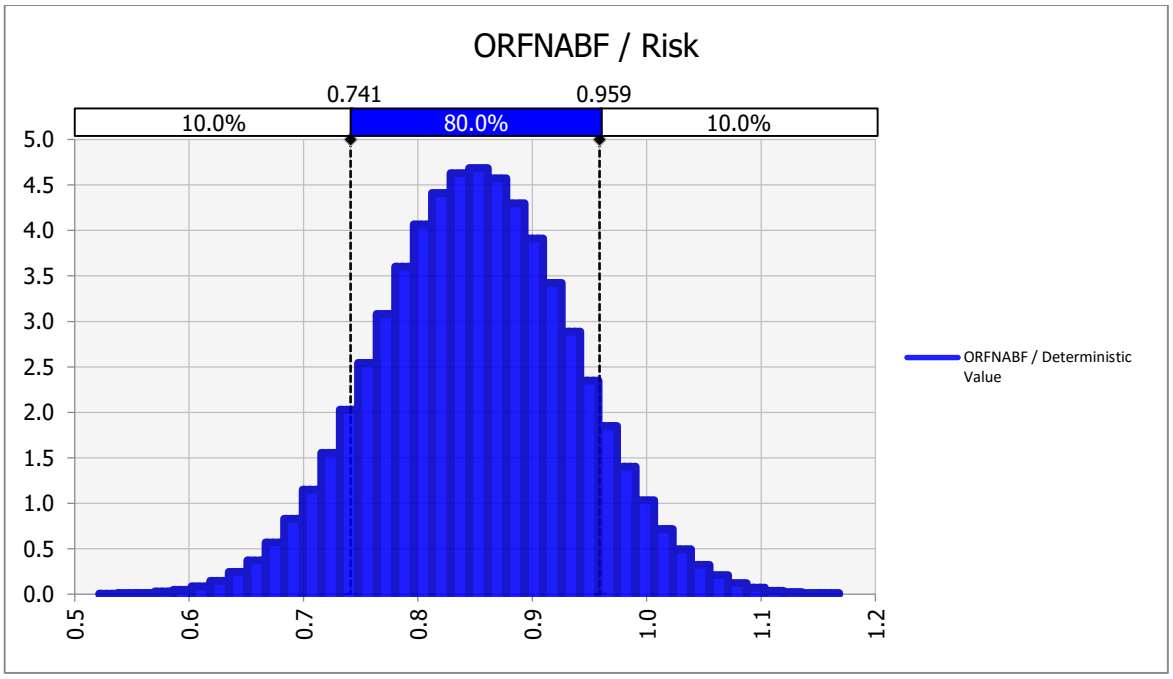

Fig. 4.10 (a): Distribution of Input Parameter (ORFNABF) for NpNABF (P10=0.959, P90=0.741)

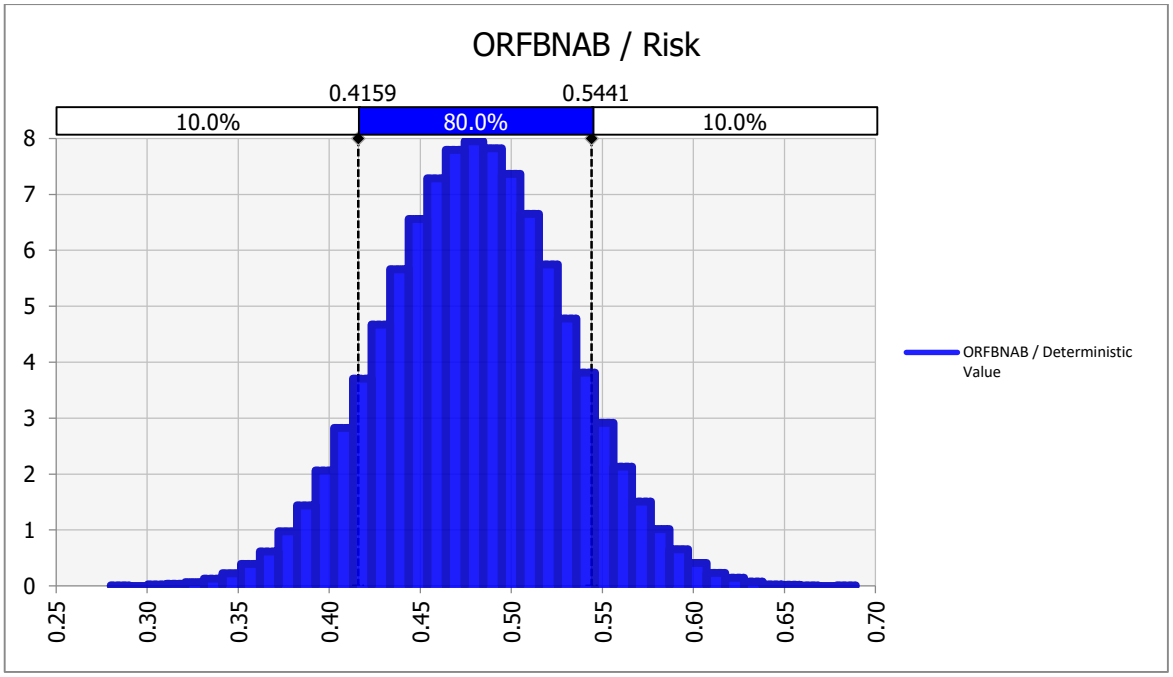

Fig. 4.10 (b): Distribution of Input Parameter (ORFBNABF) for NpNABF

(P10=0.544, P90=0.416)

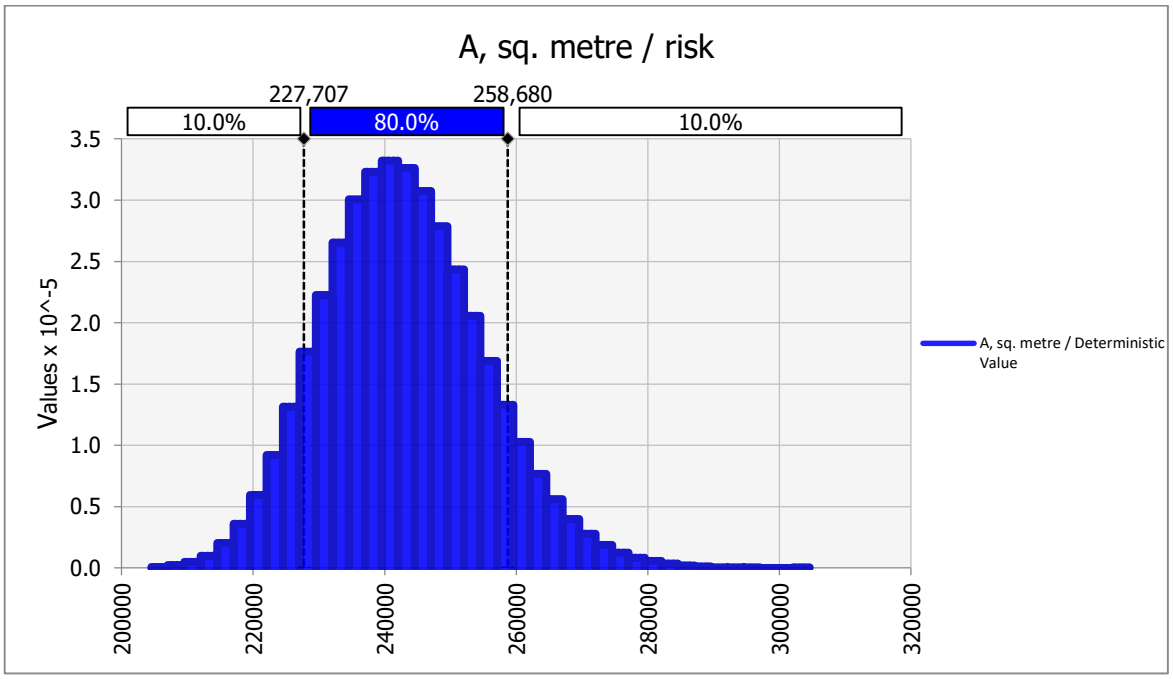

Fig. 4.10 (c): Distribution of Input Parameter (A) for NpNABF (P10=28,680 sq. m, P90=227,707sq. m)

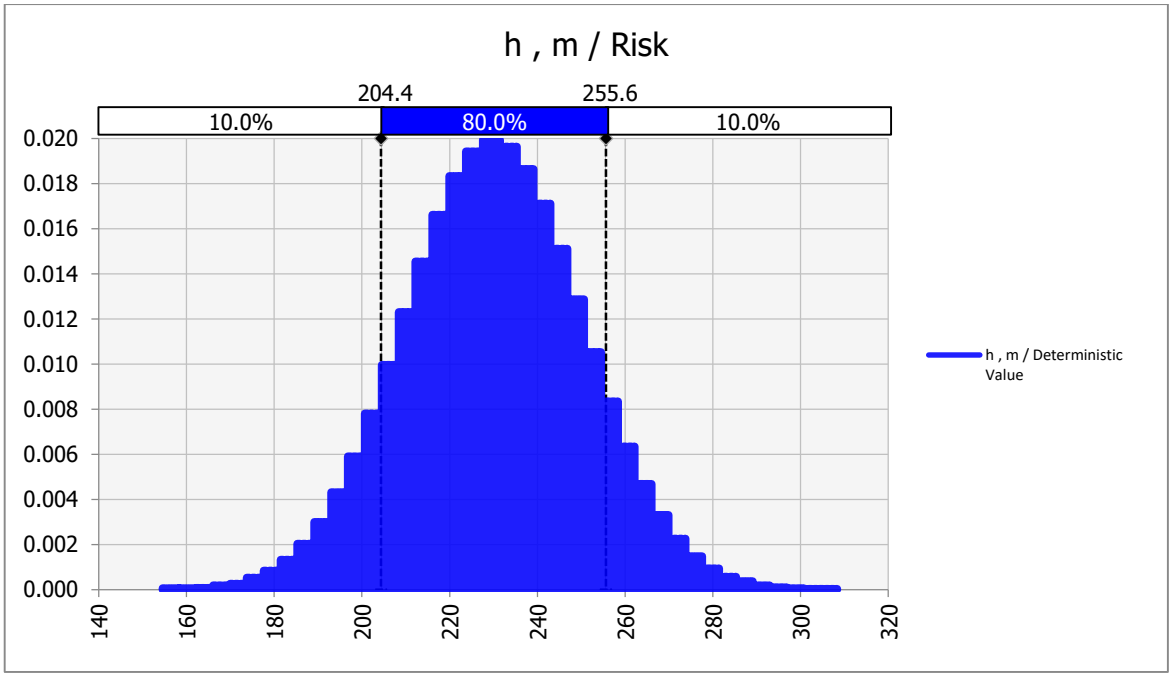

Fig. 4.10 (d): Distribution of Input Parameter (h) for NpNABF (P10=255.6 m, P90=204.4 m)

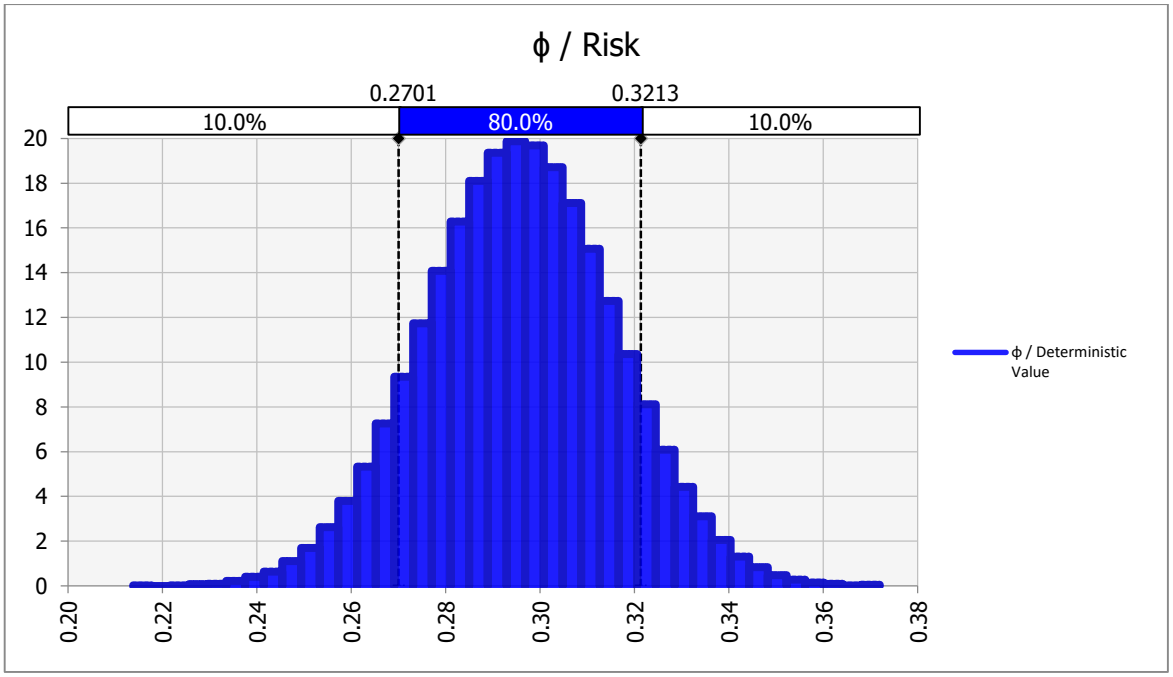

Fig. 4.10 (e): Distribution of Input Parameter (ϕ) for NpNABF (P10=32.1%, P90=27.0%)

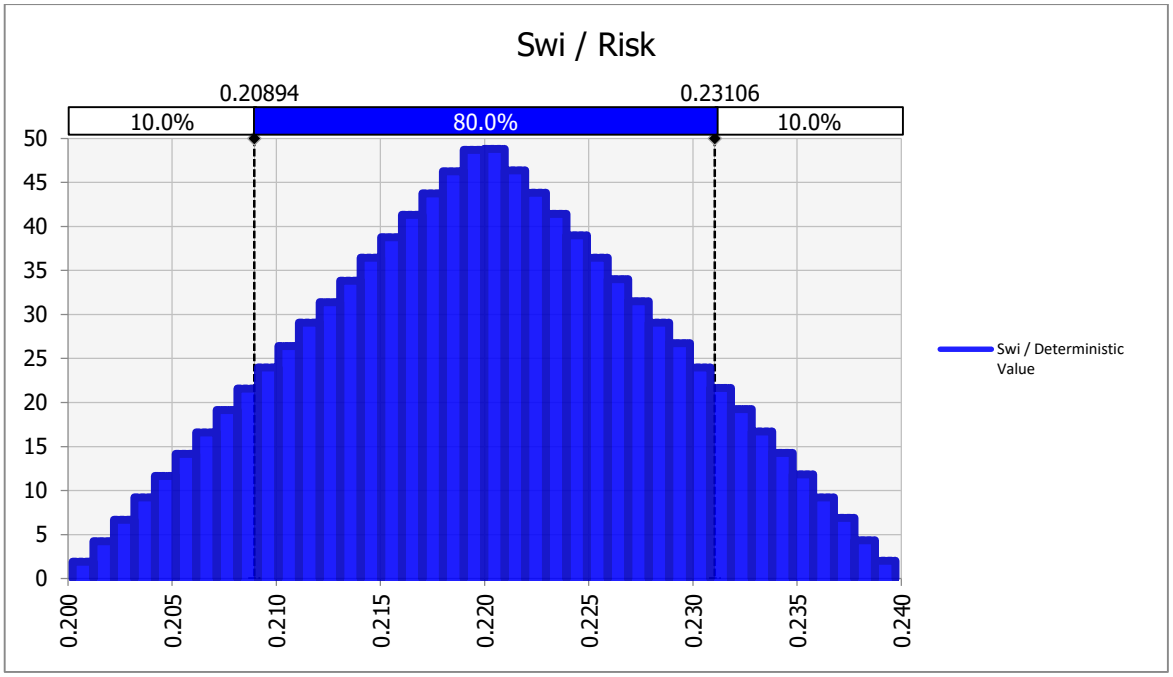

Fig. 4.10 (f): Distribution of Input Parameter Sw for NpNABF (P10=20.9%, P90=23.1%)

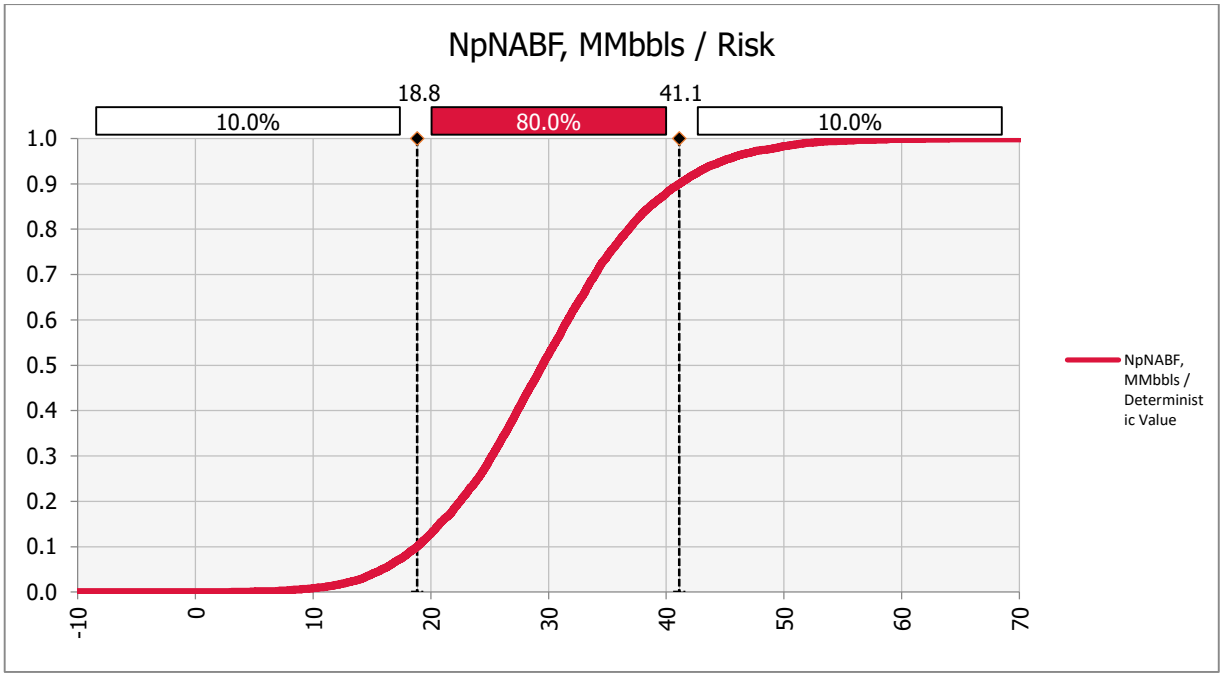

Fig. 4.11: Cumulative Ascending Probability Curve for Oil Recovery after NABF

2. Risked Threshold Oil Price

The risked or probabilistic threshold oil price is estimated using the risked input variables. These include the reserves, cost of materials, variable OPEX and CAPEX. Fixed OPEX was not part of the risked input avriables because of the assumption of its dependence on CAPEX . However, in the long run, the assumption may be far from true. The deterministic, P10 and P90 values of the risked input variables are as depicted in Table 4.19. Figures 4.11, 4.12, 4.13, 4.14, representing reserves, cost of materials, variable OPEX, CAPEX respectively; indicate the assumed distribution for the input data into the model. Monte Carlo Simulation was executed in 5000 iterations and the results obtained are as shown in Figures 4.15 and 4.16 below.

Table 4.19: Summary of Input Variables for the Threshold Oil Price E

	Deterministic		
Parameter	**Value**	**P90**	**P10**
Reserves, MMbbls	14.89	18.8	41.1
Cost of Materials, C_N, $/bbl	0.39	0.25	0.55
Total cost of Materials, MM$	5.80	5.06	6.55
Variable OPEX per depth, $/foot	8,330.00	8,257.00	9,422.00
Variable OPEX per depth, $/m	27,329.40	22,827.00	30,832.00
TVD, ft	5000.00	5000.00	5000.00
TVD, m	1524.00	1524.00	1524.00
Unit Variable OPEX, $/bbl	2.78	1.80	4.50
Unit CAPEX, $/bbl	34.91	31.70	89.87
Total CAPEX, MM$	520.00	774.00	892.00

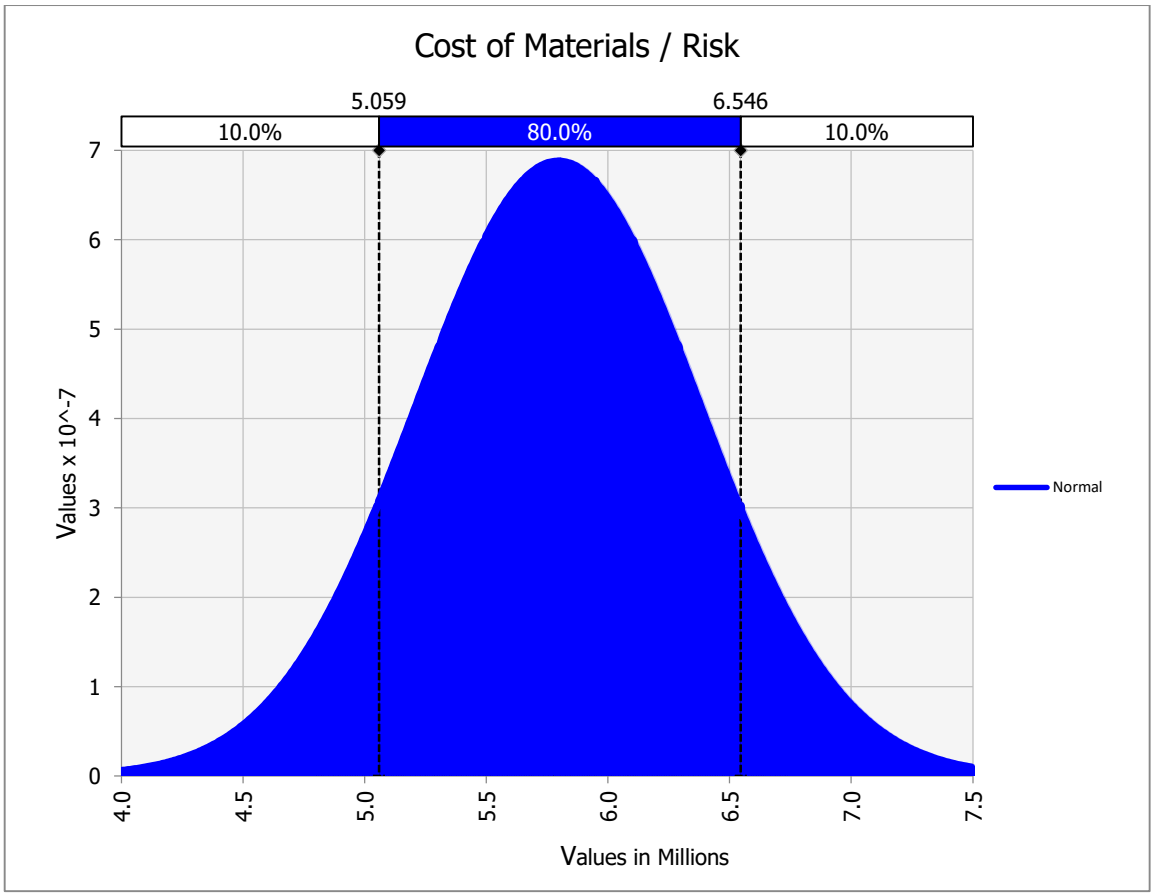

Fig. 4.12: Normal Distribution showing Variability in of Materials, $

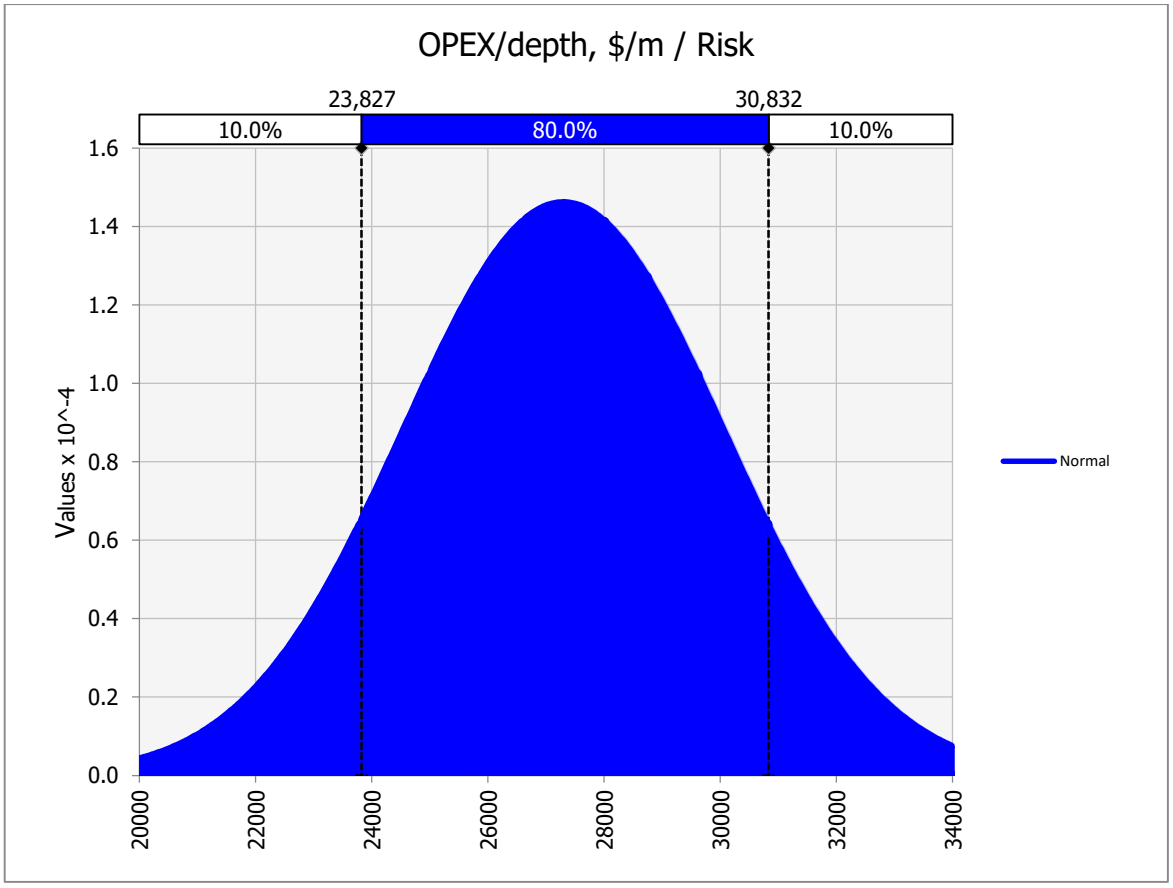

Fig. 4.13: Normal Distribution showing Variability in Injection OPEX/depth ($/m)

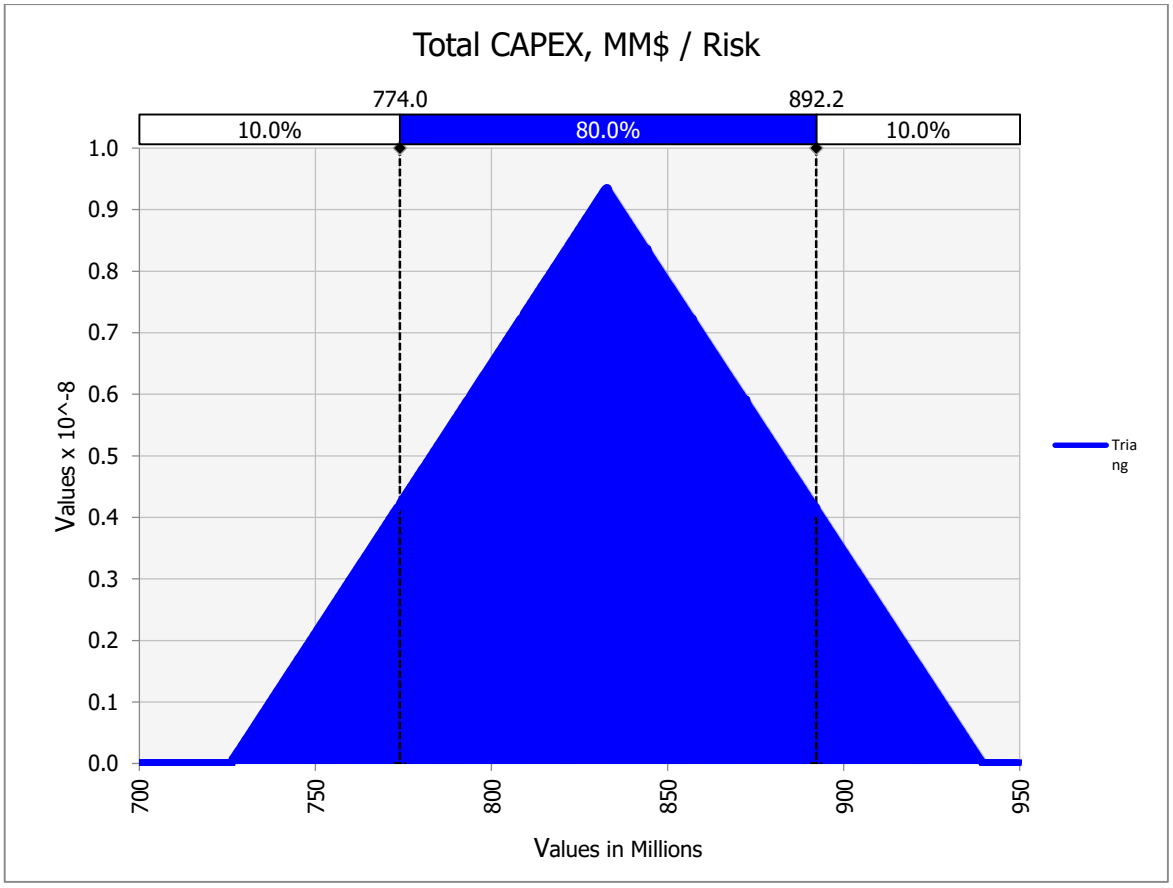

Fig. 4.14: Normal Distribution showing variability in Total Injection CAPEX, MM$

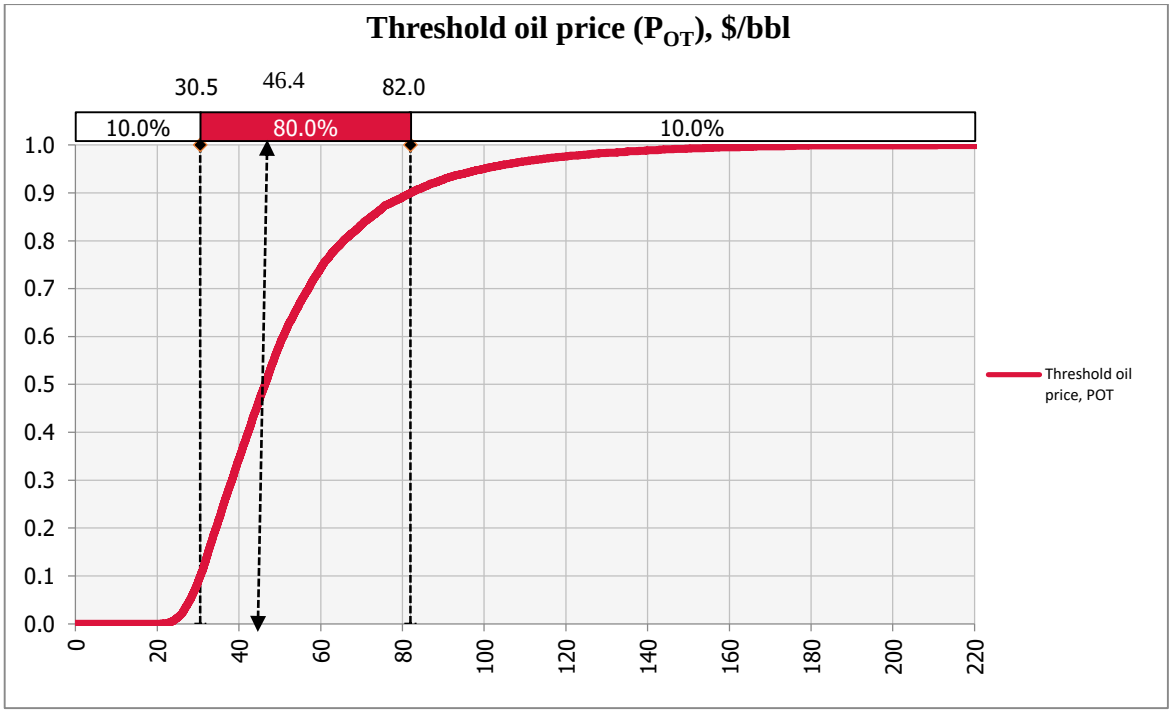

Fig. 4.15: Cumulative Asecnding Probability Curve for P10, P50 and P90 Threshold Oil Price, $/bbl.

From Figure 4.15, the optimistic oil price, P10, could be read off as $30.50/bbl. This means given low cost conditions, an oil price as low as $30.50/bbl would justify the implementation of NABF. The most likely threshold oil price, P50, was $46.10/bbl . The P90 indicates the pessimistic scenario which could be read off as $81.20/bbl. This is a red light for the applicability of NABF. It suggests that in high cost conditions, oil price may have to be as high as $81.20 before NABF could be implemented. The deterministic threshold oil price of $49.10/bbl lied between the P10 and P90 values.

Figure 4.16 below shows the impact analysis of the input variables on the threshold oil price, on a tornado diagram.. It could be observed that reserves have more spread than the total CAPEX , which in turn, has more spread than the variable OPEX. This means that reserves have more mpact on the threshold oil price compared to other input variables, hence, have the most effect on the profitability of NABF. Considerable atttention must therefore, be given to oil recovery factor as well as other input variables for reserves calculation, to prevent unrealistic estimations.

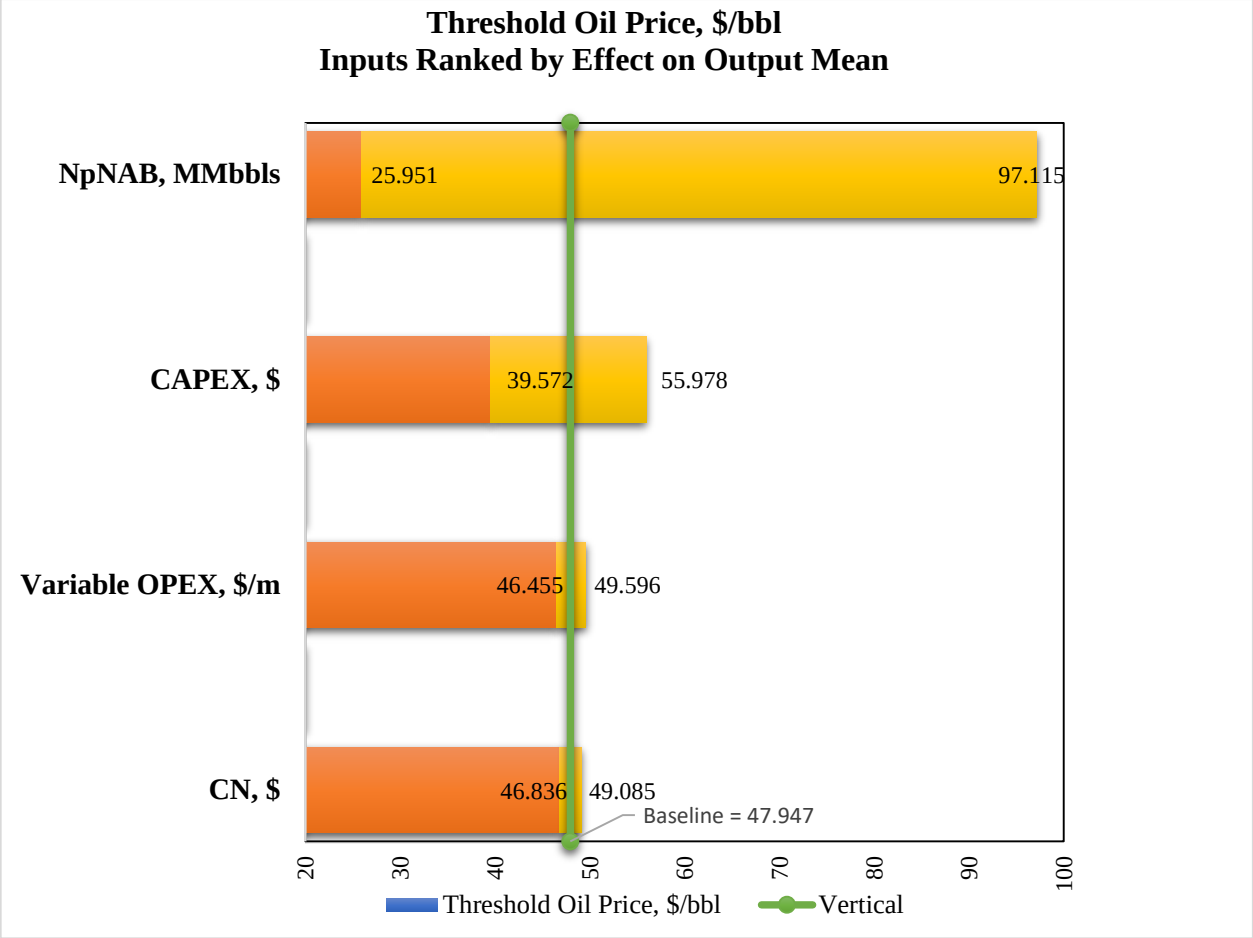

Figure 4.16: Tornado Diagram showing the impact of the input variables on Threshold Oil Price

CHAPTER FIVE

SUMMARY, CONCLUSION AND RECOMMENDATIONS

5.1 Summary

The study established the applicability of a novel nanofluid-alternating-brine flooding in Niger Delta reservoirs from both the technical and economic perspectives. The crux of the technical perspective was to be able to establish the potential of the novel synergism of brine and nanofluid flooding for the prevention or reversal of permeability impairment which arises during single nanofluid flooding especially at high concentration and low injection rate. The permeability impairment results from continuous deposition of nanoparticles at rock pore surfaces and throats; described by a novel concept nanoskin. In the same way, the intent of the economic perspective was to establish the threshold oil price for the implementation of the novel technique if at all it would be technically feasible.

The potential of nanofluid flooding was investigated based on two important factors which were nanofluid parameters *viz.*, nanofluid concentration and injection rate. Rock and fluid properties of typical reservoirs in Niger Delta were used with the assumption of generalising these properties across all fields in the Niger Delta. The study was therefore limited to reservoirs in the Niger Delta which have similar reservoir and fluid properties to the ones investigated. Porosity and liquid permeability for the samples were 17.0 - 30.0 % and 1,104.9 - 1,584.0 md, respectively. The densities of crude oil and brine were 0.88 and 1.02 g/cm^3, respectively.

In addition, the study was extended to stipulating threshold or minimum oil price for profitable implementation of the nanofluid-alternating-brine flooding process if at all it scales through the technical hurdle. This is highly imperative as it helps the investor to make informed decision. The economic analysis was not limited to point estimate (deterministic),

its purview was widened to incorporate risks from the uncertain variables such as reserves, CAPEX and OPEX.

5.2 Conclusion

From the technical and economic analysis, it can be concluded that:

1. Brine flooding (control experiment) yielded an average oil recovery factor of 71.0%.
2. Nanofluid flooding with concentration range of 0.01-3.00 wt% and injection rate range of 0.5-3.0 cm^3/min yielded an average maximum oil recovery factor of 65.0%, achieved at optimal concentration and injection rate of 2.00 wt % and 2.0 cm^3/min, respectively.
3. Nanofluid-alternating-brine flooding at the optimal nanofluid concentration and injection rate yielded an average oil recovery factor of 85.0%
4. Nanofluid-alternating-brine flooding as compared to brine flooding and single nanofluid flooding processes yielded ultimate oil recovery factor of 14.0% above that of the former and 20.0% above that of the latter.
5. Analyses of the Scanning Electron Microscopy image of the core sample after nanofluid flooding revealed permeability impairment as compared to brine flooding and nanofluid-alternating-brine flooding. The nanoskin effect which causes permeability damage in single nanofluid flooding was minimised using the nanofluid-alternating-brine flooding.
6. The analytical model derived for the nanoskin factor gave comparable results with the experimental results, although with a standard mean error of 17.4%.
7. The novel enhanced oil recovery technique is implementable within the threshold oil price N20,196.79/bbl ($49.10/bbl) using deterministic approach.
8. Risk assessment on profitability of nanofluid-alternating-brine flooding revealed that, threshold oil price ranged from 12,545.87/bbl to N33,400.81/bbl (30.50 to $81.20/bbl), with oil recovery factor as the variable with the highest impact on threshold oil price ($1= N411.34).

9. Nanofluid-alternating-brine flooding is a novel enhanced oil recovery technique with higher recovery potential than single nanofluid flooding and waterflooding. The nanoskin effect which causes permeability damage in single nanofluid flooding was minimised using the novel flooding technique. Nanofluid-alternating-brine flooding is therefore a profitable enhanced oil recovery technique that can be applied in Niger Delta sandstone formations.

5.3 Recommendations

Lipophobic Hydrophilic Polysilicon (LHP) nanoparticles have the potentials of improving recovery in sandstone rocks. A concentration window of 0.01-2.00 wt% is recommended for silica nanofluid recovery process in Niger Delta Sandstone reservoirs. An injection rate window of 0.5-2.0 cm^3/min is also recommended under the same recovery process.

For optimal recovery, a combination of 2.00 wt% concentration and 2.0 cm^3/min silica nanofluid injection rate serves as threshold values to prevent the formation of nanoskin that may damage the formation due to permeability reduction. The concept of nanoskin was introduced by the author and is defined as a thin sheet of nanoparticles deposited and retained in the rock pore surfaces and throats during nanofluid flooding which causes porosity and permeability impairment and subsequent formation damage.

The novel enhanced oil recovery technique is implementable within the range of $30.50/bbl and $82.10/bbl. The threshold oil price is highly dependent on the investor's profit margin. It can be as high as twice the total cost per barrel if profit margin is 20% of the oil price. More so, the injection depth also plays a critical role in determining the variable OPEX. Hence, NAB flooding is more favourable in shallower reservoirs as threshold oil price of implementation would be lower.

5.4 Contributions to Knowledge

The challenge of permeability damage due to nanoskin formation has been one of the limitations of single nanofluid flooding. However, the study went a step beyond the conventional single nanofluid flooding by investigating nanofluid-alternating-brine

flooding, a novel synergistic flooding technique, to overcome the problem of nanoskin formation. More so, the threshold oil price for implementation of the technique was equally stipulated within an acceptable range using the probabilistic approach. This was also a step beyond the conservative deterministic method. The study has been able to prove that nanofluid-alternating-flooding process is technically feasible and economically viable within the threshold oil price range defined.

5.5 Suggestions For Further Study

The concept of nanoskin formation is not limited to injection rate and concentration alone. It may further be extended to properties of the reservoir rock, reservoir fluid and nanoparticles such as pressure, rock grain size, salinity, temperature, clay content and other key factors that affect any enhanced oil recovery process. The additional recovery obtained for nanofluid-alternating-brine flooding may be explained by the mechanism of adsorption and desorption of nanoparticles during the alternate flooding process. However, there is need to be able to prove the mechanism experimentally, hence, future study could also be extended to micro-pore studies to understand, establish and measure the effects of mechanisms in operation during nanofluid-alternating-brine flooding.

REFERENCES

Agi, A., Junin, R. and Gbadamosi, A. 2018. Mechanism Governing Nanoparticle Flow Behaviour in Porous Media: Insight for Enhanced Oil recovery Applications. *Int Nano Lett* **8:** 49–77. https://doi.org/10.1007/s40089-018-0237-3

Ahmed, T. 2010. Reservoir Engineering Handbook. 2010. Elsevier Inc. Doi:10.1016/C2009-0-30429-8

Ajulibe, D., Ogolo, N. and Ikiensikimama, S. 2018. Viability of SiO_2 Nanoparticles for Enhanced Oil Recovery in the Niger Delta: A Comparative Analysis. Paper presented at the SPE Nigeria Annual International Conference and Exhibition, Lagos, Nigeria, August 2018. Paper Number: SPE-193423-MS. https://doi.org/10.2118/193423-MS

Akanji, L. T., Rehman, R., Onyemara, C. C., Ebel, R. and Jamal, A. 2021. A novel technique for interface analysis: Behaviour of sophorolipids biosurfactant obtained from Meyerozyma spp. MF138126 during low-salinity heavy-crude experiments. Fuel, 297, 120607. doi:10.1016/j.fuel.2021.120607

Akintola, S., Akpabio, J., Nduamaka, F. 2015. Determination of Some Petrophysical Properties of Reservoir Rocks in the Niger Delta. Journal of Scientific Research & Reports. ISSN: 2320-0227. 5.5: 388-401.

Alkhatib, A.M. and King, P.R. 2011. Applying real options theory in determining optimal policies for a surfactant flood. Society of Petroleum Engineers - SPE Enhanced Oil Recovery Conference, EORC 2.

Almahfood, M. and Bai, B. 2018. The Synergistic Effects of Nanoparticle-Surfactant Nanofluids in EOR Applications. Journal of Petroleum Science and Engineering. 171: 196-210. ISSN 0920-4105. https://doi.org/10.1016/j.petrol.2018.07.030.

Anderson, W. G. 1987. The Effect of Wettability on Capillary Pressure. Wettability Literature Survey. *Journal of Petroleum Technology*. 39.4: 1283–1300.

Aurel Carcoana. 1992. Applied Enhanced Oil Recovery. Prentice-Hall Inc. Library of Congress in Cataloguing-in-Publication data.

Beka, F. T. and Oti, M. N. 1995. The distal Offshore Niger Delta: Frontier Prospects of a Mature Petroleum Province, in, Oti, M.N., and Postma, G., eds., Geology of Deltas: Rotterdam, A.A. Balkema. 237-241.

Chengara, A., Nikolov, A., Wasan, D.T., Trokhymchuck, A. and Henderson, D. 2004. Spreading of Nanofluids driven by the Structural Disjoining Pressure Gradient. J. Colloid Interface Sci. 280: 192–201.

Clark, P.D., Clarke, R.A., Hyne, J.B. and Lesage, K.L. 1990. Studies on the Chemical Reactions of Heavy Oils under Steam Stimulation Conditions. *AOSTA J* Res 6.1: 29-39.

Cocuzza, M., Pirri, F., Rocca, V. and Verga, F. 2011. Is the Oil Industry Ready For Nanotechnologies? Offshore Mediterranean Conference and Exhibition in Ravenna, Italy, March 23-25.

Dahle, G.S. 2014. Investigation of how Hydrophilic Silica Nanoparticle affects Recovery in Berea Sandstone: An Experimental Study. Master Thesis, Department of Petroleum Engineering and Applied Geophysics, Norwegian University of Science and Technology.

Das, S.K., Choi, S.U.S., Yu, W. and Pradeep, T. 2008. Nanofluids Science and Technology. John Wiley & Sons, Inc. Publishing, Hoboken, NJ, ISBN: 0470074736.

Devendiran, D.K. and Amirtham, V.A. 2016. A review on Preparation, Characterization, Properties and Applications of Nanofluids. Renew. Sustain. Energy Rev, 60: 21–40.

Donaldson, E.C., Chilingarian, G.V. and Yen, T.F. 1989. Enhanced Oil Recovery II, Processes and Operations. Elsevier Science Publ. Co., New York.

Doust, H. 1990. Geological Society, London. Shell International, Hague. Special Publications. 50:365. January 1. https://doi.org/10.1144/GSL.SP.1990.050.01.21

Doust, H., Omatsola, E. 1990. Niger Delta, in J.D. Edwards and P. A. Santogrossi, eds., Divergent/Passive margin basins: American Association of Petroleum Geologists. Memoir 48: 201-236.

Edwards, J.D. and Santogrossi, P.A. 1990. Summary and Conclusions. In: Edwards, J.D. and Santogrossi, P.A., Eds., Divergent/Passive Margin Basins, AAPG, Tulsa. Memoir 48: 239-248.

Ekweozor, C.M. and Okoye, N.V. 1980. Petroleum Source-bed Evaluation of Tertiary Niger Delta: American Association of Petroleum Geologists Bulletin. 64:1251-1259.

El-Diasty, A.I. 2015. The Potential of Nanoparticles to Improve Oil Recovery in Bahariya Formation in Egypt: An Experimental Study. *SPE 174599. DOI:10.2118./174599 MS*

El-Diasty, A.I. and Aly, A. M. 2015. Understanding the Mechanism of Nanoparticles Application in Enhanced Oil Recovery. *SPE North Africa Technical Exhibition and Conference held at Cairo, 14-16, September.*

Enslayed, R. and Fattah, A. 2014. A Comparative Study between Nanoparticles Method and other Methods for increasing Heavy Oil Recovery. *M.Sc. thesis*, Suez University.

Evamy, D.D., Haremboure, J., Wikanerling, P., Knaap,W.A., Lolloy, F.A., and Rowlands, P.H. 1978. Hydrocarbon Habitat of Tertiary Niger Delta: American Association of Petroleum Geologists Bulletin. 62.1: 139.

Greff, J.F. and Babadagli, T. 2011. Catalytic Effect of Nano-size Metal Ions in Breaking Asphaltene Molecules during Thermal Recovery of Heavy Oil. *SPE 146604, DOI: 10.2118/146604 MS.*

Hendraningrat, L., Li. S, Torsaeter.O. 2013a. A Coreflood Investigation of Nano Enhanced Oil Recovery. *Journal of Petroleum Science and Technology* 111: 128–138.

Hendraningrat, L., Torsaeter, O., and Li, S. 2013b. A Coreflood investigation of Nanofluid Enhanced Oil Recovery in Low-Medium Permeability Berea Sandstone. *DOI: 10.2118/164106-MS.*

Jikich. S.J. 2012. CO_2 EOR: Nanotechnology for Mobility Control Studied, Technology Update, National Energy Technology Laboratory, US Department of Energy.

Joshi S., Castanier, L. M. and Brigham, W.E. 1998. Techno-Economic and Risk Evaluation of an EOR project. Society of Petroleum Engineers - SPE India Oil and Gas Conference and Exhibition held in New Delhi, India, 17-19 Feb.

Ju, B. and Dai, S.G. 2002. A Study of Wettability and Permeability Change Caused by Adsorption of Nanometer Structured Polysilicon on the Surface of Porous Media. Paper SPE-77938, presented at SPE Asia Pacific Oil and Gas Conference and Exhibition, Melbourne, Australia, 8-10 October.

Ju, B. and Fan, T. 2009. Experimental study and mathematical model of nanoparticle transport in porous media. *Powder Technology* 192: 195-202.

Ju, B., Fan, T. and Ma, M. 2006. Enhanced Oil Recovery by flooding with Hydrophilic Nanoparticles. *China Particuology* 4.1: 41-46.

Kapusta, S., Balzano, L. and Te Riele, P. M. 2011. Nanotechnology Applications in Oil and Gas Exploration and Production. Paper presented at *International Petroleum Technology Conference.* Bangkok, Thailand. 7-9 February.

Khilar, K. C. and Fogler, H. S. 1999. Migration of Fines in Porous Media. *Dordrecht: Kluwer Academic Pub.* 12: 30-52.

Klaine, S. J., Alvarez, P. J. J, Batley, G. E., Fernandes, T. F., Handy, R. D., Lyon, D. Y., Mahendra, S., McLaughlin, M. J. and Lead, J. R. 2008. Nanomaterials in the environment: Behaviour, fate, bioavailability, and effects. *Environmental Toxicology and Chemistry*. 27. 9: 1825-1851.

Kodukoli, P. and Papudesu, C. 2006. Project Valuation Using Real Options: A Practitioner's Guide. J. Ross Publishing, Inc. USA. ISBN 1-932159-43-6. 70-74

Kulke, H. 1995. Nigeria, *in*, Kulke, H., ed., Regional Petroleum Geology of the World. Part II: Africa, America, Australia and Antarctica: Berlin, Gebrüder Borntraeger. 143-172.

Latil, M., Bardon, C., Burger, J. and Sourieau, P. 1980. Enhanced Oil Recovery. Imprimerie Louis-Jean, 05002 Gap, France. ISBN 2-7108-0381-X. 208

Li, S., Hendraningrat, L. and Torsaeter, O. 2013. Improved Oil Recovery by Hydrophilic Silica Nanoparticles Suspension: 2-phase Flow Experimental Studies. Presented at International Petroleum Technology Conference. Paper Number: IPTC-16707-MS. https://doi.org/10.2523/IPTC-16707-MS. URL http://www.onepetro.org/mslib/app/Preview.do?paperNumber=IPTC-16707-MS&societyCode=IPTC.

Li, W., Zhu, J. and Qi, J. 2007. Application of Nano-nickel Catalyst in the Viscosity Reduction of Liaohe Extra-heavy Oil by Aqua-thermolysis. *Journal of Fuel Chemistry and Technology*. 35.2:176-180. DOI: 10.1016/S1872-5813(07)60016-4.

Liu, X. and Civian, F. 1993. A Multiphase Mud Fluid Infiltration and Filter Cake Formation Model. *Proceedings of the SPE International Symposium on Oilfield Chemistry*. New Orleans, USA.

Maghzi, A., Mohammadi, S., Ghanzanfari, M.H., Kharrat, Z. and Masihi, M. 2012. Monitoring Wettability Alteration by Silica Nanoparticles during Water Flooding to Heavy oils in Five-Spots System: *A Pore-level Investigation. Experimental Thermal and Fluid Science* 40: 168-176

Mian, M.A. 2011. Project Economics and Decision Analysis. 1.2: 164. Library of Congress Cataloging-in-Publication Data

Michele, L. W.T., Michael E.B., Ronald, R.C. 1999. Tertiary Niger Delta (Akata-Agbada) Petroleum System, Niger Delta Province: Nigeria, Cameron, Equatorial Guinea, Africa. U.S. Geological Survey Open File Report 99-50H.

Miranda, C. R., Lara, L. S., and Tonetto, B. C. 2012. Stability and Mobility of Functionalized Silica Nanoparticles for Enhanced Oil Recovery Applications. doi: 10.2118/157033-ms. Paper presented at the SPE International Oilfield Nanotechnology Conference and Exhibition. Paper Number: SPE-157033-MS URLhttp://www.onepetro.org/mslib/app/Preview.do?paperNumber=SPE-157033-MS&societyCode=SPE.

Moon, T. 2010. Nanofluid Technology Promises Large Scale Performance Gains from Tight Reservoirs. *JPT Online Article.*

Murat, R. C. 1972. Stratigraphy and Palaeogeography of the Cretaceous and Lower Tertiary in Southern Nigeria, in African Geology, T.F.J. DEssauvagie and A.J. Whiteman, eds: Ibadan University Press. 251- 266.

Nanowerk, 2016. Ten Things you should know about Nanotechnology. https://www.nanowerk.com/nanotechnology/ten_things_you_should_know_3.php

Nasrollahzadeh, M., Sajad, S. M., Sajjad, M., Issaabadi, Z. 2019. Applications of Nanotechnology in Daily Life. *Interface Science and Technology*. 28: 113-143. https://doi.org/10.1016/B978-0-12-813586-0.00004-3.

Negin, C., Ali, S., Xie, Q. 2016. Application of nanotechnology for enhancing oil recovery – A review. *Petroleum.* 2.3: 324-333. https://doi.org/10.1016/j.petlm.2016.10.002

Ogolo, N.A. Olafuyi, O.A and Onyekonwu, M.O. 2012. Enhanced Oil Recovery Using Nanoparticles. Paper presented at the SPE Saudi Arabia Section Technical Symposium and Exhibition, Al-Khobar, Saudi Arabia, April. Paper Number: SPE-160847-MS. https://doi.org/10.2118/160847-MS

Onyeonkwu M.A., Ogolo, N.A. 2010. Investigating the Use of Silica Nanoparticles in Enhancing Oil Recovery. Paper presented at the SPE Nigeria Annual International Conference and Exhibition, Lagos, Nigeria. July 31- August 4. Paper Number SPE-140744-MS.

Orodu, K.B., Afolabi, R.O., Oluwasijuwomi, T.D. And Orodu, O.D. 2019. Effect of Aluminum Oxide Nanoparticles on the Rheology and Stability of a biopolymer for Enhanced Oil Recovery. Journal of Molecular Liquids [online]. 288. Article ID 110864. Available from: https://doi.org/10.1016/j.molliq.2019.04.141

Ozumba, B. 2013. Geology of the Niger Delta: An Overview for Geophysics Processors. An SPDC presentation for geologists in Nigeria.

Reijers, T.J.A., S.W. Petters and C.S. Nwajide. 1996. The Niger Delta Basin, in: T.J.A. Reijers (ed.), Selected Chapters on Geology: SPDC corporate reprographic services, Warri, Nigeria. 103-114.

Rostami, P., Sharifi, M., Aminshahidy, B., Fahimpour, J. 2019. The effect of nanoparticles on wettability alteration for enhanced oil recovery: micromodel experimental studies and CFD simulation. Pet. Sci. 16: 859–873. https://doi.org/10.1007/s12182-019-0312-z.

Roustaei, A., Saffarzadeh, S. and Mohammadi, .M. 2013. An Evaluation of Modified Silica Nanoparticles' Efficiency in Enhancing Oil Recovery of Light and Intermediate Oil Reservoirs*", Egyptian Journal of Petroleum* 22: 427–433

Ruan, B. and Jacobi, A.M. Ultrasonication Effects on Thermal and Rheological Properties of Carbon Nanotube Suspensions. *Nanoscale Res. Lett*. 7: 127

Russel, W.B., Saville, D.A. and Schowalter, W.R. 1992. Colloidal dispersions. J. Chem. Technol. Biotechnol. 54: 201–202.

Saggaf, M. M. 2008. A Vision for Future Upstream Technologies. Distinguished author series. *Journal of Petroleum Technology*. 60.3: 54-55, 94-98.

Shafiai, S.H. and Gohari, A. 2020. Conventional and Electrical EOR Review: The Development Trend of Ultrasonic Application in EOR. *Journal of Petroleum Exploration and Production Technology.* 10:2923–2945. https://doi.org/10.1007/s13202-020-00929-x

Short, K.C. and Stauble, A.J. 1967. Outline of geology of Niger Delta: American Association of Petroleum Geologist Bulletin. 51.5:764-772.

Sun, Z., Zang, Y., Chen, G. and Gai. Z. 2017. Application of Nanoparticles in Enhanced Oil Recovery A Critical Review of the Recent Progress. *Energies, MDPI Journals*. Doi: 10.3390/en10030345. 10.345: 1-33.

Tiantian Zhang. 2014. Modeling of Nanoparticle Transport in Porous Media, Ph.D. Thesis, The University of Texas at Austin.

Torsaeter, O. and Abtahi, M. 2000. Experimental Reservoir Engineering Laboratory Work Book. Department of Petroleum Engineering and Applied Geophysics, NTNU.

Udoh, T. and Akanji, L., Vinagradov, J. 2018. Experimental Investigation of Potential of Combined Controlled Salinity and Bio-Surfactant CSBS in Enhanced Oil Recovery EOR Processes. Paper presented at the SPE Nigeria Annual International Conference and Exhibition, Lagos, Nigeria. Paper Number SPE-193388-MS.

Wasan, D.T. and Nikolov, D. A., 2003. Spreading of Nanofluids on Solids. J .Nat. 423: 156–159.

Wasan, D.T., Nikolov, A. and Kondiparty, K. 2011. The Wetting and Spreading of Nanofluids on Solids: Role of the Structural Disjoining Pressure. Curr. Opin. *Colloid Interface Science*.16: 344–349.

Weber, K. J and Daukoru, E.M. 1975. Petroleum geology of the Niger Delta: Proceedings of the Ninth World Petroleum Congress. Geology: London, Applied Science Publishers, Ltd. 2: 210-221

Wei, Y. and Huaqing, X. 2011. A Review of Nanofluids: Preparation, Stability Mechanisms and Applications. *Journal of Nanomaterials*. Article ID 43587

Wen, D. and Ding, Y. 2005. Experimental Investigation into the Pool Boiling Heat Transfer of Aqueous based–Alumina Nanofluids. J. Nanopart. Res., 7: 265–274. [CrossRef]

Willhite, G. P. 1986. Waterflooding. *SPE Textbook Series* 3. Shell Company and Society of Petroleum Engineers Foundation Fund. ISBN 1-55563-005-7. Richardson, TX

Yu, H., Hermann, S., Schulz, S.E., Gessner, T. and Li, W.J. 2012. Optimizing Sonication Parameters for Dispersion of Single-walled Carbon Nanotubes. *Chem. Phys.* 408: 11–1

Zhong, P., Wei, W. and Wei, L. 2013. Economic evaluation of EOR project based on options differential equation method. Paper presented at International Conference on Computational and Information Sciences, Shiyang China. 21-23, June.

Zolotukhin, A. and Ursin, J. 2000. Introduction to Petroleum Reservoir Engineering. Hyskoleforlaget, Norwegian Academic Press. ISBN 9788276340655. URL http://books.google.no/books?id=eiwAGQAACAAJ.

APPENDICES

APPENDIX A

Nanofluid Flooding with Changing Injection Rate for 0.01 wt % Silica Nanofluid

Injection rate (cm^3/min)	Time (min)	PV of Nanofluid Injected	Vol. of oil recovered (cm^3)	Recovery factor
0.5	5	2.5	0.372	0.024
	10	5.0	0.822	0.053
	15	7.5	1.271	0.082
	20	10.0	1.426	0.092
	25	12.5	1.612	0.104
	30	15.0	1.752	0.113
	35	17.5	1.938	0.125
	40	20.0	2.000	0.129
	45	22.5	2.000	0.129
	50	25.0	2.000	0.129
1.0	55	30.0	2.077	0.134
	60	35.0	2.124	0.137
	65	40.0	2.139	0.138
	70	45.0	2.232	0.144
	75	50.0	2.294	0.148
	80	55.0	2.294	0.148
	85	60.0	2.294	0.148
	90	65.0	2.294	0.148
	95	70.0	2.372	0.148
2.0	100	80.0	2.294	0.148
	105	90.0	2.294	0.148
	110	100.0	2.294	0.148
	115	110.0	2.294	0.148
	120	120.0	2.294	0.148
	125	130.0	2.294	0.148
	130	140.0	2.294	0.148
3.0	135	155.0	2.294	0.148
	140	170.0	2.294	0.148
	145	185.0	2.294	0.148
	150	200.0	2.294	0.148
	155	215.0	2.294	0.148
	160	230.0	2.294	0.148
	165	245.0	2.294	0.148

I. Nanofluid Flooding with Changing Injection Rate for 0.50 wt % silica nanofluid

Injection rate (cm^3/min)	Time (min)	PV of Nanofluid Injected	Vol. of oil recovered (cm^3)	Recovery factor
0.5	5	2.5	0.448	0.025
	10	5.0	1.199	0.067
	15	7.5	1.468	0.082
	20	10.0	1.683	0.094
	25	12.5	1.862	0.104
	30	15.0	2.076	0.116
	35	17.5	2.238	0.125
	40	20.0	2.327	0.130
	45	22.5	2.327	0.130
	50	25.0	2.327	0.130
1.0	55	30.0	2.470	0.138
	60	40.0	2.721	0.152
	65	55.0	2.900	0.162
	70	75.0	3.043	0.17
	75	100.0	3.401	0.19
	80	130.0	3.544	0.198
	85	165.0	3.992	0.223
	90	205.0	3.992	0.223
	95	250.0	3.992	0.223
2.0	100	260.0	4.207	0.235
	105	270.0	4.439	0.248
	110	280.0	4.493	0.251
	115	290.0	4.529	0.253
	120	300.0	4.547	0.254
	125	310.0	4.547	0.254
	130	320.0	4.547	0.254
3.0	135	335.0	4.547	0.254
	140	350.0	4.565	0.255
	145	365.0	4.565	0.255
	150	380.0	4.582	0.256
	155	395.0	4.600	0.257
	160	410.0	4.600	0.257
	165	425.0	4.600	0.257

II. Nanofluid Flooding with Changing Injection Rate for 2.0 wt % silica nanofluid

Injection rate (cm^3/min)	Time (min)	PV of Nanofluid Injected	Vol. of oil recovered (cm^3)	Recovery factor
0.5	5	2.5	0.692	0.040
	10	5.0	0.727	0.042
	15	7.5	1.194	0.069
	20	10.0	1.765	0.102
	25	12.5	2.249	0.130
	30	15.0	2.578	0.149
	35	17.5	2.630	0.152
	40	20.0	2.699	0.156
	45	22.5	2.699	0.156
	50	25.0	2.699	0.156
1.0	55	30.0	2.387	0.138
	60	35.0	2.630	0.152
	65	40.0	3.287	0.190
	70	45.0	3.460	0.200
	75	50.0	4.152	0.240
	80	55.0	5.017	0.290
	85	60.0	5.294	0.306
	90	65.0	5.294	0.306
	95	70.0	5.294	0.306
2.0	100	80.0	5.346	0.309
	105	90.0	5.415	0.313
	110	100.0	5.917	0.342
	115	110.0	6.263	0.362
	120	120.0	6.297	0.364
	125	130.0	6.297	0.364
	130	140.0	6.297	0.364
3.0	135	155.0	6.297	0.364
	140	170.0	6.297	0.364
	145	185.0	6.297	0.364
	150	200.0	6.297	0.364
	155	215.0	6.297	0.364
	160	230.0	6.297	0.364
	165	245.0	6.297	0.364

III. Nanofluid Flooding with Changing Injection Rate for 3.0 wt % silica nanofluid

Injection rate (cm^3/min)	Time (min)	PV of Nanofluid Injected	Vol. of oil recovered (cm^3)	Recovery factor
0.5	5	2.5	0.154	0.010
	10	5	0.185	0.012
	15	7.5	0.354	0.023
	20	10	0.524	0.034
	25	12.5	0.616	0.040
	30	15	0.662	0.043
	35	17.5	0.693	0.045
	40	20	0.708	0.046
	45	22.5	0.708	0.046
	50	25	0.708	0.046
1.0	55	30	0.755	0.049
	60	35	0.801	0.052
	65	40	0.893	0.058
	70	45	9.548	0.620
	75	50	1.047	0.068
	80	55	1.109	0.072
	85	60	1.201	0.078
	90	65	1.201	0.078
	95	70	1.201	0.078
2.0	100	80	1.201	0.078
	105	90	1.201	0.078
	110	100	1.201	0.078
	115	110	1.201	0.078
	120	120	1.201	0.078
	125	130	1.201	0.078
	130	140	1.201	0.078
3.0	135	155	1.201	0.078
	140	170	1.201	0.078
	145	185	1.201	0.078
	150	200	1.201	0.078
	155	215	1.201	0.078
	160	230	1.201	0.078
	165	245	1.201	0.078

APPENDIX B

Cores Used for SEM Analysis

I. Sample No: Y5

Brine	
PV injected	Recovery factor, %
0.5	0.0
1.1	9.7
1.6	17.4
2.1	28.4
2.6	40.6
3.2	55.5
3.7	62.6
4.2	69.7
4.7	70.3
5.3	71.0
5.8	71.0
6.3	71.0
6.8	71.0

II. Sample No: Y6

Nanofluid Flooding	
PV Injected of Nanofluid	Recovery Factor, %
0.5	6.9
1.0	8.1
1.5	12.1
2.0	13.9
2.5	23.7
2.9	32.4
3.4	45.1
3.9	50.3
4.4	50.9
4.9	50.9
5.4	51.4
5.9	53.8
6.4	55.5
6.9	56.1
7.4	56.6
7.8	57.2
8.3	57.8
8.8	57.8
9.3	57.8
9.8	64.2
10.3	64.7
10.8	64.7
11.3	65.3
11.8	65.3
12.3	65.3
12.7	65.3
13.2	65.3
13.7	65.3
14.2	65.3
14.7	65.3
15.2	65.3
15.7	65.3
16.2	65.3

III. Sample No: Y8

Nanofluid-Alternating-Brine Flooding	
PV injected	Recovery factor, %
0.6	1.9
1.2	7.8
1.7	14.9
2.3	24.0
2.9	31.2
3.5	51.9
4.0	59.7
4.6	67.5
5.2	69.5
5.8	71.4
6.4	72.7
6.9	73.4
7.5	73.4
8.1	74.0
8.7	75.3
9.2	77.3
9.8	77.9
10.4	79.9
11.0	79.9
11.6	79.9
12.1	81.8

APPENDIX C

Oil Recovered from the BF, NF, NABF applied incrementally

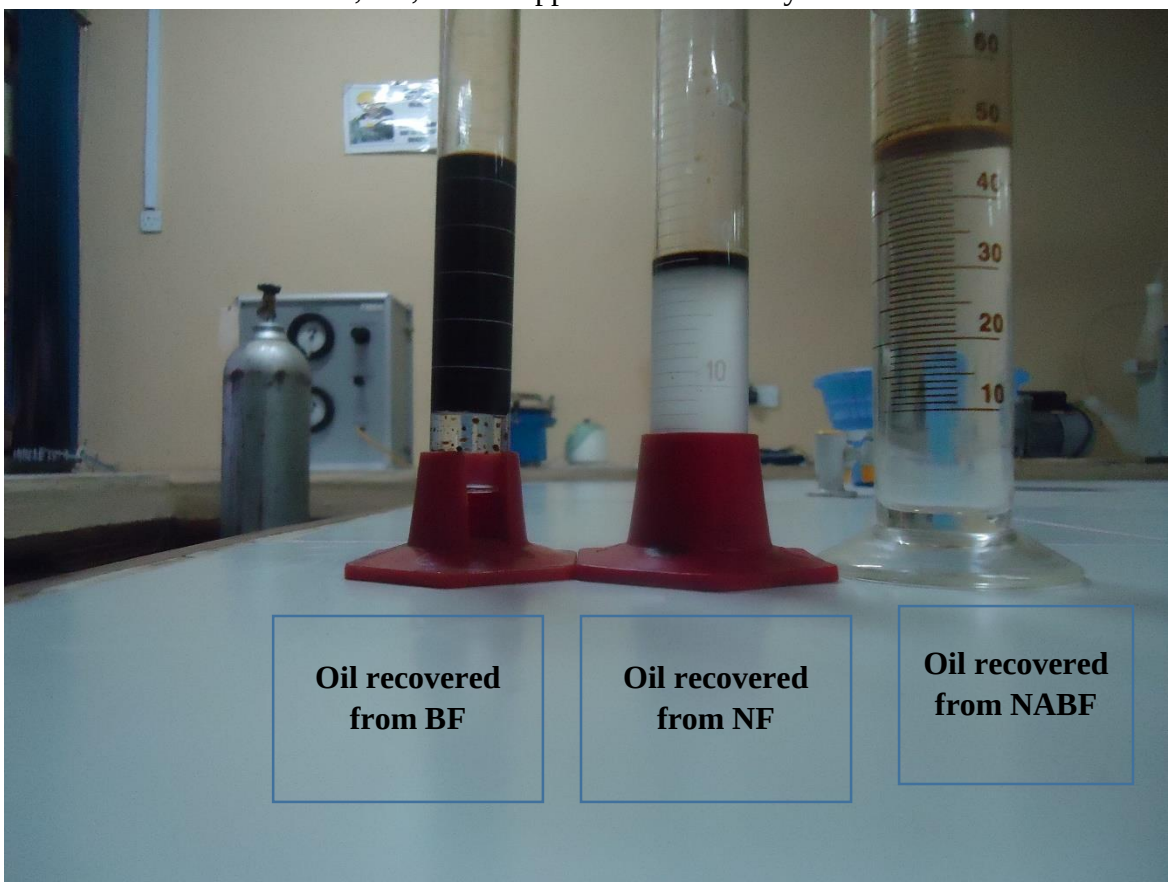

APPENDIX D

Images of SEM FOR Samples Y5, Y6 and Y8 at Various Resolutions and Magnification

Y5: Dry Sample, Y6: NF Sample Y8: NABF Sample

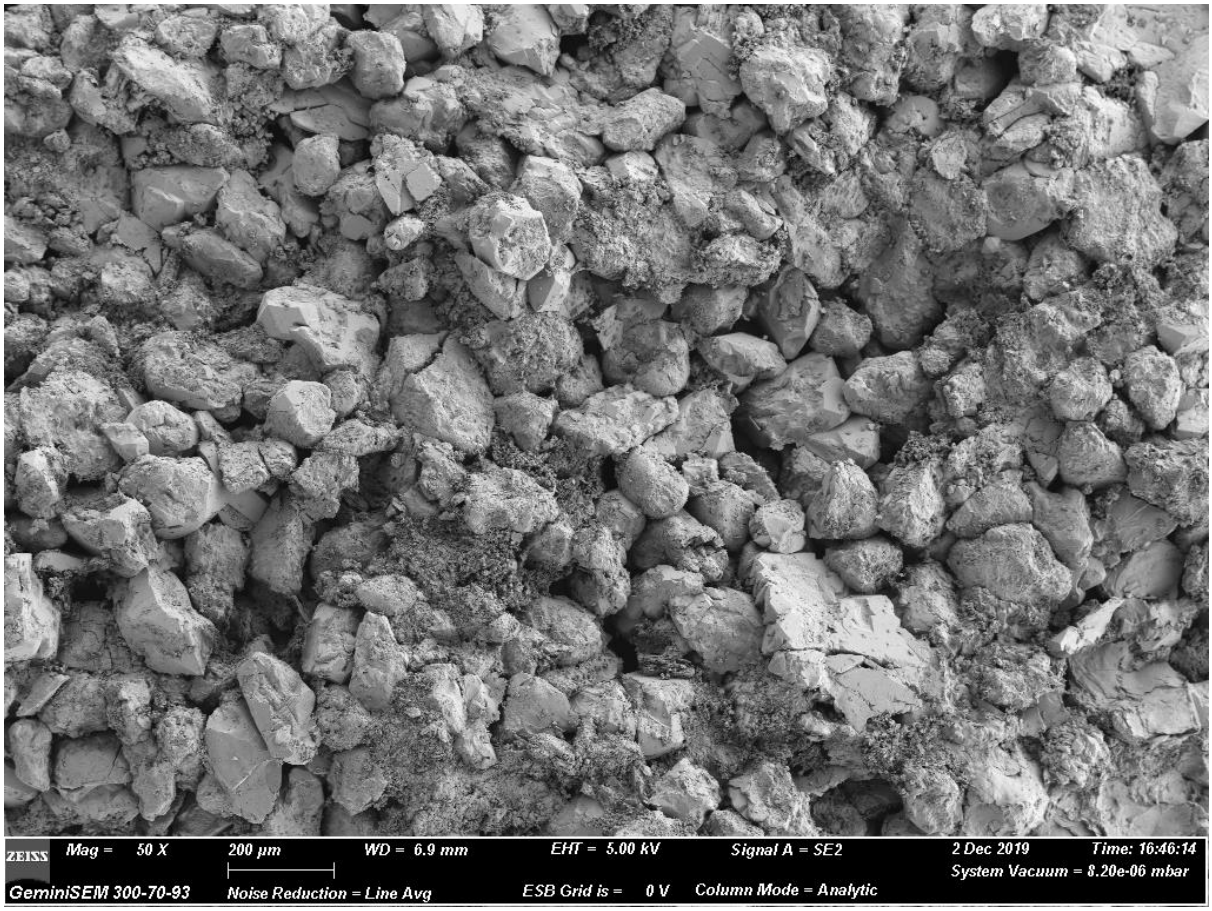

Sample Y5 – magnification = 50x resolution = 200 µm

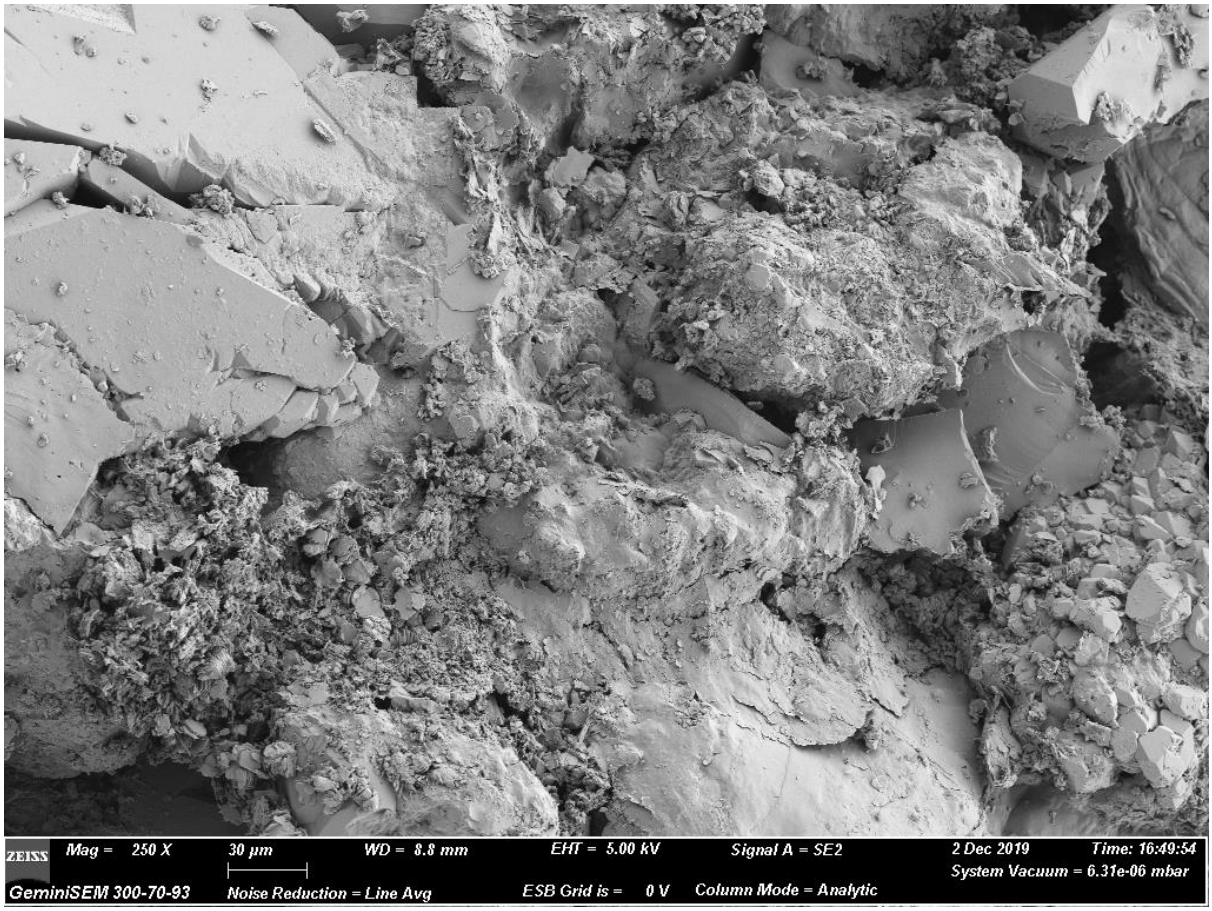

Sample Y5 – magnification = 250x resolution = 30 µm

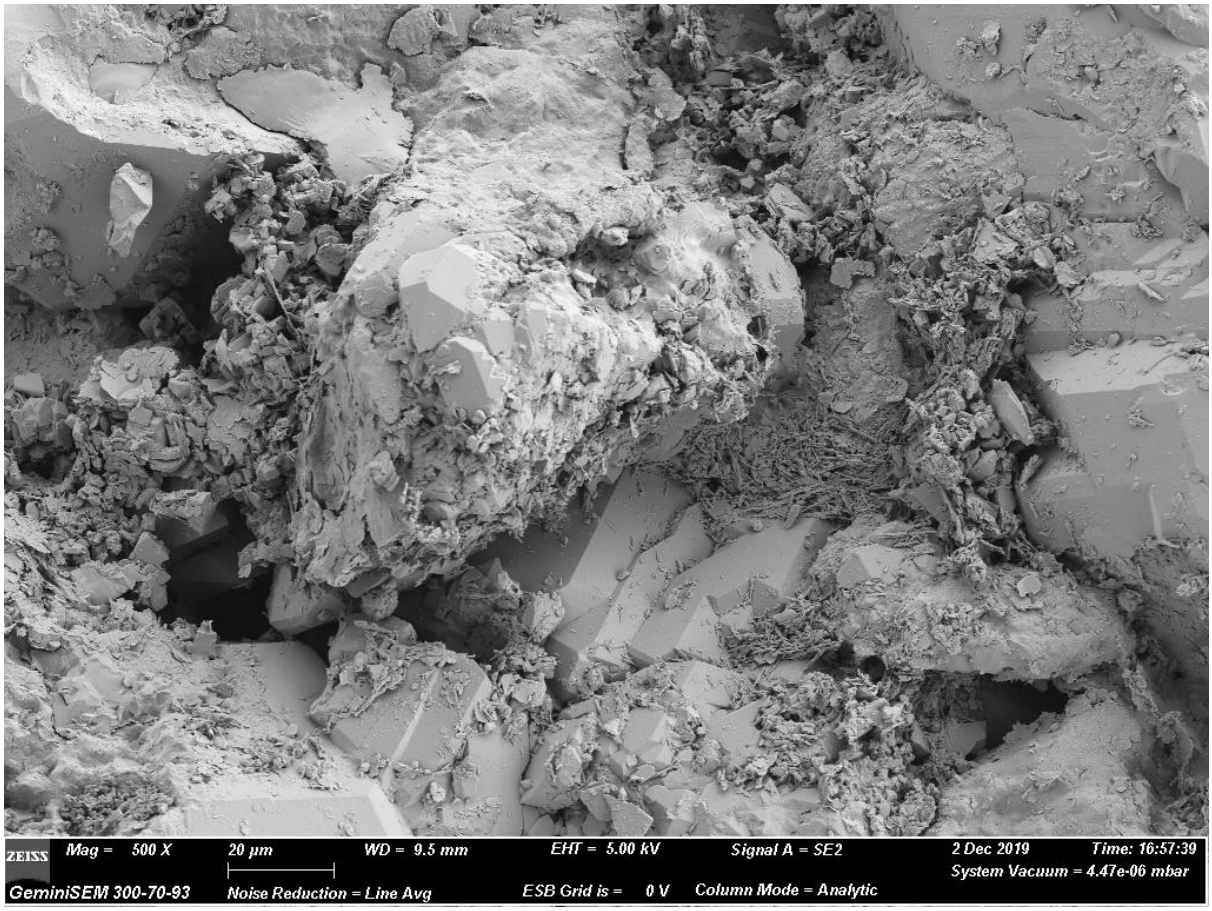

Sample Y5 – magnification = 500x resolution = 20 µm

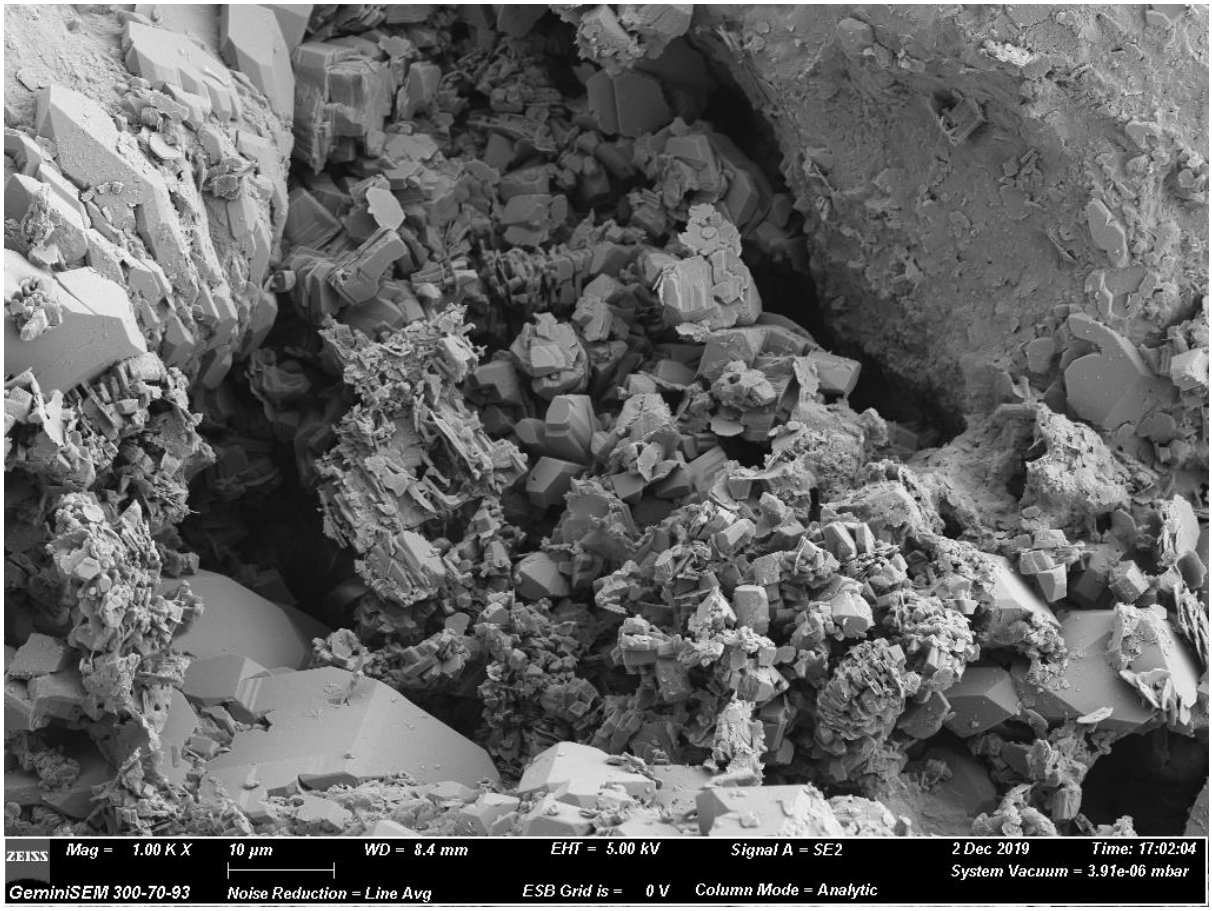

Sample Y5 – magnification = 1000x resolution = 10 µm

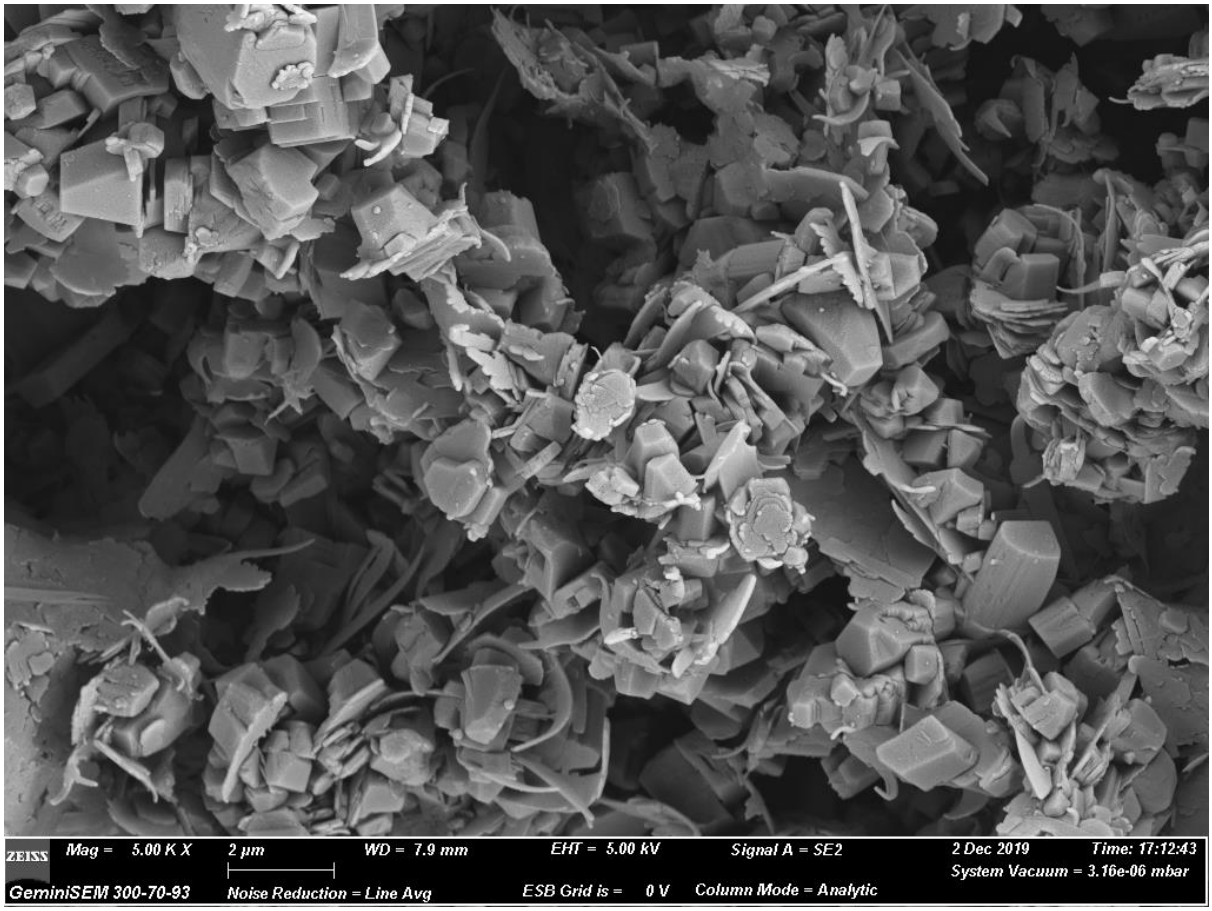

Sample Y5 – magnification = 5000x resolution = 2 µm

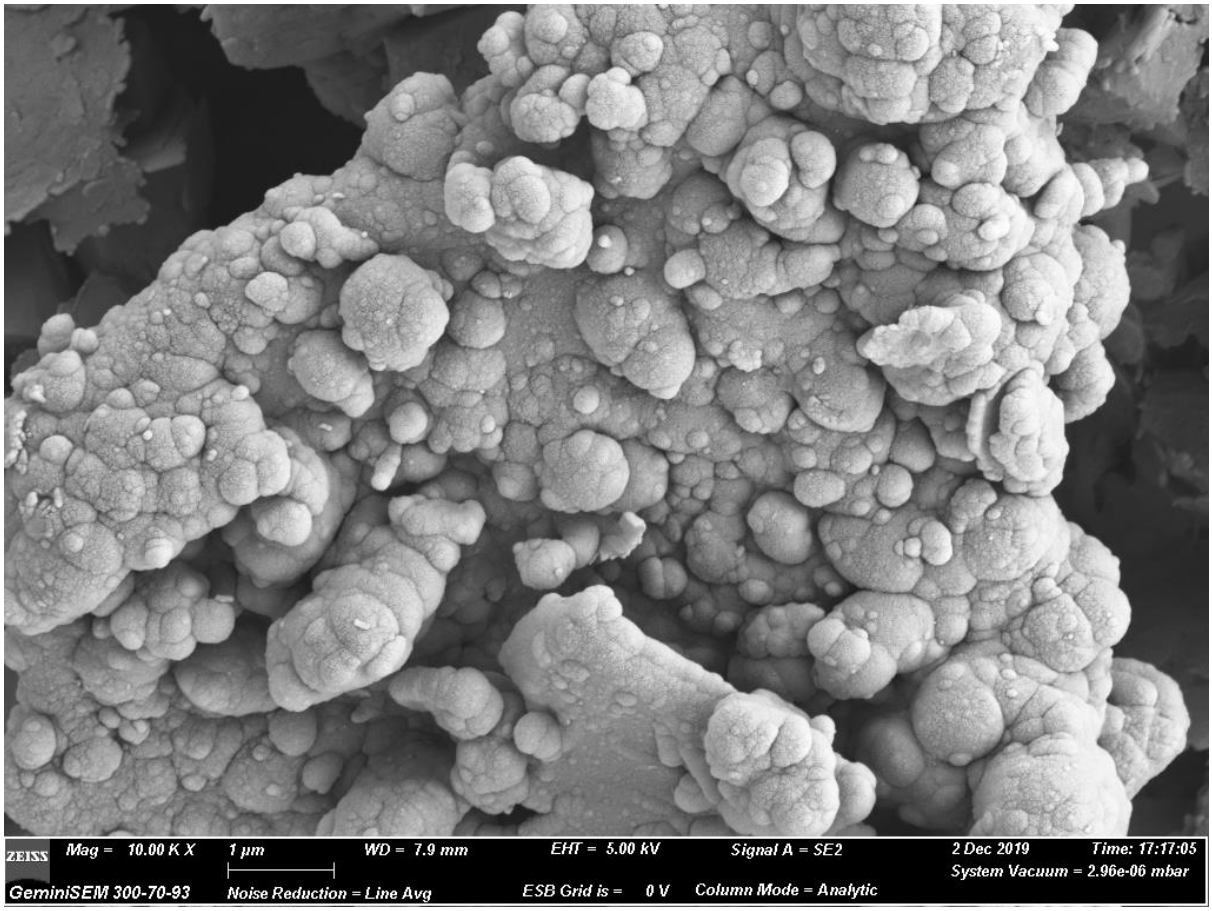

Sample Y5 – magnification = 10000x resolution = 1 µm

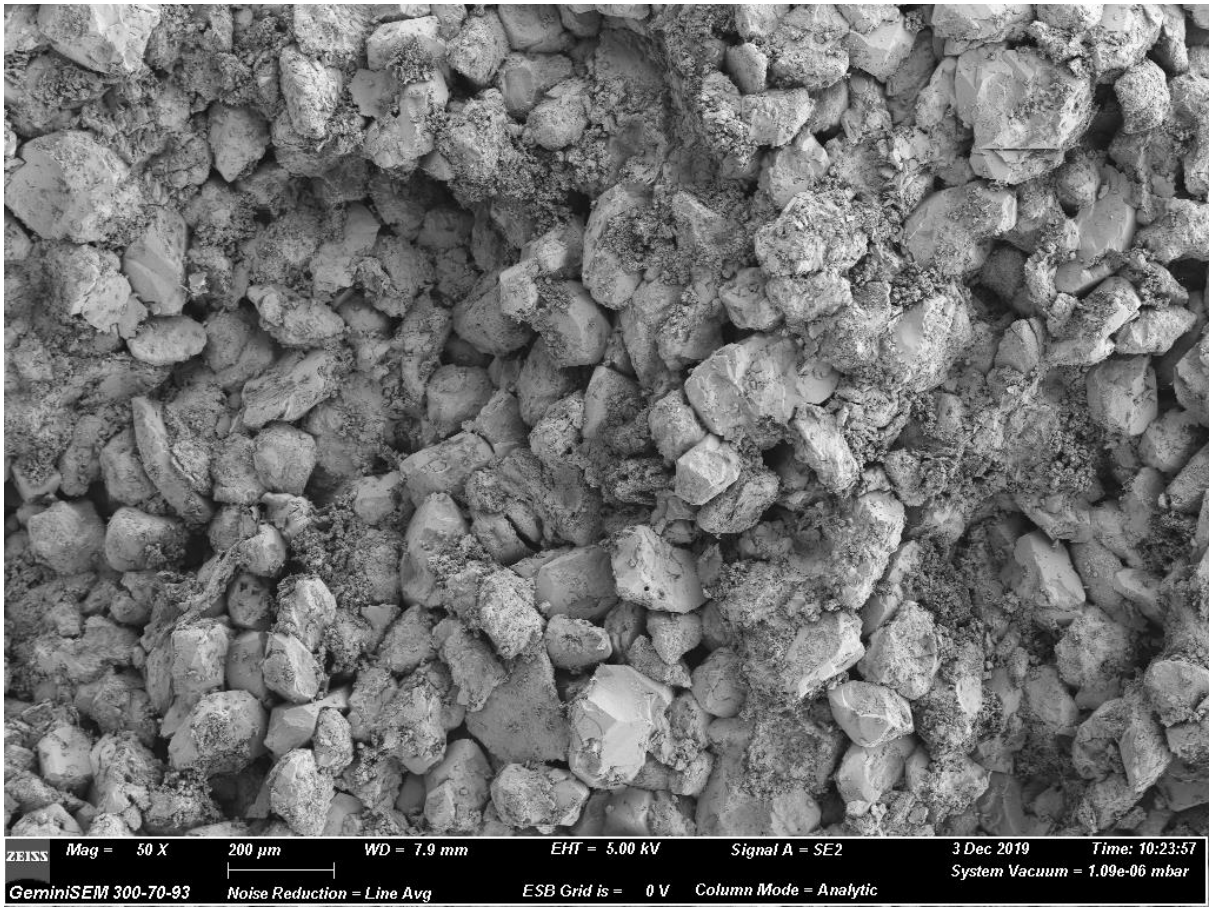

Sample Y6 – magnification = 50x resolution = 200 µm

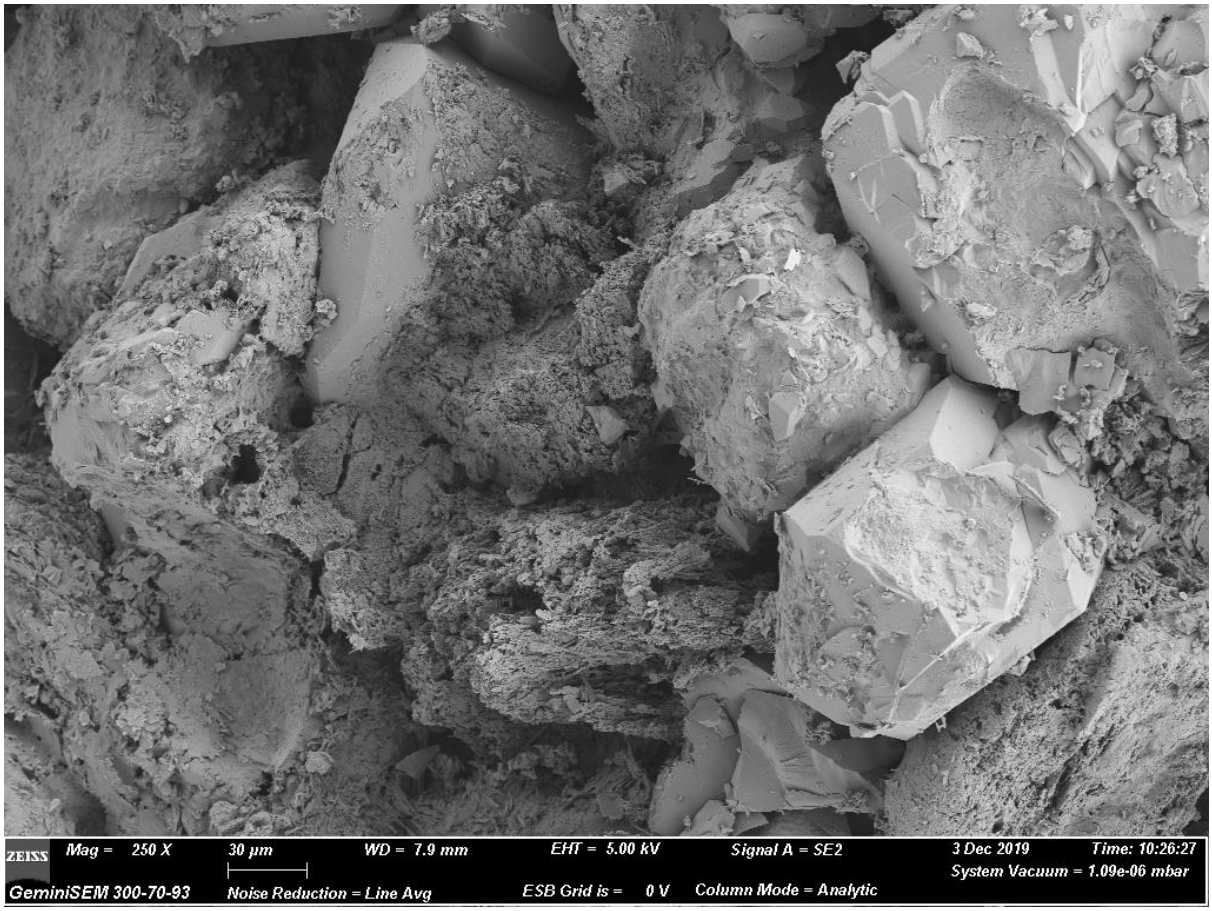

Sample Y6 – magnification = 250 x resolution = 30 µm

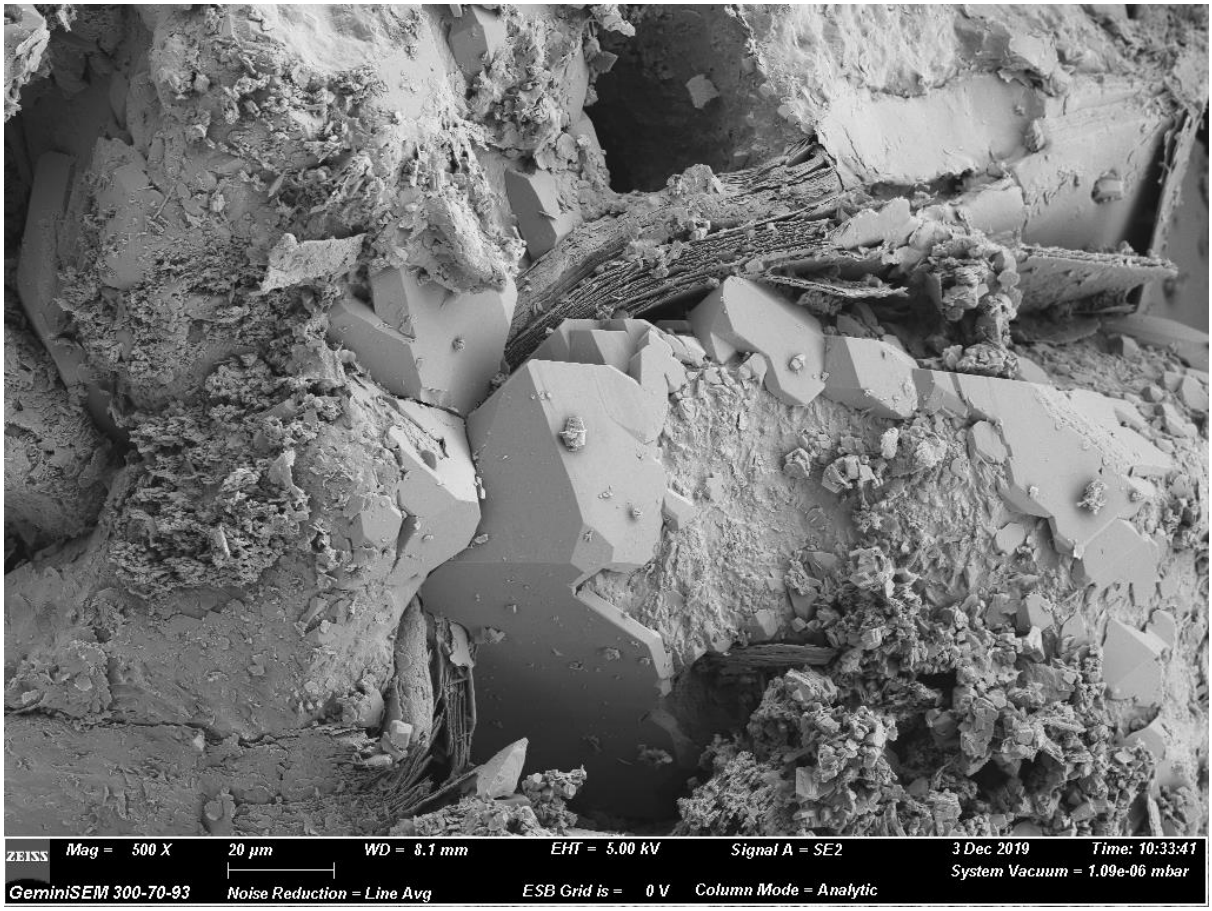

Sample Y6 – magnification = 500x resolution = 20 µm

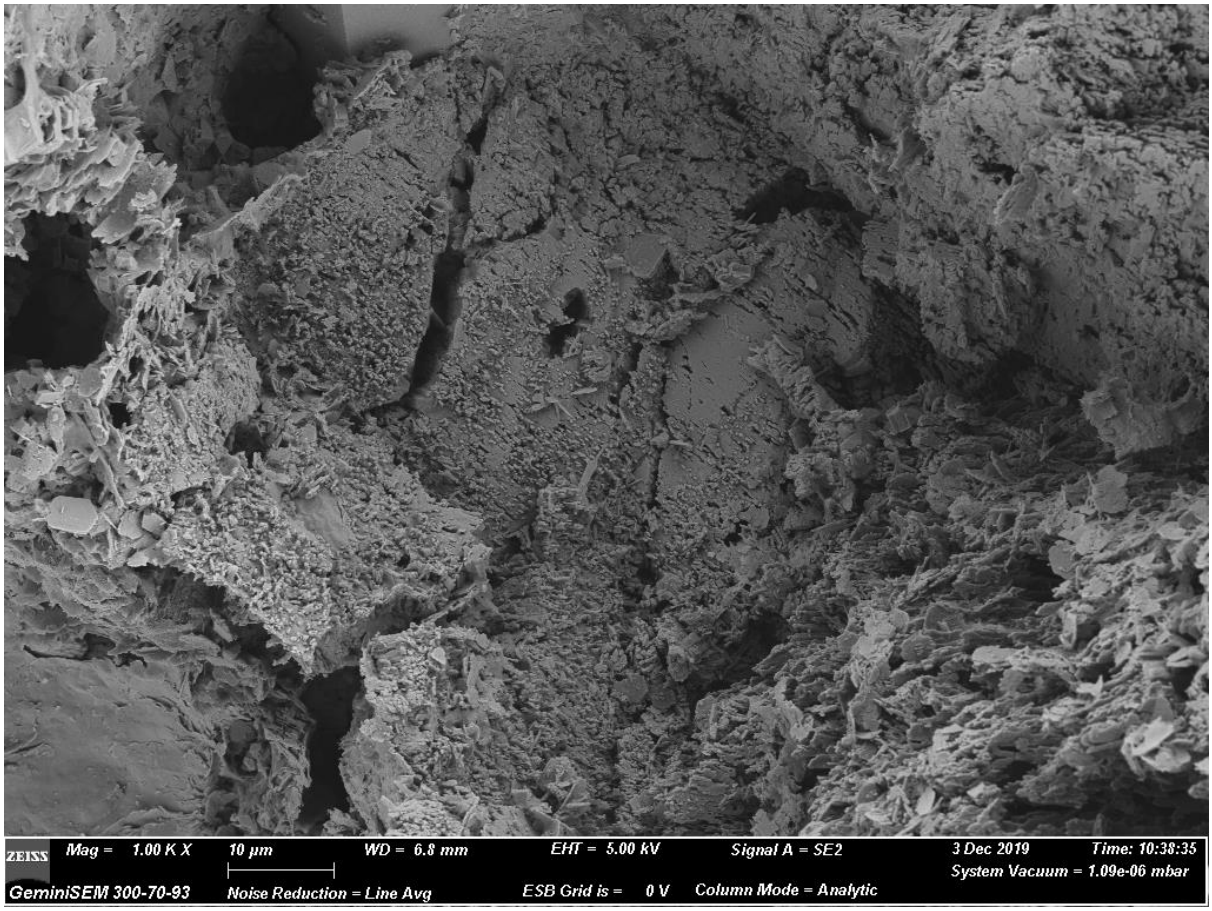

Sample Y6 – magnification = 1000x resolution = 10 µm

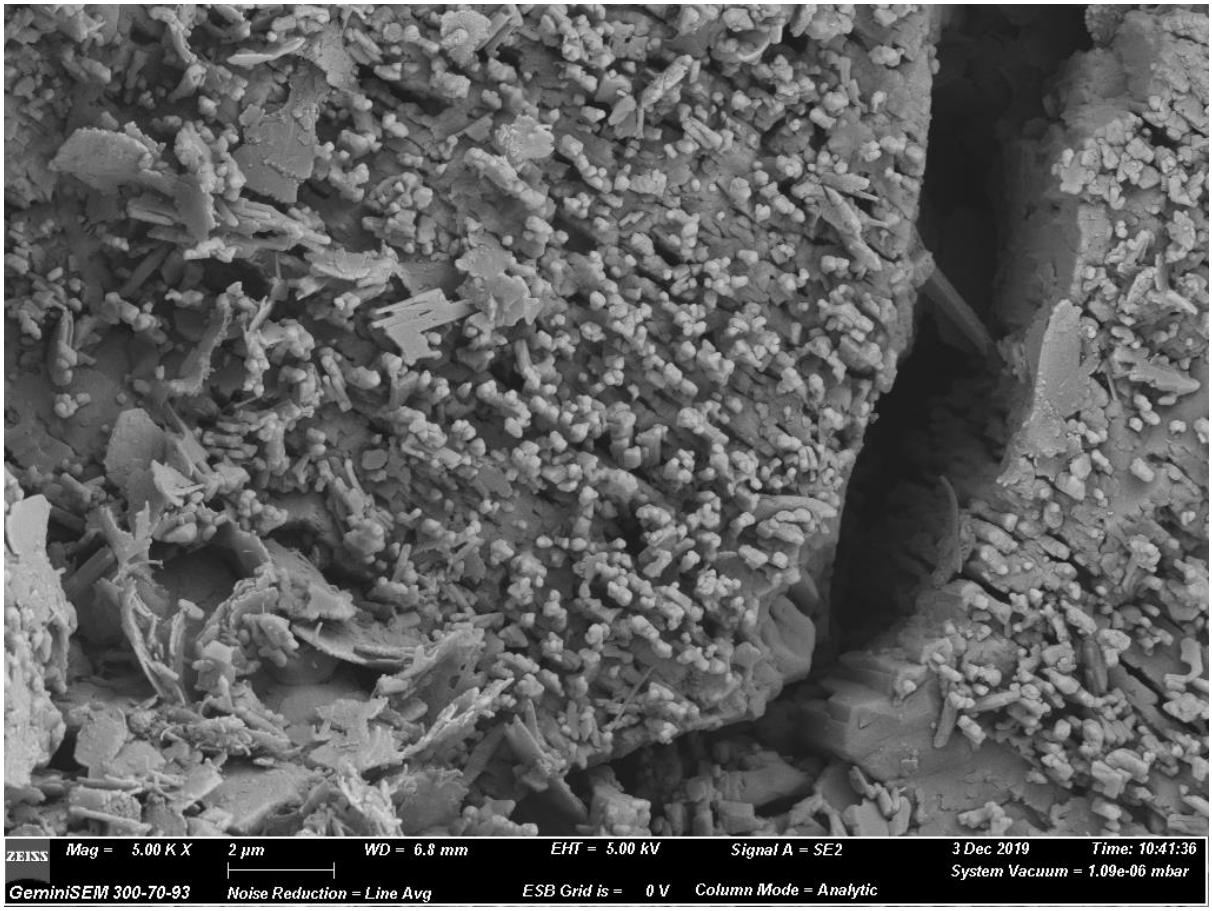

Sample Y6 – magnification = 5000x resolution = 2 µm

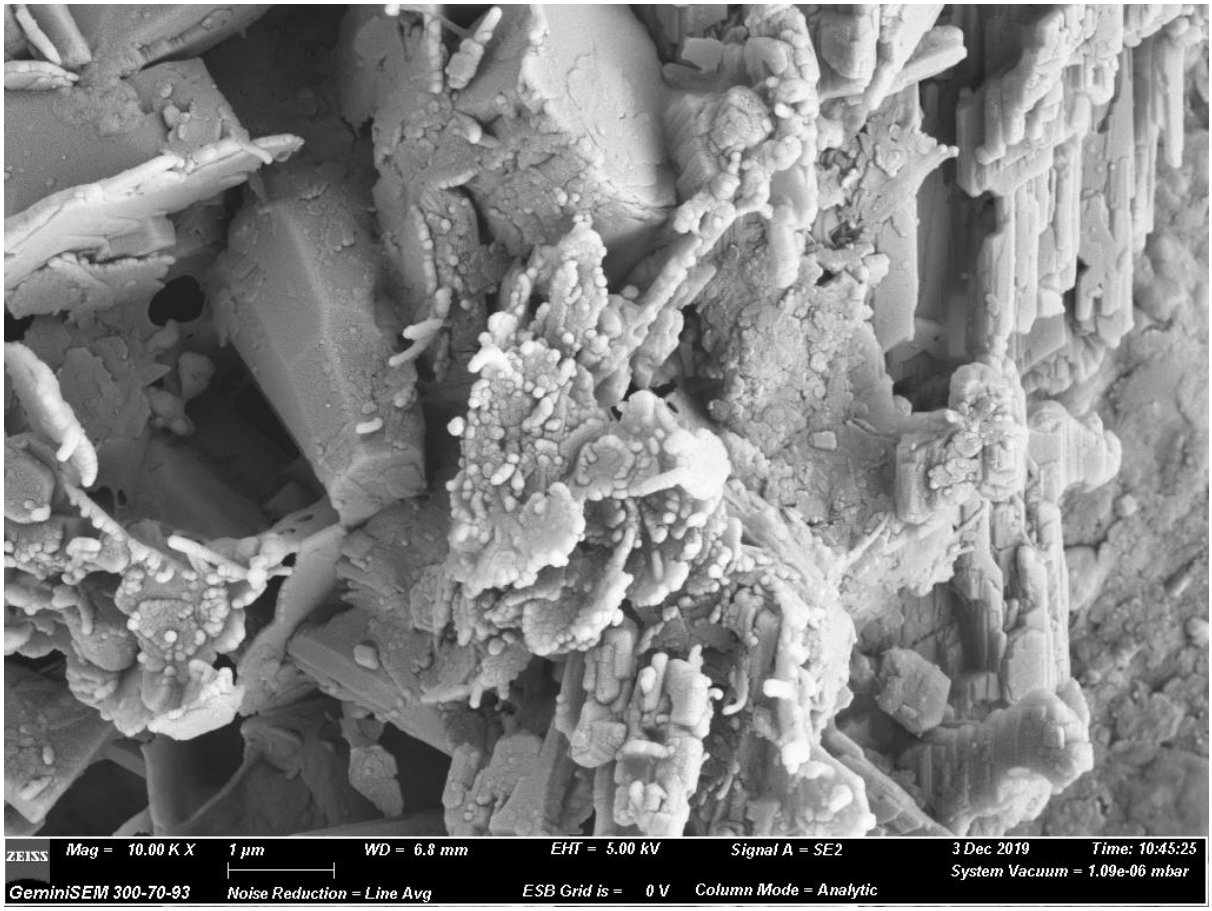

Sample Y6 – magnification = 10000x resolution = 1 µm

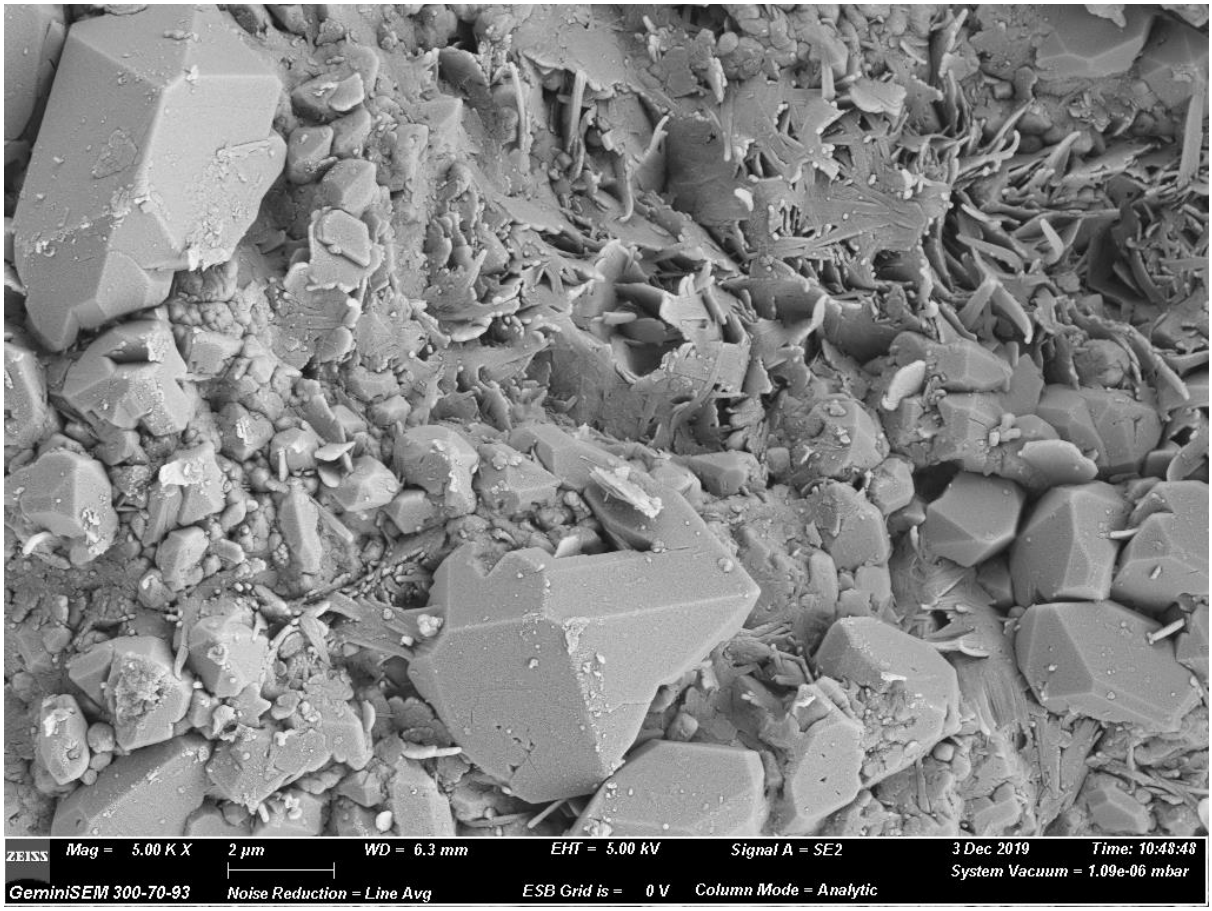

Sample Y6 – magnification = 5000x resolution = 2 µm

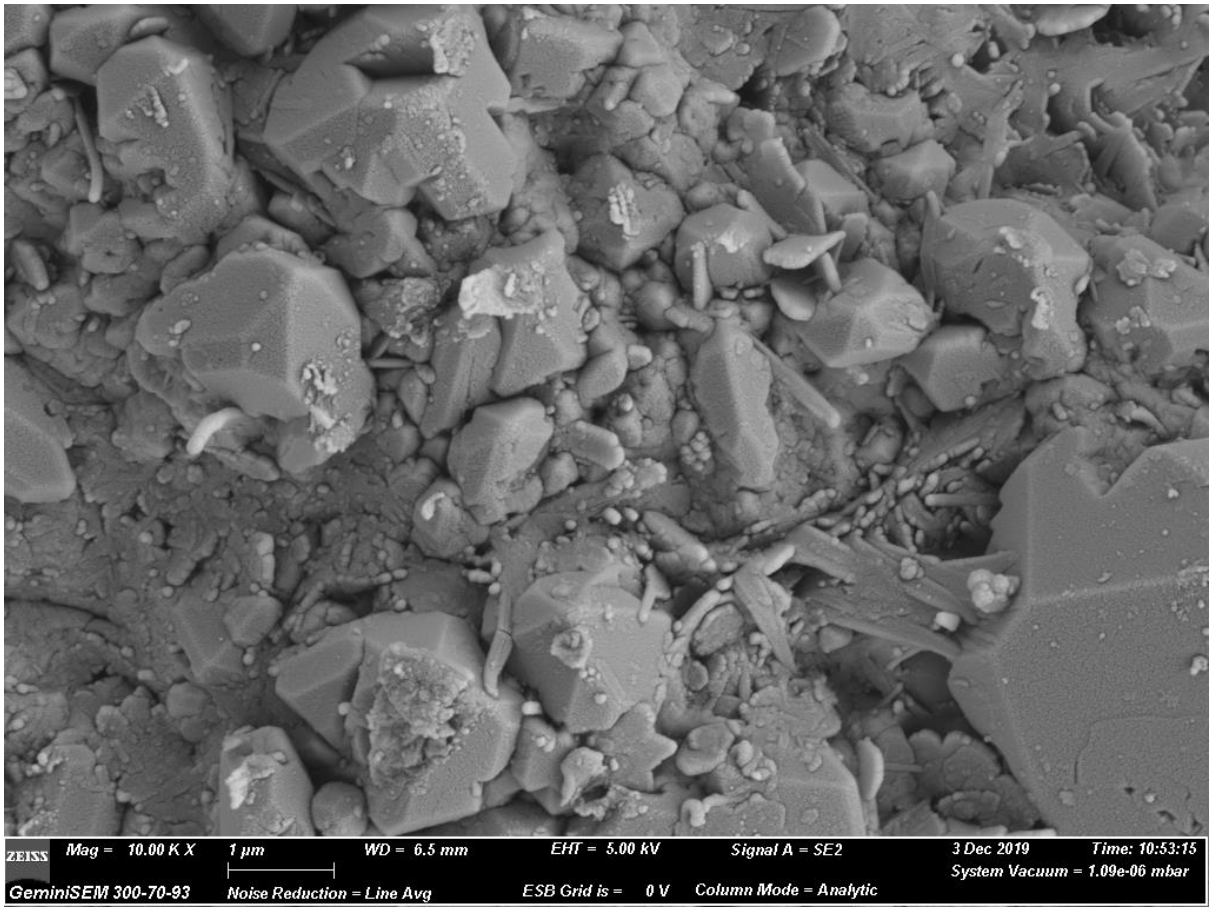

Sample Y6 – magnification = 10000x resolution = 1 µm

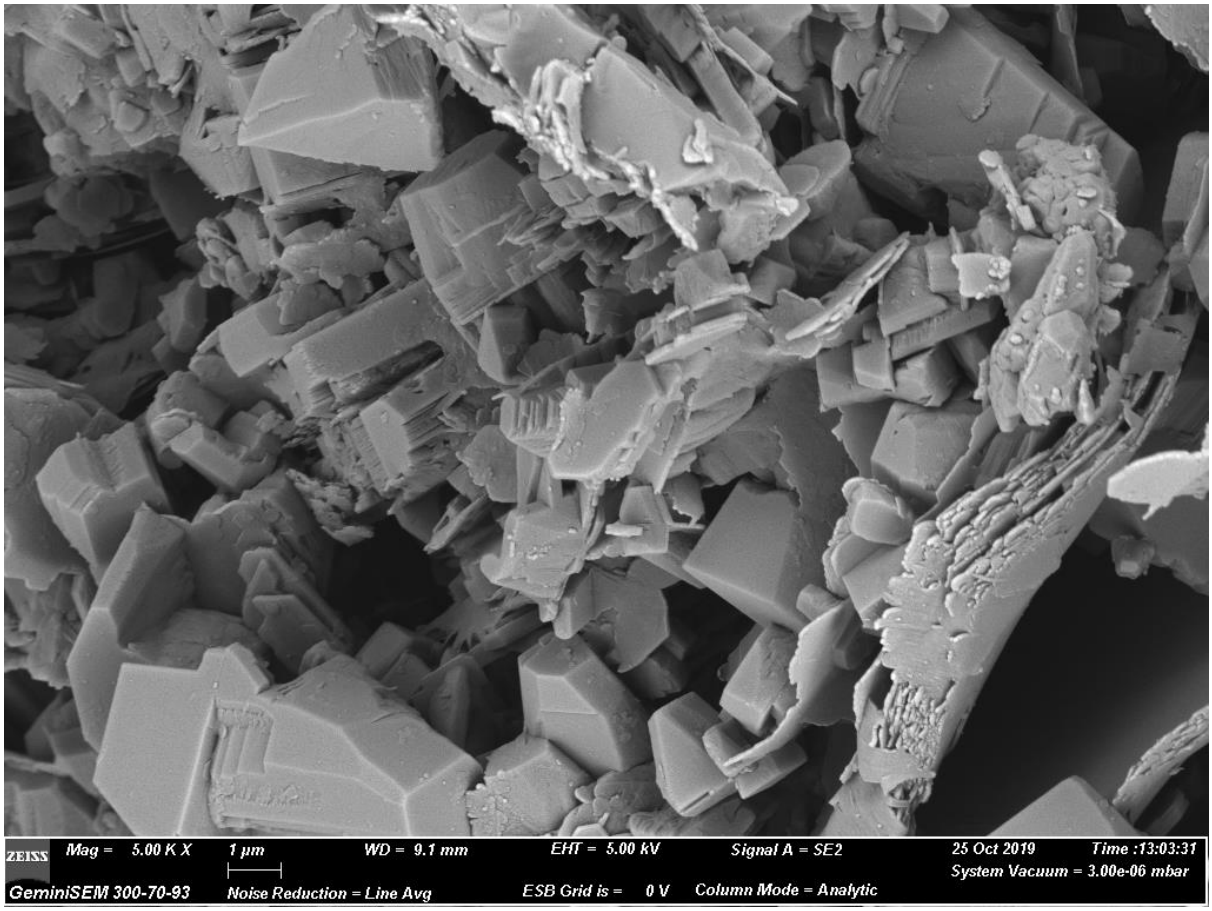

Sample Y8 – magnification = 5000x resolution = 1 µm

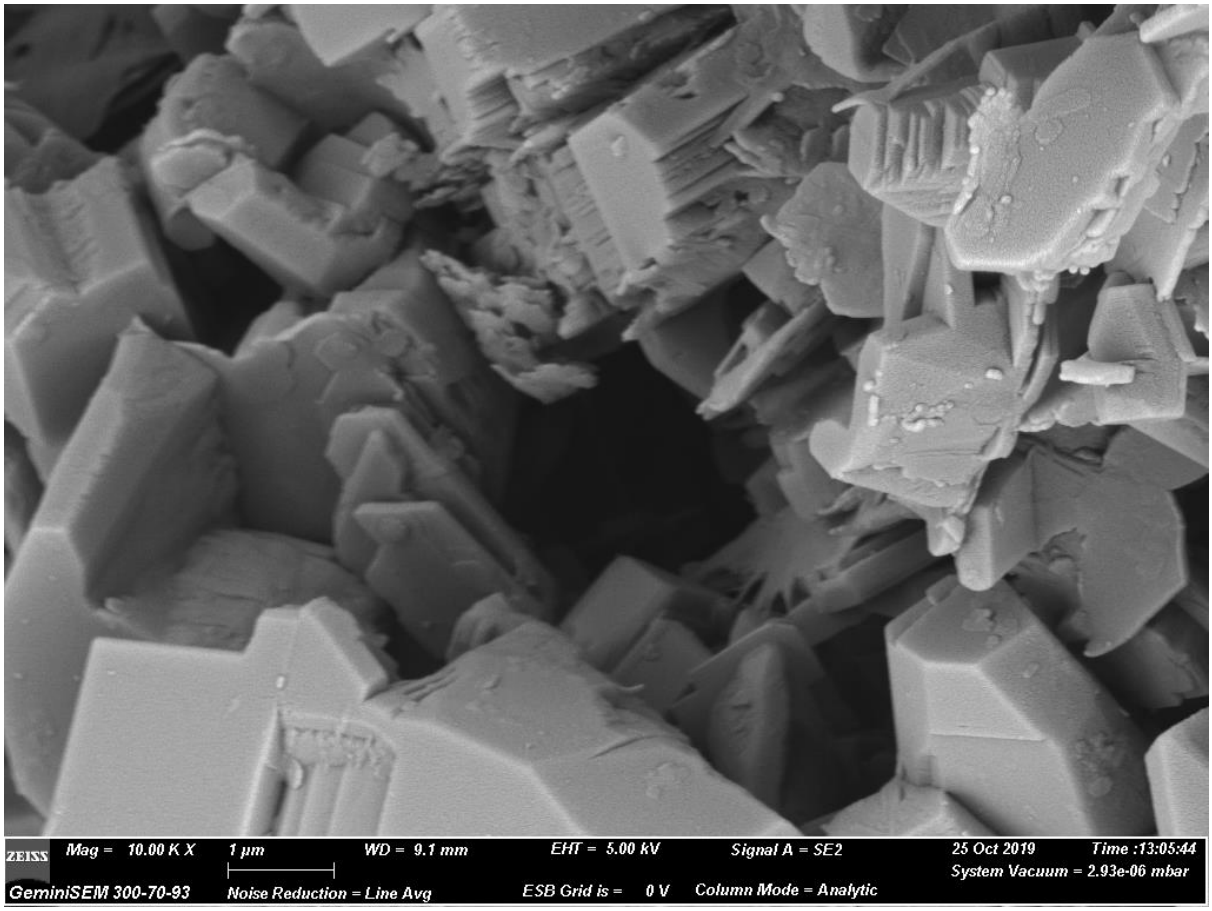

Sample Y8 – magnification = 10000x resolution = 1 µm

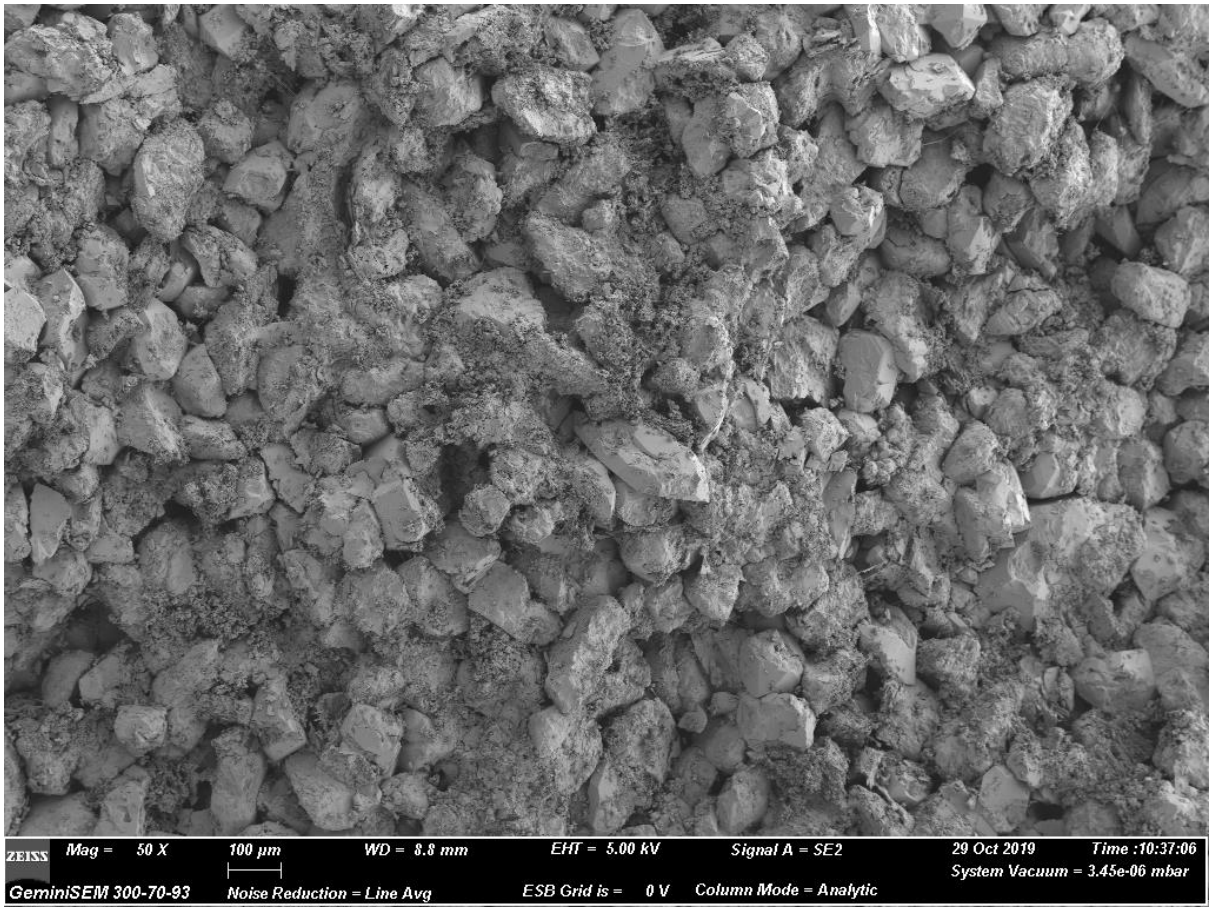

Sample Y8 – magnification = 50x resolution = 100 µm

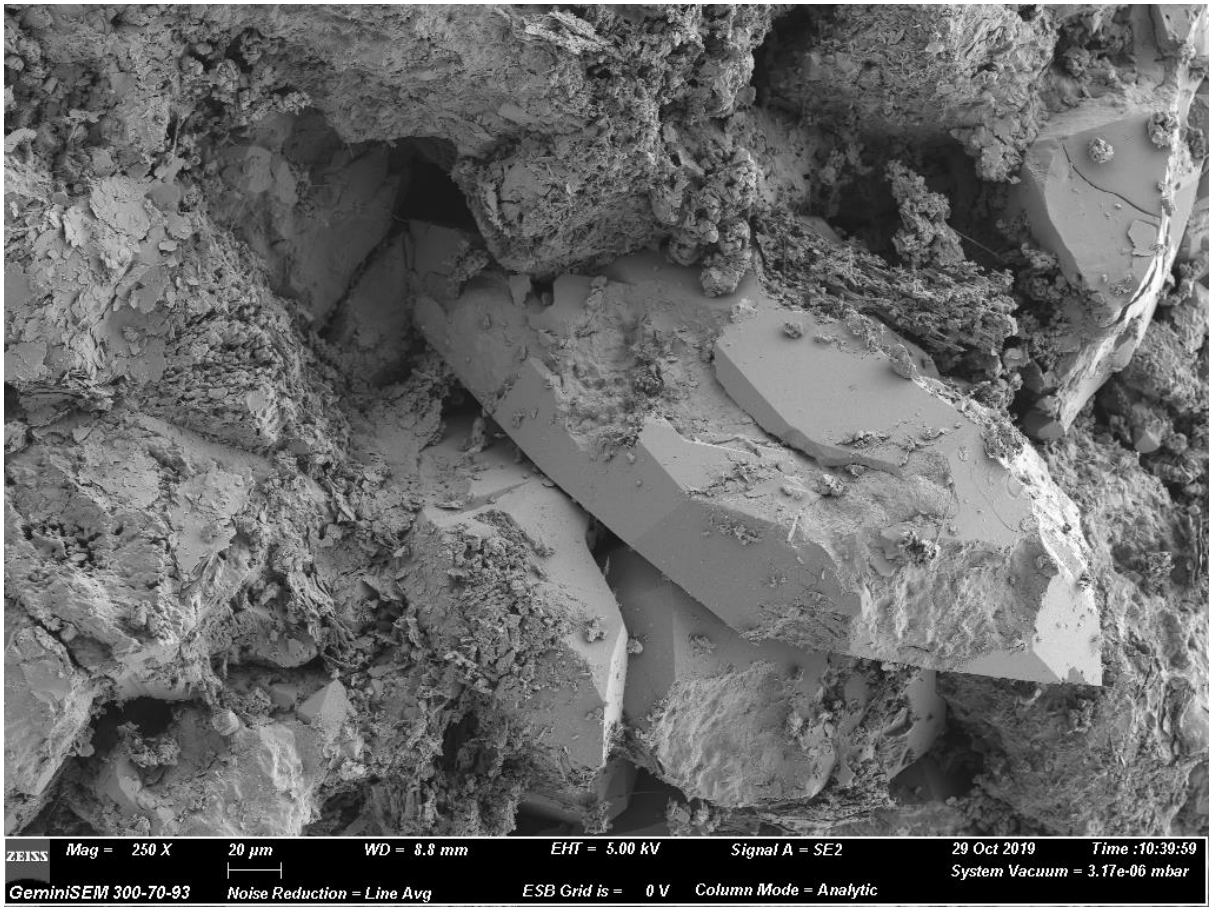

Sample Y8 – magnification = 250x resolution = 20 µm

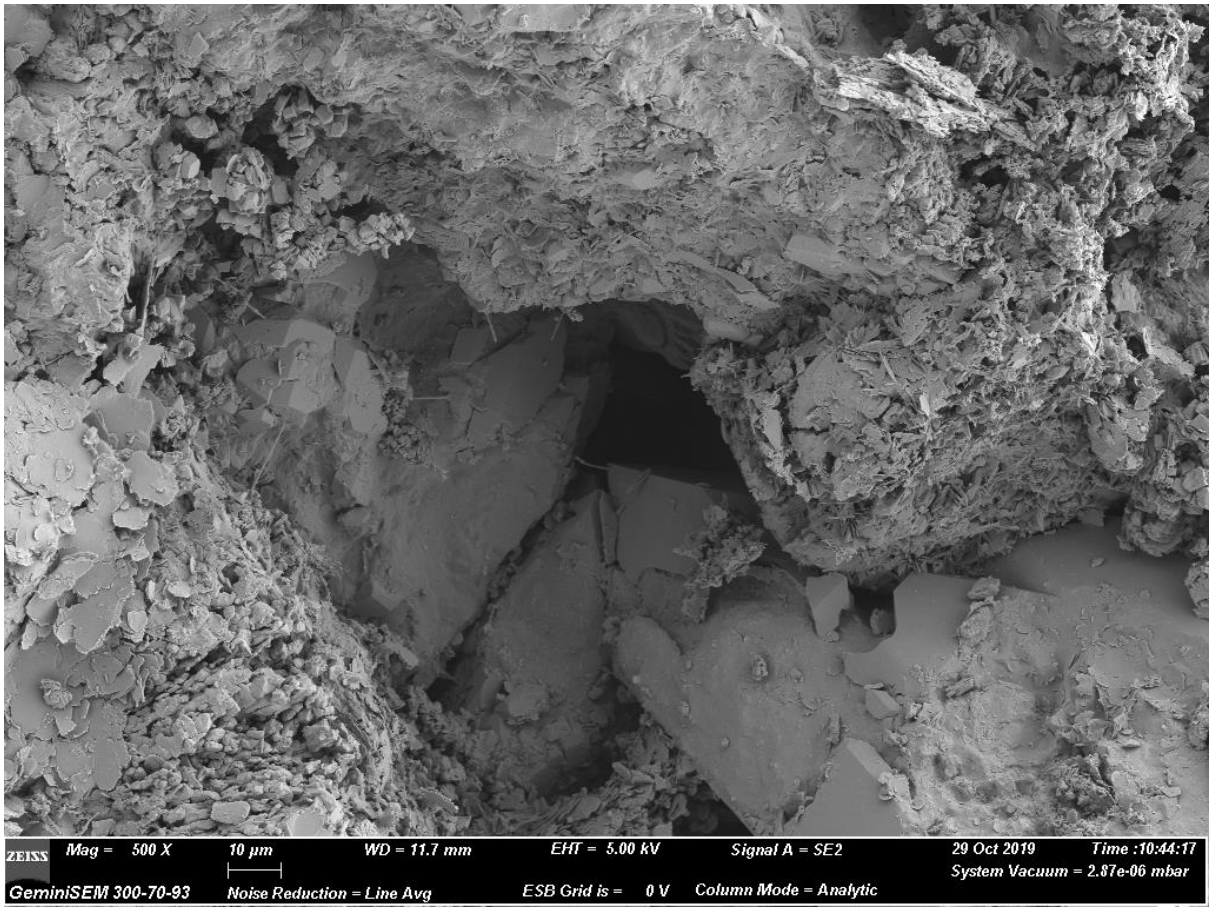

Sample Y8 – magnification = 500x resolution = 10 µm

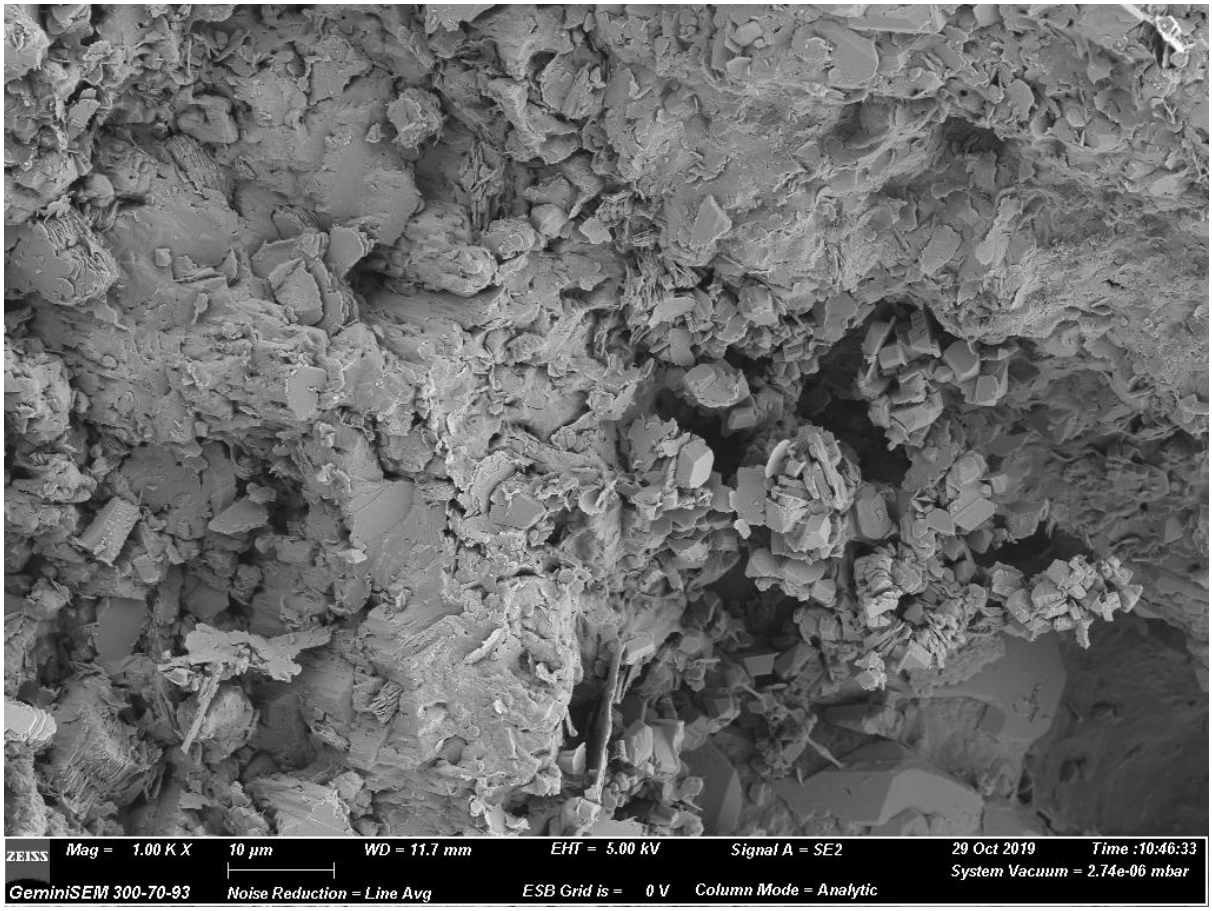

Sample Y8 – magnification = 1000x resolution = 10 µm

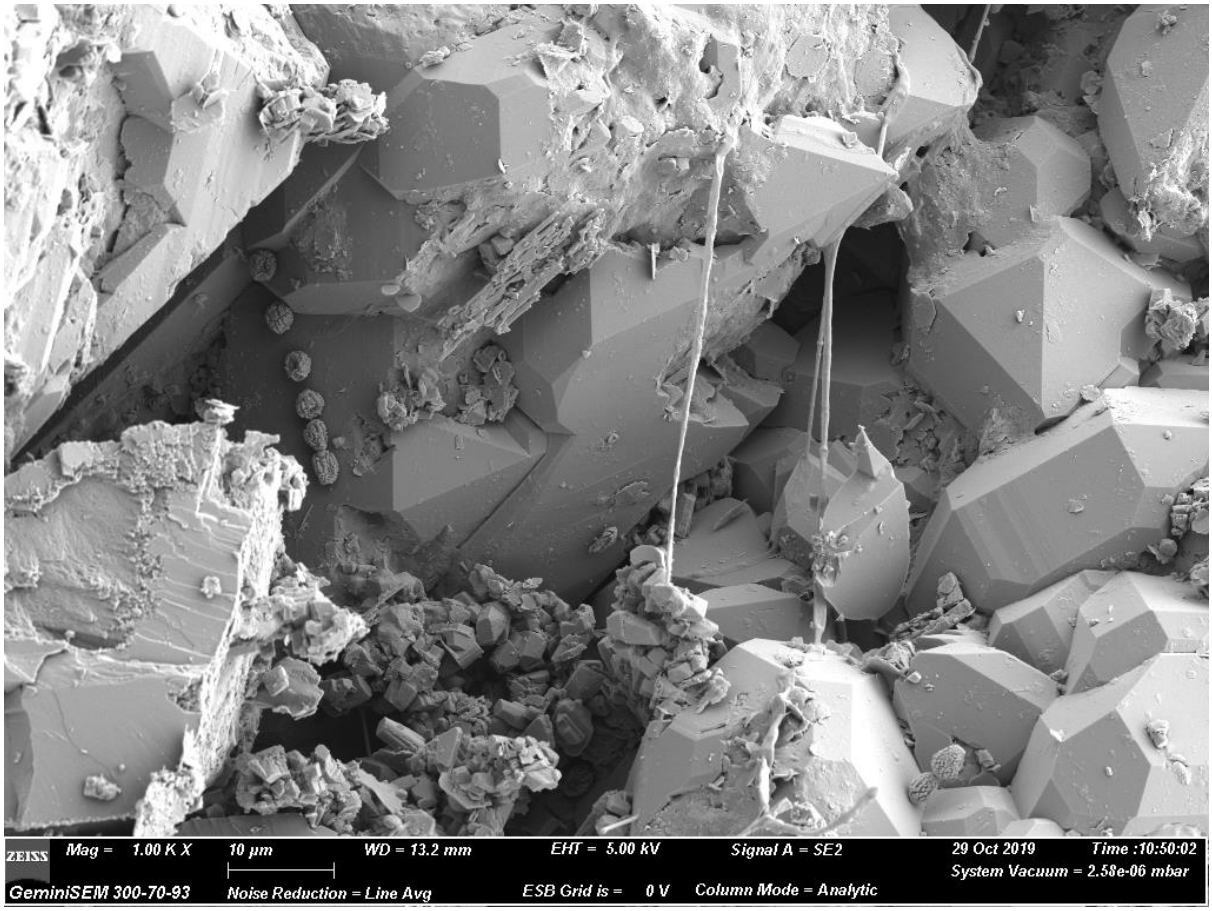

Sample Y8 – magnification = 1000x resolution = 10 µm

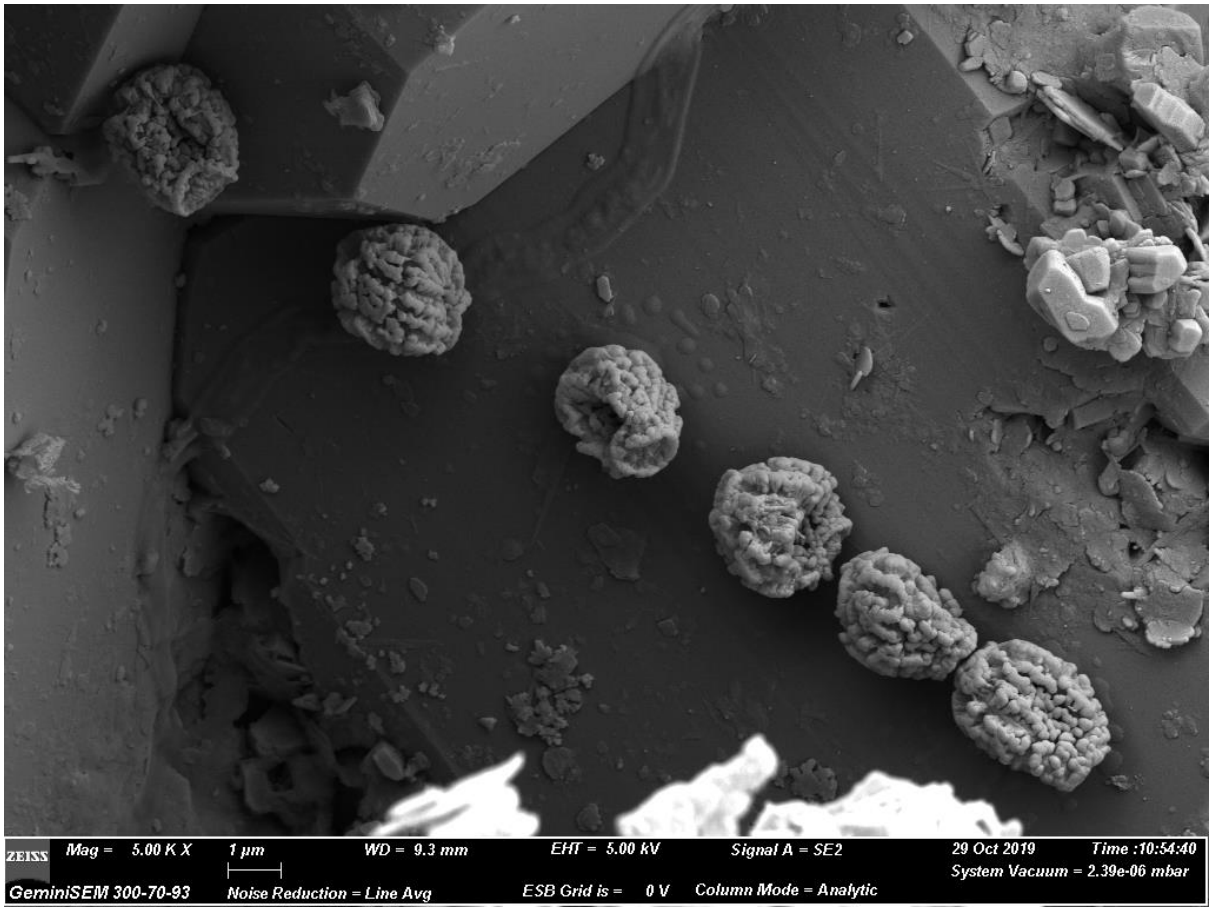

Sample Y8 – magnification = 5000x resolution = 1 µm